Recombinant Truncated Diphtheria Toxin for Possible Therapeutic Applications

Thesis submitted by

ASHOK KUMAR

For the award of the degree

of

Doctor of Philosophy

DEPARTMENT OF BIOTECHNOLOGY

INDIAN INSTITUTE OF TECHNOLOGY GUWAHATI

GUWAHATI - 781039, ASSAM, INDIA

FEBRUARY, 2014

Dedicated to my Family for their love, encouragement and support.

TH-1245_08610607

Department of Biotechnology

Indian Institute of Technology Guwahati

STATEMENT

I do hereby declare that the matter embodied in this thesis is the result of investigation carried out by me in the Department of Biotechnology, Indian Institute of Technology Guwahati, Guwahati, India, under the guidance of Dr. Biplab Bose.

In keeping with the general practice of reporting scientific observations, due acknowledgements have been made wherever the work described is based on the findings of other investigators.

February, 2014

Ashok Kumar
(Roll No. 08610607)

TH-1245_08610607

Department of Biotechnology

Indian Institute of Technology Guwahati

Date: 12.02.2014

CERTIFICATE

This is to certify that the thesis entitled "**Recombinant Truncated Diphtheria Toxin for Possible Therapeutic Applications**", is being submitted by **Mr. Ashok Kumar (Roll No. 08610607)** for the award of degree of Doctor of Philosophy is an authentic record of the results obtained from the research work carried out under my direct supervision & guidance in the Department of Biotechnology, Indian Institute of Technology Guwahati, India.

The investigations in connection with this work have been carried out by the candidate himself and the data obtained are genuine. The results embodied in this thesis have not been submitted to any other University or Institute for the award of any degree.

February, 2014

Dr. Biplab Bose

(Research Supervisor)

TH-1245_08610607

Acknowledgements

All things are destined to end, but memories. It is with sense of immense relief and feelings of achievement and satisfaction at the conclusion of this thesis that I turn to the pleasant opportunity to acknowledge and record my sincere gratitude to all those who made this work possible. In the race against the clock in which one almost inevitably becomes enmeshed when preparing a thesis, it is true relief to be surrounded by people who show sympathy and who continue to believe in what you are doing.

I wish to express my deep sense of gratitude and reverence to my esteemed supervisor Dr. Biplab Bose for his ongoing support, encouragement and constructive suggestions and for giving me the opportunity to work in such an inspiring environment and "state-of-art" facility at the Centre for Excellence (DBT Programme Support Laboratory), Department of Biotechnology, IIT Guwahati. His dedication and commitment to research and teaching is truly inspiring and remarkable. The amendment he did in my thesis has taught me the importance of quality work. I will remain endebited to him forever. Thank you very much sir for everything.

I am very much thankful to the members of my doctoral committee, Prof. Dr. S. S. Ghosh., Dr. A. M. Limaye, and Dr. Subrata K. Majumder for evaluating my work, giving critical comments and valuable suggestions which ultimately shaped the progress of my work. I am extreamly thankful to Prof. P. Goswami, Dr. A. Ramesh and Dr. L. Sahoo for their priceless suggestions, discussions and support throughout my PhD. I would sincerely like to acknowledge Dr. Gopal Das, Department of Chemistry, whose valuable suggestions often gave new perspectives and to carry forward my work.

With deep sense of appreciation, I owe my thanks to the present and past HODs of the Department of Biotechnology, Prof. Venkata Dasu Veeranki, Prof. A. Goyal and Prof. P. Goswami for creating excellent facilities and a great atmosphere at the department. I feel

TH-1245_08610607

privileged to have been able to work with intelligent, interesting and most of all very co-operative present and past members of the Department of Biotechnology as well as at the Centre for Nanotechnology.

I am really in dearth of words in expressing my sincere acknowledgement, gratitude and respect to my senior Dr. Asim Bikas Das for his guidance, support and encouragement. He helped me in every possible way. His constant criticism, uninhibited assistance and readiness to help at all stages have helped me to bring this thesis to a logical conclusion. I owe him a lot and remain indebted to him. Thank you Dada for your time, input, persistent efforts and enlightenment over the time.

I'm heavily indebted to my present and past lab members, Pojul, Mahesh, Priya, paulomi, Ritika, Sukanya, who have provided me with ongoing support, inspiration and enjoyable working environment. I'm especially grateful to my senior friends Dr. Vinod, Dr. Urmila, Dr. Shadab, Dr. Kaushik da for their unassessable fondness which made my stay at IITG a gratifying and memorable one. I also extend my thanks to Chokalingam, Kohila, Subhamoy, Manab, Sudeep, Sandipan, Nidhi, Gouri, Mitun, Ankana, Reddy, Souvika, Sagarika, Abhay, Rishi, Manjit, Himangshu, Seraj, Amresh, Shilpa, and former Ph.D. students, who have been of exceptional support during my PhD. Most especially, the sharing of news and views with my friends (Asim, Urmila, Vinod, Pojul) during mid-morning and evening tea at institute coffee shop or KV gate tea stall used to give me utmost relaxation from my tedious work. I have thoroughly enjoyed my years in IIT Guwahati campus. The departmental picnics and my trips to different parts of Assam with friends were the most enjoyable and memorable days of my PhD life. I duly acknowledge the technical help and cooperation rendered to me by our departmental staff (Mr. Nurul, Mrs. Anita, Mr. Niranjan, Mrs. Prarthana, and Mr. Sharan).

A very special vote of thanks goes to my friend Kaushik for his unconditional support and help without which it might have been a little harder for me to compile this thesis. I owe more than a formal thanks to Kaushik. I am indeed fortunate for the good wishes and zestful association with him. I wish him all the very best for his career.

TH-1245_08610607

Words are inadequate to express my feelings for my parents, (Late) Mr. Dharam Dev Ram and Mrs. Yashoda Devi, who taught me the values of honesty and hard work. Their love, support, and encouragement throughout my life heightened my strength to fulfill my goal. Today, whatever I am, I owe to them. Their unconditional love and belief is invaluable to me. Without their blessings, I could not have achieved my goal. No choice of words will suffice to adequately register the love, care and encouragement provided by my dearest wife, Joita, my little sweet son, Aryan(Putlu) & my parents'-in-laws who not only stood by me during the times of trial and listened patiently to me but also made things less troublesome by giving constant motivation & encouragement that give me energy to do more hard work. Finally, I want to remember all my professors & teachers during the course of my education who taught me to think, to do work in more widely and broader way. Many thanks to all of them.

…….and finally I express and extend my humble devotion to the almighty God for instilling in me enough strength, tenacity and conviction to see through this onerous task and without his blessings this work could never have been completed.

February, 2014 ***Ashok Kumar***

TH-1245_08610607

Contents

TH-1245_08610607

TH-1245_08610607

TH-1245_08610607

TH-1245_08610607

Abbreviations

ANOVA	Analysis of variance
bp	Base pair
CM	Carboxymethylated
DT	Diphtheria toxin
DAB	3, 3′-diaminobenzidine tetrahydrochloride
DAPI	4', 6-Diamino-2-phenylindole dihydrochloride
DEPC	Diethylpyrocarbonate
DMEM	Dulbecco's Modified Eagle Medium
DMSO	Dimethyl sulfoxide
DNA	Deoxyribonucleic acid
dNTP	Deoxyribonucleotide triphosphate
EDTA	Ethylene-diamine-tetraacetic acid
EDC	1-ethyl-3-(3-dimethylamino-propyl)carbodiimide hydrochloride
ELISA	Enzyme-linked immunosorbent assay
EGF	Epidermal growth factor
EGFR	Epidermal growth factor receptor
ERK	Extracellular signal-regulated kinase
FBS	Fetal bovine serum
FITC	Fluorescein isothiocyanate
GAPDH	Glyceraldehyde 3-phosphate dehydrogenase
HB-EGF	Heparin-binding epidermal growth factor
HPLC	High performance liquid chromatography
hr	Hour

TH-1245_08610607

HRP	Horseradish peroxidase
IPTG	Isopropyl β-D-thiogalactopyranoside
JNK	c-Jun N-terminal kinase
kDa	Kilodalton
K_a	Association rate constant
K_d	Dissociation rate constant
K_D	Dissociation constant
LED	Light emitting diode
MAPK	Mitogen-activated protein kinases
mg	Milligram
min	Minutes
ml	Milliliter
mM	Millimolar
MTT	3-(4,5-Dimethylthiazol-2-yl)-2,5-diphenyl-tetrazolium bromide
NHS	N-hydroxysuccinimide
ng	Nanogram
nm	Nanometer
nM	Nanomolar
OPD	O-phenylenediamine dihydrochloride
PBS	Phosphate buffered saline
PCR	Polymerase chain reaction
PI3K	Phosphatidylinositol 3-kinase
PMSF	Phenylmethanesulfonylfluoride
PDB	Protein database
PVDF	Polyvinylidene fluoride
RDT	Receptor-binding domain of Diphtheria toxin
RIPA	Radioimmunoprecipitation assay

TH-1245_08610607

RNA	Ribonucleic acid
rpm	Revolutions per minute
RT	Room temperature
RU	Response unit
SPR	Surface Plasmon resonance
THF	Tetrahydro-furan
µg	Microgram
µl	Microliter
µM	Micromolar

TH-1245_08610607

Abstract

Toxicity of bacterial toxins, like Diphtheria toxin, has been widely utilized to create therapeutic agents that can kill target cells. For example, immunotoxins have been developed by fusing antibodies to Diphtheria toxin. Antibodies home the toxin to specific cells, overexpressing the antigens, and the toxin kills the target cells. Many of these toxins have receptors on certain cells. However, the receptor-binding ability of such toxins remains largely unutilized.

Diphtheria toxin (DT) binds to its cell surface receptor called Heparin-binding EGF-like growth factor (HB-EGF). Subsequently, the toxin gets internalized and causes cytotoxicity through its catalytic domain. Interestingly, HB-EGF is overexpressed in various cancer cells. Therefore, HB-EGF is a good target for homing chemotherapeutic agents. An HB-EGF-binding protein can be used for this purpose. HB-EGF is also involved in oncogenic signaling and known to facilitate tumor growth, metastasis and angiogenesis. Therefore, an HB-EGF-binding protein can also be used to block oncogenic signaling of HB-EGF.

In the present work, we have exploited the receptor-binding ability of DT for therapeutic utilities. We have cloned, expressed and purified the receptor-binding domain of DT (RDT) using an *E.coli* expression system. We show that RDT binds to HB-EGF on cell surface. It was observed that RDT binds to HB-EGF with an affinity equivalent to that of full-length DT.

Using fluorescence spectroscopy, we show that curcumin, a potential chemotherapeutic agent, binds to RDT. Binding to RDT increases the fluorescence and fluorescence lifetime of curcumin. Curcumin-RDT complex

TH-1245_08610607

binds to HB-EGF and associates with human glioblastoma cells (U-87 MG) expressing HB-EGF. This increases accumulation of curcumin in-and-around the cells, leading to enhanced uptake. This increase in uptake enhances the anti-proliferative effect of curcumin and induces apoptosis of these cells even at a lower dose.

Certain chemotherapeutic agents like Etoposide and Irinotecan increase expression and shedding of HB-EGF. Being oncogenic, such increase of soluble HB-EGF reduces the efficacy of these therapeutic agents. As RDT binds to HB-EGF, it may block or sequester signaling through HB-EGF. We have used these chemotherapeutic agents in combination with RDT and have shown that RDT enhances the potency of these drugs.

TH-1245_08610607

1 Introduction

Issues of solubility, stability, bioavailability, toxicity, and targeted delivery of drugs are persistent challenges of drug development. Various approaches starting with chemical modification to encapsulation have been used to circumvent these problems, particularly for hydrophobic drugs. Macromolecules and biomimetic molecules have also been used. Nanocarriers, made up of albumin and casein, have been developed to increase drug solubility and stability. Antibody-tagged delivery vehicles are created to deliver drugs to specific cells. Cell penetrating peptides have been developed that can increase cellular uptake of drugs. All these approaches lead to decrease in dosage of the drug, thereby reducing side effects. An associated approach is to use combination of drugs or drug and adjuvants to enhance the potency of the drug. Increase in drug potency lowers the required dosage, leading to lesser side effects.

Cell surface molecules overexpressed on diseased cells are good target for cell-specific drug delivery. Ligands to such molecules, like antibody-fragments, can be used to home a drug to those cells. HB-EGF is one such target molecule, which is overexpressed in several cancer cells. It is a membrane bound molecule, which gets released through ectodomain shedding. HB-EGF-expressing cells can be targeted using HB-EGF-binding molecules. Such HB-EGF-binding molecules can have dual effects. Apart from homing a therapeutic molecule, such a binder may block signaling through HB-EGF. Both membrane-bound and soluble HB-EGF are known to induce oncogenic signaling. Blocking such signaling may potentiate a conventional chemotherapeutic agent.

TH-1245_08610607

Interestingly, Diphtheria toxin (DT) is a natural ligand of HB-EGF. DT binds to cell surface HB-EGF and is internalized through receptor-mediated endocytosis. Therefore, mutated non-toxic DT or its receptor-binding domain can be used to target HB-EGF. In this work, we have cloned and expressed the receptor-binding domain of DT (RDT). We have shown that RDT binds to HB-EGF. Further, RDT binds to curcumin, a potential chemotherapeutic agent. Curcumin provided as curcumin-RDT complex has higher cellular uptake and cytotoxicity. Certain chemotherapeutic agents like Etoposide and Irinotecan, increase expression and shedding of HB-EGF. Increase in HB-EGF would offset the cytotoxic effects of these drugs. We have shown that when provided in combination with these cytotoxic agents, RDT increases the potency of these drugs possibly through blocking or sequestration of HB-EGF.

The present thesis is organized into separate sections. After this introductory chapter, existing literature on issues in drug development and possible approaches of using Diphtheria toxin (DT) to solve these issues has been extensively reviewed in Chapter 2, Review of Literature. Chapter 3 describes Materials and Methods used in the present work. Additional information on common reagents, kits, cells used in different experiments is given in the appendix. The results of our experiments and a thorough discussion on those have been provided in Chapter 4, Results & Discussion. The conclusions drawn from our present work, along with their implications and future scopes are discussed in Chapter 5.

TH-1245_08610607

2 Review of Literature

Rapid developments in biochemistry and molecular technology have led to advancement in drug discovery. Large numbers of newer drugs are designed through rational approaches [1, 2]. Even then, certain persistent issues like solubility, stability, bioavailability, toxicity and targeted delivery of drugs, limits clinical uses of many of these molecules [3].

Many therapeutic agents are small hydrophobic molecules and have low solubility in water. These drugs usually require high doses and toxic organic solvents to achieve desired bioavailability and for prolonged pharmacological activity [3, 4]. Some therapeutic molecules are unstable in aqueous environment and require higher dosage to achieve the desired effect. Dose escalation increases unwanted side effects too. This problem is aggravated as most of these molecules are not cell or tissue specific and get distributed throughout the body through systemic circulation. This necessitates high dose of the drug to achieve desired concentration at the required site. This eventually leads to enhanced side effects and toxicity.

2.1 Enhancement of solubility and stability of drugs:

Several approaches have been used to increase solubility of drugs. The commonest approach is to create chemical analogues having better solubility [5]. Such chemical modification includes derivatization, complexation, and salt formation [6] Another approach is to encapsulate the drug in a carrier. Derivatives of cyclodextrins having a hydrophilic exterior and lipophilic core are used to form noncovalent Lipophilic drug-cyclodextrin inclusion complexes, resulting in increased aqueous solubility and chemical stability of poorly water soluble drugs [7-10]. Further, encapsulation of drugs in liposomes

TH-1245_08610607

[11] and polymeric micelles [12, 13] also improves the solubility and bioavailability of poorly water soluble drugs. Several proteins have been used to develop novel carrier systems that increase solubility and stability of drugs. Human serum albumin, casein, collagen and β-lactoglobulin [14-17] have been used to develop nano-carriers to increase the solubility, bioavailability as well as stability of many drugs like Methotrexate, Paclitaxel, Celecoxib, Retinol and Curcumin.

2.2 Enhancement of cellular uptake of drugs:

Potency of a drug also depends upon its uptake in target cells. Absence of any facilitated uptake mechanism necessitates use of high dose. One can reduce the dosage but still generate the desired outcome by developing a drug delivery system that helps in cellular uptake of the drug.

Cell-penetrating peptides (CPPs) like Protein transduction domains (PTDs) are small parts of viral proteins that act as molecular transporters. They are typically composed of approximately 10-30 amino acids in length containing a high abundance of positively charged amino acids such as such as arginine and/or lysine (polycationic) or exhibit an alternating pattern of polar/charged and non-polar, hydrophobic residues (amphiphilic) [18]. CPPs get internalized by a cell through endocytosis. This is facilitated by strong ionic interaction between the positively charged amino acids of CPP and negatively charged plasma membrane constituents [19, 20]. As these molecules have higher endocytic rate, CPPs can work as molecular carrier to increase cellular uptake of a drug. Protein transduction domain and cell penetrating peptides have been shown utility in enhancing the cellular uptake of multiple types of macromolecular cargo including peptides, proteins, antisense oligonucleotides and siRNA [21-24].

TH-1245_08610607

An example of such cell-penetrating peptide (CPP TAT) is a highly basic region comprising amino acids 48-57(TAT_{48-57}) from the nuclear transcription activator (TAT) protein of the human immunodeficiency virus type 1 (HIV-1) [25-27]. CPP TAT fused to a cargo like protein (>50 amino acids) or peptide (<50 amino acids) has been shown to have enhanced internalization into living mammalian cells [28]. Particulate systems are well known to deliver drugs with higher efficiency [29, 30]. Various particulate drug delivery systems have been developed, such as polymeric microspheres [31], nano-particles [32, 33], liposomes [29, 34, 35], and solid lipid nano-particles (SLNs) [36]. Polymer-lipid hybrid nanoparticle (PLN) system is a lipid-based nanoparticle formulation and has been developed to enhance the cellular uptake and retention of drugs in cancer cells [31, 37, 38]. Wong et al. in 2006 [39] developed a complex of a nanoparticle containing drug like Doxorubicin (Dox) with P-glycoprotein (PgP) inhibitors to form Dox-PLN. PgP is a membrane associated glycoprotein overexpressed in breast cancer and resists entrance of several drugs including Dox. The polymer inhibited membrane PgP and enhanced the cellular uptake and retention of DOX associated with the nanoparticle. It has shown to increase the uptake of Dox compared to free Dox in PgP-overexpressing breast cancer cells.

2.3 Drug combination to enhance potency:

Problem of solubility, stability and non-specificity necessitate use of higher doses to achieve a desired effect. One way to circumvent this is to increase the potency of the drug. Combination therapy is a way to increase drug potency [40]. In this two or more drugs are used in combination to potentiate individual effect [41]. This lowers the required dosage of individual drugs and lowers side effects [42, 43].

TH-1245_08610607

Based on molecular mechanisms, drug synergism can be of three types, namely anti-counteractive actions, complimentary action and facilitating actions. In anti-counteractive actions, the counteractive or neutralizing actions by the cell against one drug's therapeutic effect is reduced by the other drug, therefore resulting in synergism. Combination of cisplatin and topotecan is an example of the mechanism. Cisplatin binds to the major groove of DNA. The cell counteracts and bypasses the replication across cisplatin–DNA with mutagenic translesional bypass. Topotecan reduces this counteraction by inhibiting topoisomerase I and stabilizing covalent topoisomerase–DNA complexes to block DNA replication forks and therefore, resulting in synergism [44-46]. In complementary actions, one drug complements the action of other drug synergistically. It involves potentiation of the action of one drug by the other or producing an additive effect due to their equivalent actions on different targets of related pathways. An example of such action is observed in celecoxib and emodin combination, which synergistically represses the growth of certain cancer cells. Celecoxib is a cyclooxygenase 2 (CoX 2) inhibitor. Inhibition of CoX2 inactivates protein kinase AKT resulting into apoptosis, thereby suppression of cancer growth. Emodin also suppresses cancer growth by inhibiting tyrosine kinases ($p185^{neu}$, an ErbB receptor kinase protein) and downregulating AKT. Emodin, thus, complements celecoxib's inactivation of AKT and ultimately leads to apoptosis in a synergistic fashion [47]. In facilitating actions, Drugs in combination produce synergistic effect. Two drugs may have different mechanism of action but the result of actions by one of the drug enhances the activity or effect of other drug. This can be explained by a combination of gentamicin and vancomycin, which produces synergistic antibacterial action against penicillin-resistant bacterial strains. Gentamicin targets bacterial ribosome and disrupt protein synthesis. Vancomycin selectively inhibits cell-wall peptidoglycan synthesis, RNA synthesis and alters cell membrane permeability. The alteration in cell-membrane permeability by

TH-1245_08610607

vancomycin enhances gentamicin penetration into bacterial cells, thereby increasing its effect [48].

A rational combination of antibodies against some cell surface receptors and chemotherapeutic agents has been developed. Such combinations have also shown promising results in several cancers. Monoclonal antibodies against EGFR and HER2, namely, cetuximab and trastuzumab, in combination with cisplatin enhanced the cytotoxic effects of cisplatin through DNA-damaging. Such combinations are effective in breast as well as gastric cancer and have advanced into different phases of clinical trials [49-51].

2.4 Targeted delivery of drugs:

Conventional drug delivery systems involve homogeneous distribution of drugs throughout the body via the systemic blood circulation system. Due to distribution throughout the body, only a small portion of the medication reaches the affected site. Therefore, a high dose of the drugs is required for desired effects. This lack of specific affinity towards a pathological site and requirement of higher doses of drugs causes non-specific toxicity and other side effects.

Targeted drug delivery has emerged as an attractive strategy for enhancing the potency of a drug. It involves delivering the drug in a dosage form that preferentially gets delivered to the pathological site. Several such targeted delivery systems (Figure 2.1) have been developed of which a few are approved and are in clinical use for various diseases whereas others are under trials [52].

Liposome based therapeutic system improves the delivery of drugs to target site in several cancers. A liposome can be reformulated to achieve targetable property by association with cell specific antibody. Therefore, a chemotherapeutic agent entrapped in such modified liposome gets delivered to specific cell. Doxorubicin is entrapped in liposomes (Doxil) is being used in

TH-1245_08610607

patients with multiple myeloma [53], Kaposi sarcoma [54], ovarian [55] and breast cancer [56]. Formulations like polymer drug conjugates such as Oncaspar (PEG-L-Asparginase) have been used in leukemia patients [57]. Targeted nanomedicine formulations such as polymeric micelles containing Paclitaxel (Genexol-PM) is been approved for breast, lung and ovarian cancer. Abraxane (albumin based nanoparticle containing Paclitaxel) have shown promising results in breast cancer patients [58].

Cell surface molecules are often used for delivery of drugs to a target cell. Many such molecules are differentially over-expressed in diseased cells. Therefore, a molecule that can specifically bind to such a cell surface molecule can be used to home a therapeutic payload to those cells over-expressing the molecule. This eventually leads to increased cellular uptake of drugs by those specific cells and enhances the potency of the drug. There are a number of reports where a ligand or an antibody against such receptors has been used for targeted drug delivery in various diseases including cancers. Jennifer *et al.* in 2000 [59], targeted Folic acid receptor which is highly over-expressed in ovarian carcinomas and delivered drugs coupled with folic acid, to folate receptor-positive tumor cells. In another approach, IL-2 fused with the enzymatic domain of Diphtheria toxin, was used for targeting and preventing the expansion of IL-$2R^+$ T cells [60]. IL-$2R^+$ T cells are involved in a variety of T-cell mediated diseases, including transplant rejection, autoimmunity, and delayed-type hypersensitivity (DTH). Similarly, transferring receptors has been targeted to deliver therapeutic molecules to malignant cells over-expressing transferring receptors [61-64]. In another approach, Zhang *et al*. in 2009 [65] developed a drug delivery vehicle consisting of non-toxic recombinant heavy chain of botulinum neurotoxin-A coupled to dextran via a linker. It has been used for targeting neuromuscular synapses, which express the receptors for this neurotoxin. Townsend et al. in 2007 [66] conjugated C fragment of tetanus toxin (TTC) to nanoparticles through a crosslinker and shown that it targets neuroblastoma cells *in vitro*. TTC

TH-1245_08610607

specifically binds to neurons and therefore TTC conjugated nanoparticle can serve as drug delivery vehicles to target central nervous system. Besides coupling with therapeutics, in the following year, Bouter et al. [67] functionalized spherulites (multi-lamellar lipid vesicles) with non-toxic B-subunit of Shiga toxin (STxB). STxB binds to glycosphingolipid Gb3 (globotriaosyl ceramide) overexpressed in various tumors. It was shown that STxB-functionalized spherulites get internalized into HeLa cells in a receptor dependent manner. Mayer *et al,* in 2004 [68] developed an Antibody-directed enzyme pro-drug therapy (ADEPT) where adeno-carcinomas expressing carcino-embryonic antigen (CEA). They linked bacterial enzyme carboxy-peptidase CP either chemically or genetically to tumor-targeting monoclonal anti-CEA antibody and given intravenously. Once the antibody-enzyme has cleared from the circulation, a pro-drug was given which gets converted to active drug in the tumor by the targeted enzyme. Such antibody based system for targeted delivery of drugs has advanced significantly over the past few years.

Several Antibody drug conjugates (ADCs) has been developed for delivery of anti-cancer drugs to target cells. The first U.S. Food and Drug Administration (FDA) approved ADC is used in patients with relapsed acute myelogenous leukemia [69]. It consisted of a recombinant monoclonal antibody (Gemtuzumab) against CD33 expressed on most leukemic blast cells and was linked to calicheamycin. Another, FDA approved ADC for clinical use in patients with Hodgkin's Lymphoma consists of an antibody (Brentuximab) against tumor necrosis factor receptor (CD30) conjugated to Lymphoma drug (Adcetris) [70]. CD30 is a tumor marker for Hodgkin's Lymphoma. A similar approach in patients with HER2-positive breast cancer with ADC, Trastuzumab emtansine (T-DM1), has shown positive results in pre-clinical and is currently under phase III of clinical trials [71]. Several other ADCs are under different phases of clinical trials [72].

TH-1245_08610607

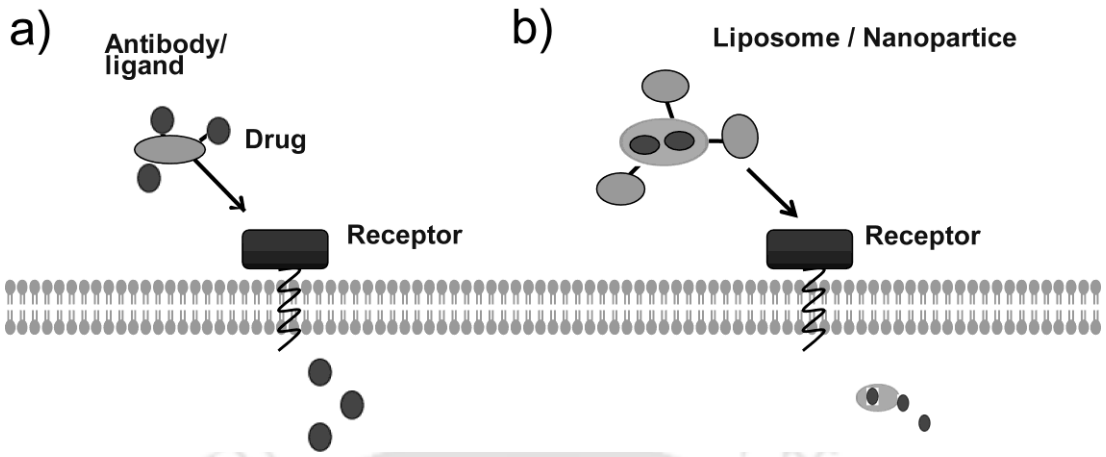

Figure 2.1. Different methods of Targeted delivery of drug. A cell surface receptor may be used in two different ways. A ligand or antibody of the receptor may be used either by (a) conjugating it with a drug or (b) a drug loaded nanoformulations like liposomes or nanoparticles may be crowned with it. The antibody or the ligand delivers the drug to cells expressing that receptor.

2.5 HB-EGF as a therapeutic target:

Heparin-binding EGF-like growth factor (HB-EGF) is a cell surface molecule. HB-EGF is expressed as a membrane anchored molecule that is released in soluble form by ectodomain shedding [73]. The primary role of HB-EGF is to act as a growth and survival factor. HB-EGF binds to EGFR and ErbB4 and activates downstream pathways. HB-EGF is over-expressed in several types of cancers, e.g., glioma, pancreatic, liver, and gastric cancer and is involved in multiple aspects of tumor development, progression, angiogenesis and metastasis and development of drug resistance [74-77]. Therefore, HB-EGF has emerged as a potential therapeutic target for development of novel anti-cancer therapy.

TH-1245_08610607

Targeting HB-EGF for therapeutic benefits offers a dual advantage. HB-EGF promotes cellular growth through multiple signaling pathways. Blocking HB-EGF by a ligand would stop those oncogenic signaling pathways leading to inhibition of cell growth and proliferation. Further, it can also be utilized in specific delivery of a therapeutic cargo to cells over-expressing HB-EGF. Attempts have been made to inhibit HB-EGF and its associated signaling cascades. Blocking antibodies (mAbs) against HB-EGF have been developed [78-80]. They block HB-EGF signaling leading to inhibition of cell proliferation and angiogenesis [78]. These antibodies may be used for treatment of cancer. Miyamoto *et al.* [81] have shown that such HB-EGF antibody is effective against ovarian cancer in *in-vivo* models. Additionally, such antibody can be used for targeted drug delivery. Nishikawa *et al.* [82] encapsulated doxorubicin in PEGylated liposomes and crowned those liposomes with an anti-HB-EGF antibody. They have shown that this targeted drug delivery system is effective against breast cancer *in-vivo* models.

2.6 Domain architecture of HB-EGF:

HB-EGF is a 208 amino acid long protein with an apparent molecular weight of 20-22 kDa. HB-EGF exists in multiple secreted isoforms containing between 73 and 87 amino acids [83]. These HB-EGF forms are generated by N-terminal proteolytic cleavages of that occur during processing of the initial primary translation product to produce a mature HB-EGF. These forms of HB-EGF also differ in their C termini or in patterns of post-translational modification like *O*-glycosylation at putative glycosylation sites [84].

Similar to other members of the EGF family, HB-EGF has an ectodomain, a single membrane-spanning domain and a cytoplasmic domain [85]. The HB–EGF precursor as shown in Figure 2.2, includes an N-terminal signal peptide domain (1-23 amino acids), a pro-peptide domain (24-62 amino acids), mature

TH-1245_08610607

HB–EGF domain (63-149 amino acids), a juxtamembrane domain (150-160 amino acids), a trans-membrane domain (161-184 amino acids) and short cytoplasmic (185-208 amino acids) domain. The mature HB-EGF domain consists of an epidermal growth factor (EGF)-like motif having a heparin-binding region. The EGF-like domain of HB-EGF, typical of all members of the EGF family, has a conserved six cysteine residues, which forms three intra-molecular disulfide bonds and their spacing are highly conserved. Mature soluble HB–EGF is released from the membrane-anchored precursor by proteolytic cleavage [86].

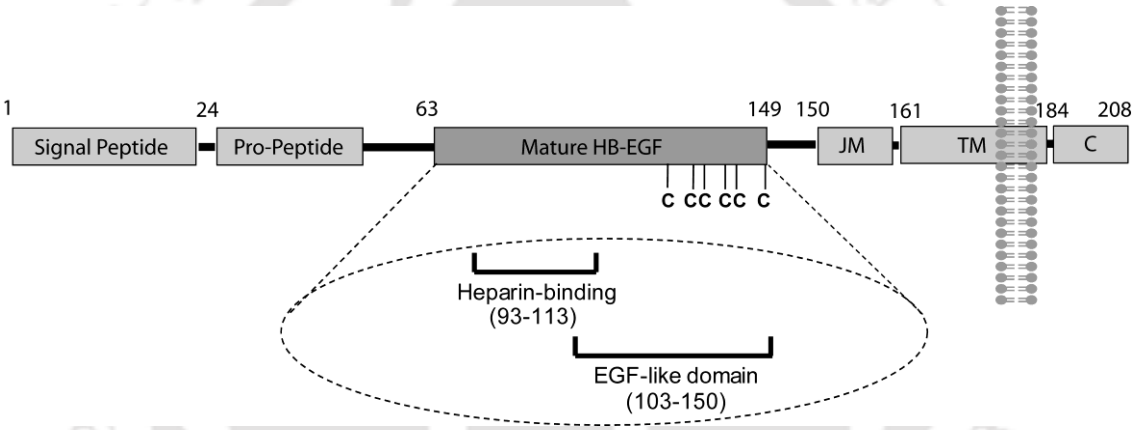

Figure 2.2. Domain architecture of Heparin-binding epidermal growth factor (HB-EGF). HB-EGF (1-208 amino acids) has a signal peptide, pro-peptide region, a mature HB-EGF region, a short juxta-membrane sequence (JM) followed by a hydrophobic trans-membrane domain (TM) with a short cytoplasmic domain (C) at the C-terminus.

2.7 Expression of HB-EGF:

HB-EGF was first identified as a secreted product of macrophage and macrophage-like U-937 cells [84, 87]**.** The human HB-EGF gene spans 14-kb of DNA and contains 6 exons and 5 introns. Its locus has been mapped to chromosome 5 in humans [88]**.** The longest form of an HB-EGF cDNA cloned so far is 2.36 kb in length [89]. HB-EGF is generally expressed at a very low level in

TH-1245_08610607

some normal adult tissues like lung [90], heart [91], brain and skeletal muscle [92]. It regulates cellular activities such as proliferation, migration and differentiation [93] and blastocyst implantation [94]. However, there is growing evidence that HB-EGF is over-expressed in various cancers, including breast cancer [95], pancreatic [76, 96, 97], liver [74], esophageal, melanoma, prostate cancers [98], colon [99], gastric [77], ovarian [100], hepatic [101] and bladder cancers [102-104] as well as in glioblastoma [75].

2.8 Role of HB-EGF in physiological processes:

HB-EGF plays critical roles in wound healing [105]. Its expression increases during wound/injury as observed in wound fluid obtained from porcine partial-thickness excisional wounds [106]. The level was back to normal with the healing of the wound. Additionally, human monocytes, which play an important role in wound healing, also release HB-EGF upon activation. HB-EGF is also involved in myogenesis. A DNA binding transcription factor (MyoD), involved in myogenesis, modulates HB-EGF transcription in skeletal muscle cells during this process. Cell surface HB-EGF interacts with adjacent cells and promotes myotube and myofibril formation. HB-EGF facilitates cell-cell interactions between the endometrium and conceptus during embryo implantation and placentation [107]. HB-EGF acts as a potent mitogen and regulates smooth muscle cell (SMC) growth *in vivo*. It is synthesized and secreted by cultured fetal human vascular SMC and initiate SMC migration and proliferation [108]. HB-EGF is ubiquitously present in the epithelial cells of the renal proximal tubules and plays a role in the formation of proximal renal tubules in normal kidneys. HBEGF has been shown to act as an autocrine growth factor for normal human urothelial cells. HB-EGF within the urothelium acts as a regulator of cell cycling or regeneration in response to mucosal injury. HB-EGF is also essential for proper growth and normal functioning of cardiac

TH-1245_08610607

muscle cells. It regulates proliferation and differentiation of mesenchymal cells into mature atrioventricular valves structures [91, 109].

2.9 Role of HB-EGF in pathological processes:

HB-EGF is involved in a number of pathological processes, including cardiac hypertrophy [110], smooth muscle cell hyperplasia [111], pulmonary hypertension [112], atherosclerosis [111], and oncogenic transformation [113]. HB-EGF is over-expressed in several types of cancers and is involved in proliferation and migration of cancer cells [114], angiogenesis [115], and development of drug resistance [116]. There is growing evidence that over-expression of HB-EGF plays crucial roles in tumorigenesis in cancers including breast cancer [95], pancreatic cancer [76, 96, 97], and glioblastoma [75]. Bladder cancer cells have been shown to express both soluble and membrane-anchored HB-EGF which induces growth, migration as well as angiogenesis [102-104]. HB-EGF has been shown to promote cell migration and invasion in prostate cancers [98], colon cancer [99]. It was also found to participate in the epithelial-mesenchymal transition (EMT) in gastric and ovarian cancer cells [77, 100]. Moreover, increased HB-EGF expression increases DNA synthesis and mitogenesis in pre-malignant hepatocytes suggesting role for HB-EGF in hepato-carcinogenesis [74, 101]. Further, HB-EGF is involved in the development of resistance against conventional chemotherapeutic agents [117] in several types like ovarian [118], Lung [119] and advanced gastric [120].

2.10 Certain chemotherapeutic agents increase HB-EGF:

Several chemotherapeutic agents like Paclitaxel, Etoposide increase HB-EGF (Table 4.1). Etoposide and Irinotecan activate NF-kB and AP-1 leading to enhanced expression of HB-EGF [117]. On the other hand, Paclitaxel and Cisplatin activate metalloproteases that induces ecto-domain shedding of HB-EGF [121]. Both the process increases soluble HB-EGF that enhances survival

TH-1245_08610607

and growth signals for cancer cells. This leads to decrease in potency of those chemotherapeutic agents.

Table 4.1. Chemotherapeutic agents that increase HB-EGF

Drug	Mechanism of action	Effect on HB-EGF	Cancer type	Ref.
Paclitaxel (Taxol)	Disrupt Cytoskeletal assembly	Increases shedding	Ovarian	[118, 122]
Etoposide	Inhibits Topoisomerase II	Increases Expression	Cervical	[123]
Irinotecan	Inhibits Topoisomerase I	Increases expression & shedding	Colorectal, cervical, Pancreatic.	[124]
Cisplatin	Cross-links DNA	Increases shedding	Ovarian, Gastric	[119]
Doxorubicin	Inhibits Topoisomerae (S phase)	Increases expression & shedding	Leukemia, cervical, Panceatic.	[117, 125, 126]
5 Fluorouracil (5-FU)	Nucleotide analogs	Increases shedding	Gastric cancer	[120]

2.11 Molecular Signaling of HB-EGF:

HB-EGF can activate signal transduction pathways both as a soluble protein as well as membrane-anchored one. HB-EGF mediated signaling involves the Ras/Erk-MAP kinase and PI3-K/Akt pathways that are involved in growth, proliferation, and survival [127, 128]. The signaling pathways of HB-EGF are briefly described in Figure 2.3. Akt and Erk1/2 are the key molecules in these two pathways. HB-EGF mediated downstream signaling pathways and their functions are discussed here.

TH-1245_08610607

2.12 Ras/Erk/MAP Kinase Signaling Pathway:

HB-EGF, like other members of the (EGF)-like super family of proteins, binds with one or more ErbB receptor tyrosine kinases. HB-EGF binds and activates both EGFR (ErbB1) and ErbB4 receptors. The activated ErbB receptors form homo- or hetero-meric receptor complexes following HB-EGF binding and undergo auto-phosphorylation on specific tyrosine residues that mediate downstream signaling cascades [129]. The phosphorylated receptor complex interacts directly or through Shc1 (Src homology 2 domain containing transforming protein 1) with an adapter protein Grb2 (Growth factor receptor bound protein 2), which in turn recruits the son of sevenless (SOS) to the activated receptor dimer. SOS then activates RAS leading to the activation of RAF-1. RAF-1 subsequently phosphorylates MEK1 and MEK2 which activate respectively ERK1 and ERK2 [130, 131]. This pathway results in increased transcription of Bcl-2 family members and inhibitor of apoptosis proteins (IAPs), thereby promoting cell survival and proliferation. HB-EGF also promotes G1-phase progression in the cell cycle by upregulating the expression of cyclin D through this Ras-MAPK signaling cascade [77, 132].

2.13 PI3 Kinase/Akt Signaling Pathway:

HB-EGF also promotes cell survival through the activation of PI3 kinase/Akt signaling [133]. The catalytic subunit of PI3-kinase phosphorylates phosphatidylinositol (4, 5) bisphosphate (PtdIns(4,5)P_2) leading to the formation of PtdIns(3,4,5)P_3. PI 3-kinase can also activate Ras, resulting in the activation of Erk signaling, thereby facilitating cross-talk between survival pathways. A key downstream effector of PtdIns(3,4,5)P_3 is Akt (PKB). Akt promotes cell survival through the transcription of anti-apoptotic proteins.

Additionally, the carboxy-terminal fragment of HB-EGF (HB-EGF-CTF) that remains after ectodomain cleavage activates a receptor-independent pathway.

TH-1245_08610607

It has been shown to inhibit the transcription-repressing capabilities of promyelocytic leukemia zinc finger (PLZF) protein and Bcl6 through either nuclear export or degradation, respectively [132, 134]. This result in enhanced expression of cyclin A and cyclin D2, together with increased cell cycle transition.

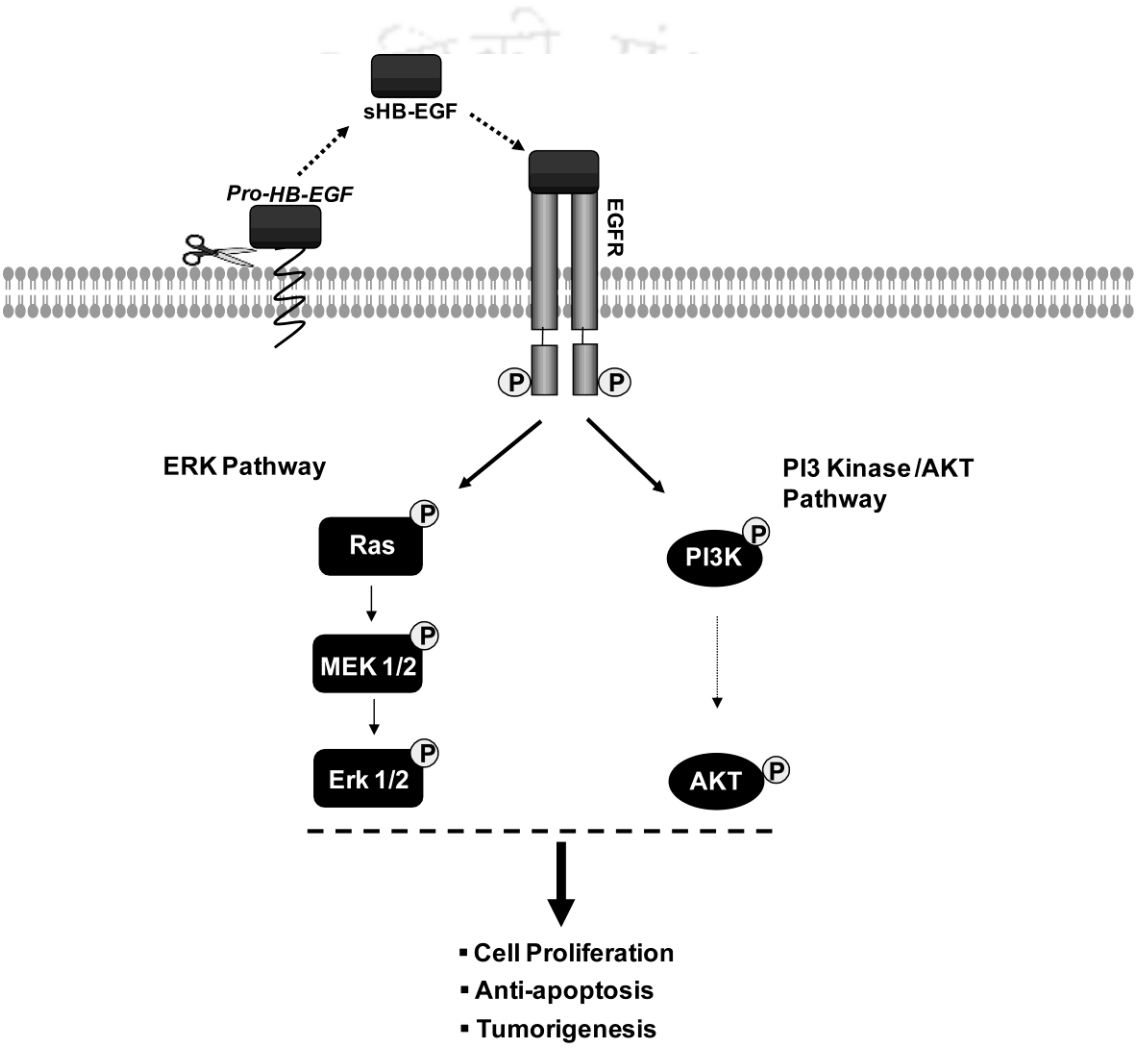

Figure 2.3. HB-EGF activates MAPK and AKT signaling pathway. HB-EGF binds and activates EGFR. Trans-activation of EGFR subsequently activates Erk1/2 and Akt. Activation of these two pathways eventually leads to cell proliferation, through modulation of molecules involved in cell cycle progression.

TH-1245_08610607

2.14 Diphtheria Toxin:

HB-EGF is also the receptor of Diphtheria Toxin (DT) [135]. DT is an exotoxin synthesized and secreted from the bacterium *Corynebacterium diphtheria* DT kills eukaryotic cells by inactivating elongation factor 2 (EF-2), an essential component of the protein translation machinery [136]. DT is globular protein composed of a single polypeptide chain of 535 amino acid residues having an approximate molecular weight of 63,000 daltons. It is synthesized as a single, intact pro-enzyme having two fragments connected by a loop containing a proteolysis site and a disulfide bond (Figure 2.4a).

2.15 Structural & functional aspects of DT:

DT is composed of three distinct domains. The ribbon diagram of the X-ray crystal structure of DT (Figure 2.4b) shows that the toxin has: (1) An N-terminal ADP-ribosyltransferase (catalytic domain, C, residues 1-190) which is involved in cellular toxicity. (2) A membrane spanning domain, (trans-membrane domain, T, residues 191-378) that facilitates the translocation of catalytic domain across the cell membrane, and (3) A C-terminal receptor-binding domain, (R-domain, residues 379-535) that binds to the EGF-like domain of HB-EGF [137, 138]. The DT binds on the surface of the target cell through the Diphtheria toxin receptor HB-EGF [139]. On binding to cell surface HB-EGF, DT is internalized through receptor-mediated endocytosis [140]. The affinity of the DT molecule with HB-EGF is relatively high. The apparent dissociation constant of the DT-HB-EGF complex has been estimated to be 10^{-8} – 10^{-9} M [141, 142].

TH-1245_08610607

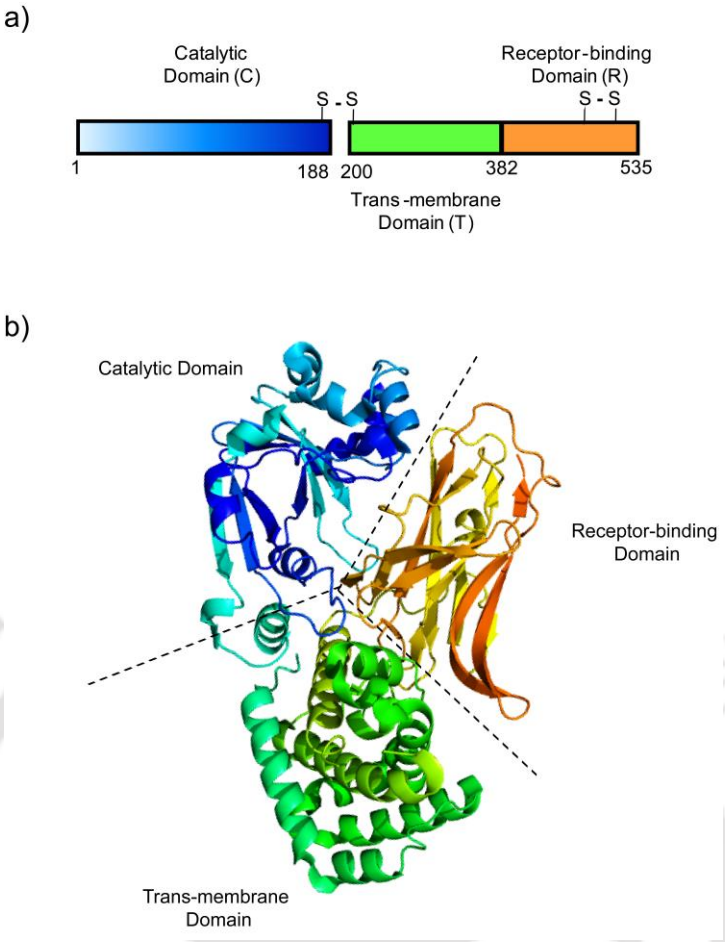

Figure 2.4. Structure of Diphtheria toxin (DT). (a) a schematic diagram showing composition of DT. DT has three domains, a catalytic (1-188 a.a residues), a trans-membrane domain (200-382 a.a residues) and a receptor-binding domain (382-535 a.a residues). (b) Ribbon diagram of the X-ray crystal structure of DT. The figure is derived from the X-ray crystal structure of DT (PDB ID: 1F0L).

The intoxication of a cell by DT involves four distinct steps (Figure 2.5). DT binds to cell surface HB-EGF through the R-domain [143]. Subsequently, it gets internalized by receptor-mediated endocytosis [143]. Once in the endosome, the acidic environment causes structural change in DT. The T-domain gets inserted in the endosomal membrane facilitating translocation of the catalytic domain to cytoplasm [144]. Eventually, the catalytic domain catalyzes the transfer of an ADP-ribosyl group from NAD^+ to a specific modified histidine (diphthamide)

TH-1245_08610607

on the elongation factor 2 (EF-2) [145]. This results in inhibition of protein synthesis that leads to cell death.

2.16 DT in therapeutics:

The toxicity of DT has been widely utilized for the development of number of therapeutic agents that can kill target cells. For example, immuno-toxins have been developed by coupling or fusing genetically, antibodies or peptides to the toxic domain of DT. One such immuno-toxin is DAB389-IL-2 where receptor-binding domain of DT is genetically replaced with interlukin-2 (IL2). It has been approved by the US Food and Drug Administration (FDA) for cutaneous T-cell lymphoma after successful Phase I, II and III trials [146]. Many such targeted DT toxins are in developmental stages of either preclinical or clinical trials phase I/II [147, 148]. Clinical investigations of the efficacy and toxicity of DT-based immuno-toxins have shown significant progress in haematological malignancies such as leukemias, Hodgkin's lymphoma and multiple myeloma [149]. Clinical trials of human transferrin coupled to a binding defective mutant of DT (transferrin-CRM107) in brain tumors (GBM) have shown therapeutic response in animal studies and early clinical trials [150-152].

DT binds to cell surface HB-EGF and gets endocysed. Therefore, it should get preferentially taken by cells that over-express HB-EGF. Several types of tumor cells over-express HB-EGF. In 1982, even when HB-EGF was not discovered, Silvio *et al.* tried DT in a clinical trial in solid tumors and got temporary but partial remission [153]. Subsequently, a non-toxic mutated DT, CRM197 has been tested in clinical trials to block oncogenic signaling by HB-EGF [154]. Limited success was achieved in those clinical trials [153]. However, CRM197 is regularly used to block HBEGF in cell biology experiments [155]. Several *in-vitro* and *in-vivo* studies have shown that DT or CRM197 can block oncogenic signaling of HB-EGF, leading to reduction in tumor growth [156-159]. CRM197

TH-1245_08610607

inhibits HB-EGF mediated proliferating of cells over-expressing EGFR [160]. Breast cancer cells, MDA-MB 231, over-express HB-EGF, and treatment with CRM197 causes apoptosis of these cells and inhibits tumor growth in nude mice [161].

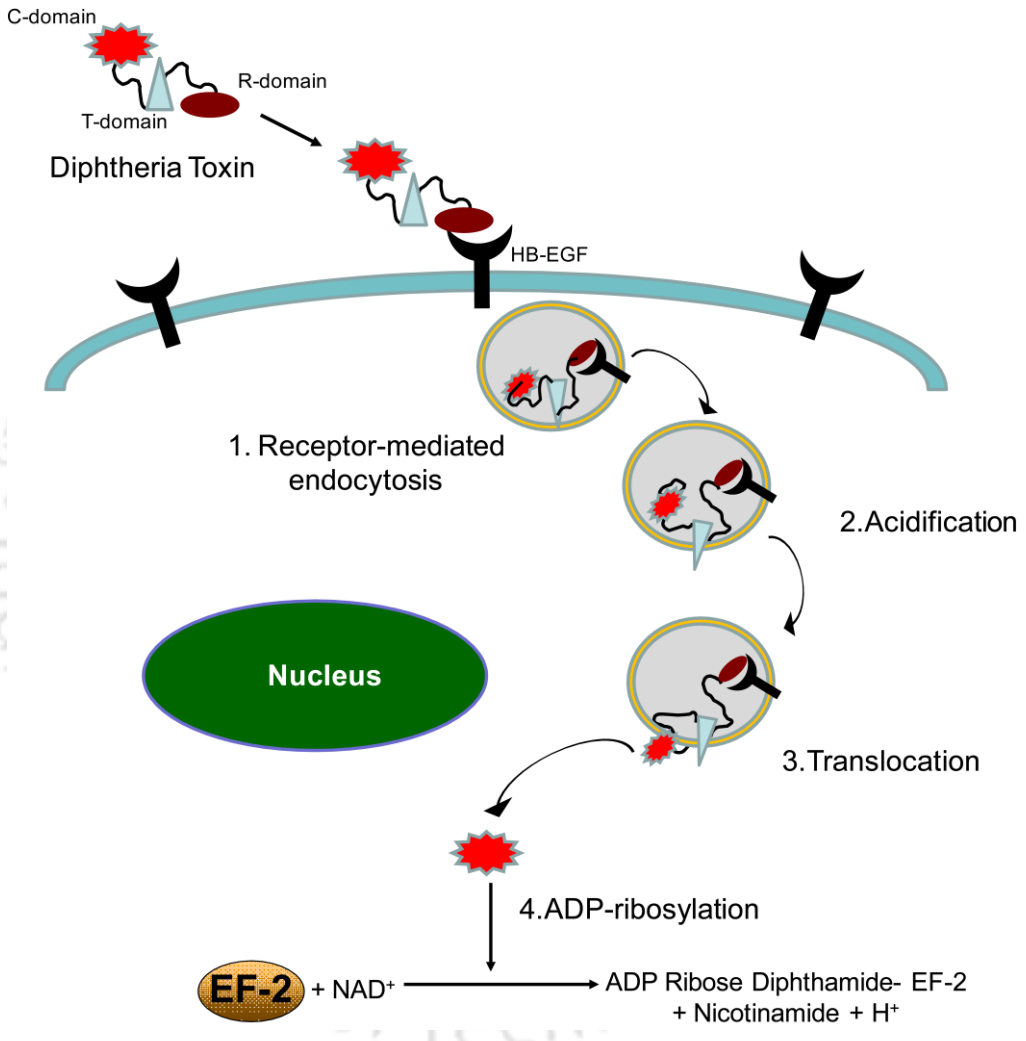

Figure 2.5. Mechanism of action of DT. (1) DT binds to HB-EGF by its R-domain and gets internalized into cell through HB-EGF mediated endocytosis.(2) Following internalization, acidification in endosome leads to structural change in DT and (3) Translocation of C-domain facilitated by T-domain.(4) the catalytic domain catalyzes ADP ribosylation on EF-2. This inhibits protein synthesis and causes cell death.

TH-1245_08610607

As discussed earlier, several chemotherapeutic agents increase expression and shedding of HB-EGF. This counteracts the cytotoxic effects of these drugs. Yagi *et al*. [122] have shown that treatment with Paclitaxel increases HB-EGF in ovarian cancer cells. They have established that mutated non-toxic DT, CRM197, can block/sequester HB-EGF and potentiate the cytotoxicity of Paclitaxel in these cells *in vitro* and *in vivo.* Similar potentiation was observed in combination treatment of gastric cancer cells with Paclitaxel and CRM197 [120]. Treatment with doxorubicin along with RDT showed enhanced antitumor effect in T-cell acute lymphoblastic leukemia (T-ALL) [162].

As DT binds to cell surface HB-EGF, mutated non-toxic DT or its fragments can be used to deliver drugs to cells expressing HB-EGF. Using CRM197 conjugated to horseradish peroxidise (HRP), Gilliard *et al.* [163] have shown that CRM197 can be used for targeted delivery. HB-EGF is expressed in the cerebral blood vessel endothelial and glial cells [164]. It has been shown that CRM197 increases permeability of blood brain barrier (BBB) and crosses it to deliver molecular cargo [165].

Based on these evidences, one can suggest that a non-toxic mutated DT, like CRM107 or its fragment that binds to HB-EGF can be used for therapeutic purposes. We can achieve two goals using such a protein. It can be used to deliver a drug preferentially to a cell that is over-expressing HB-EGF. Further, it will be useful to block or sequester HB-EGF to reduce oncogenic signaling. In this fashion, it may be used to potentiate other chemotherapeutic agents.

TH-1245_08610607

3 Materials & Methods

Details of the common reagents used in this work along with their source are given in appendix.

3.1 Bacterial cell culture:

E. coli strains and clones were stored at -80 °C as glycerol stocks (20% glycerol) and were cultured in LB medium or 2xTY medium containing suitable antibiotics. *E. coli* strains used in this work and the composition of culture media are given in Table A2 and A3 respectively in the appendix.

3.2 Maintenance of mammalian cell lines:

Human cervical adeno-carcinoma cell line HeLa, human glioblastoma cell lines U-87 MG and U-373 MG, human breast cancer cell line MCF-7, human colon adeno-carcinoma cell line HT29, and human embryonic kidney cell line HEK293, were procured from NCCS, Pune, India. They were maintained in DMEM (Sigma-Aldrich) with high glucose, with 10% fetal bovine serum and 1 X antibiotic–antimycotic (Gibco) at 37 °C with 5% CO_2, in a humidified incubator. Medium was replenished at intervals of 3 days. Cells were sub-cultured by trypsinization once they reached 80-90% confluence. After removal of medium, the monolayer of cells was washed with sterile PBS and 0.5 ml to 1 ml of Trypsin (0.25%) / EDTA (0.02%) was added to the flask and kept at 37 ^{0}C. After few minutes, trypsin was aspirated out of the flask and cells were flushed with the medium to make a uniform cell suspension. Around 30% of the cell suspension was transferred to a new flask having fresh growth media and cells were kept at 37 °C with 5% CO_2. Medium and other

TH-1245_08610607

reagents used in mammalian cell culture are given in Table A4 and A5 in appendix.

3.3 Cell growth and proliferation assay:

Viability of the cells in different treatment conditions was measured by an MTT (3-[4, 5-dimethylthiazole-2-yl]-2, 5-diphenyl tetrazolium bromide) based colorimetric assay [25]. Briefly, cells were seeded at a density of 1×10^4 cells per well in a 96-well cell culture plate. After 24 hr of seeding, cells were treated as per the requirement of the experiment and kept for required duration. At the end of the incubation period, MTT (Hi-Media) at a concentration of 5 mg/mL in PBS (pH 7.4) was added to each well (10% v/v), followed by further incubation for 4 hr at 37 °C. The medium was then aspirated and the formazan crystals that formed were dissolved in 100 µl of DMSO. The percentage of metabolically active cells after treatment relative to the untreated controls was then determined on the basis of the production of insoluble purple formazan crystals through cleavage of the tetrazolium ring by mitochondrial enzymes. The results were assessed in a 96-well format ELISA microplate reader (Infinite M200, Tecan, Switzerland) by measuring the optical density (OD) at a wavelength of 550 nm and 670 nm. Cell viability (%) related to control wells containing cell culture medium without treatment was calculated by

$$\text{Cell Viability (\%)} = \frac{(\text{O.D}_{550} - \text{O.D}_{670})_{\text{Treated}}}{(\text{O.D}_{550} - \text{O.D}_{670})_{\text{Control}}} \times 100$$

3.4 Protein estimation:

The total protein content in a sample was estimated by either Bradford assay [104] or by Lowry's method [105]. Protein content was estimated by following

TH-1245_08610607

the 96-well plate assay format. BSA was used as protein standard. BSA was dissolved in same buffer system which was used during sample preparation.

3.5 Protein estimation by Bradford assay:

The protein samples in PBS were estimated by Bradford assay. Bradford reagent was purchased from Sigma-Aldrich. As per the manufacturer's protocol, 200 µl of protein sample was mixed with 200 µl Bradford Reagent and kept at room temperature for 15 min. After incubation, 200 µl of the reaction mixture of each sample was transferred to the 96-well plate and the optical density was measured at 595 nm.

3.6 Protein estimation by Lowry's method:

The protein samples which were prepared using RIPA buffer, was estimated according to the Lowry's method. 100 µl of diluted crude protein sample was mixed with 500 µl of freshly prepared complex forming reagent (2% Na_2CO_3 in 0.1 N NaOH : 1.0% $CuSO_4.5H_2O$: 2% potassium sodium tartrate ≡ 100:1:1). The reaction mixture was vortexed and incubated at room temperature for 10 min. 50 µl of freshly prepared Folin's reagent and diluted with distilled water (1:1) was added to the reaction mixture and vortexed for 5 s. This reaction mixture was incubated in the dark at room temperature for 30 min. After 30 min of incubation, 200 µl of the reaction mixture from each sample was transferred to 96-well plate and the optical density was measured at 660 nm.

3.7 Quantification of DNA and RNA:

Quantities of DNA and RNA in samples were measured by spectrophotometry. Samples were diluted in water and optical densities were measured at 260 nm and at 280 nm. 1 O.D at 260 nm was considered to represent 40 µg of single stranded RNA and 50 µg of double stranded DNA.

TH-1245_08610607

Concentrations of DNA and RNA samples were calculated from the optical densities by using suitable dilution factors.

3.8 Agarose gel electrophoresis:

DNA samples were resolved by agarose gel electrophoresis using agarose gel (0.8-1.5%, containing 0.5 μg/ml of ethidium bromide) in 1 X TAE at 80 V until the desired resolution was achieved. The DNA fragments were visualized on a UV-Trans-Illuminator and imaged using gel documentation system (Gel logic 1500, Kodak).

3.9 Elution of DNA sample from agarose gel:

PCR amplified products, digested plasmids and inserts were eluted out of agarose gel by using QIAquick Gel Extraction Kit, as per manufacturer's protocol. For gel elution of DNA, required fragments were excised from the gel and stored at –20 °C for further use. Three volumes of Buffer QG was added to one volume of gel (i.e. 300 μl for 100 mg of gel slice) and heated at 50 °C to melt and dissolve the gel. One gel volume of iso-propanol was added to the sample and mixed. A QIAquick spin column was placed in a 2 ml collection tube. 750 μl of sample was applied to the column to bind DNA, followed by centrifugation at maximum speed for 1 min. The flow through was discarded and 500 μl of QG buffer was added to the column. After centrifugation for 1 min, 0.75 μl of PE buffer was added to wash the column and centrifuged. Another hard spin was given for 1 min to remove residual traces of wash buffer. 50 μl of nuclease-free water was added to the column to elute out the DNA. After incubation for 3-4 min at room temperature, DNA was eluted out by centrifugation at maximum speed for 1 min. Eluted DNA was stored at -20 °C for further use.

TH-1245_08610607

3.10 Plasmid DNA Isolation (Mini-Prep Method):

Plasmid DNA was isolated from 3 ml of over night cultures by alkaline lysis method [166]. Reagents used for plasmid isolation are given in Table A5 in appendix. A single *E.coli* colony carrying a recombinant plasmid was grown for 14-18 hr in LB medium containing specific antibiotic, at 37 °C with shaking at 180 rpm. The culture was harvested and the cells were resuspended in 100 µl of solution I. The cells were lysed with 200 µl of freshly prepared solution II. Thorough mixing of the contents was done by gently inverting the tube. Bacterial genomic DNA and bacterial cell debris were differentially precipitated by adding 150 µl of ice cold solution III and incubating on ice for 5 min followed by centrifugation at 12000 g for 10 min at 4 °C. The supernatant was transferred to a fresh tube and equal volume of phenol/chloroform (1:1 v/v; here chloroform means chloroform/isoamyl alcohol (24:1 v/v) was added. The resulting mixture was mixed gently by inversion and the phases were separated by centrifugation at 12,000 g for 10 min at 4 °C. The aqueous phase was aspirated out in a fresh tube and 2 volumes of ethanol were added to precipitate the plasmid DNA. After incubation at room temperature for 10 min, plasmid DNA was precipitated by centrifugation at 12,000 g for 10 min at 4 °C. The DNA pellet was washed with 70% ethanol, air-dried and resuspended in the required amount of nuclease-free water.

3.11 Isolation of RNA from mammalian cells:

Total RNA was isolated from mammalian cell line for preparation of cDNA. RNase free materials were used for isolation of RNA and for all downstream processing. All plasticwares including micropipette tips and centrifuge tubes were treated by 0.1% DEPC for 2 hr at 37 °C, followed by removal of DEPC by autoclaving. Total RNA was extracted by TRI reagent (Sigma-Aldrich). 1 ml of TRI reagent was used to isolate RNA from 5-7 × 10^6 cells in 25 cm^2 culture flasks. RNA was isolated according to the manufacturer's protocol. After

TH-1245_08610607

addition of the reagent on monolayer of cell, the cell lysate was passed several times through a syringe to form a homogenous lysate. To ensure complete dissociation of nucleoprotein complexes, samples were allowed to stand for 5 min at room temperature. Then, 0.2 ml of chloroform per ml of TRI Reagent was added. After 30-60 s of vigorous shaking, samples were allowed to stand for 10 min at room temperature. Resulting mixture was centrifuged at 12,000 *g* for 15 min at 4 °C. The aqueous phase having RNA was transferred to a fresh tube and 0.5 ml of isopropanol per ml of TRI Reagent was added to precipitate the RNA. After incubation at room temperature for 10 min with occasional mixing by inversion, the sample was centrifuged at 12,000 g for 10 min at 4 °C. The supernatant was removed and the RNA pellet was washed with 1 ml of 75% chilled ethanol and re-centrifuged at 12,000 g for 10 min at 4 °C. The RNA pellet in ethanol was either stored at –70 °C for long-term storage or was air-dried and dissolved in suitable amount of sterile water and stored at –20 °C for immediate use.

3.12 Removal of Genomic DNA contamination from RNA:

To remove the genomic DNA contamination, each RNA sample was treated with RNase-free DNase (Promega) according to the manufacturer's protocol with some modification. The composition of reaction mix was as follows:

RNA	5.00 µg
RNase-Free DNase 10 X Reaction Buffer	5.00 µl
RNase-Free DNase (1,000 U/ml)	5.00 µl
Nuclease-free water to final volume	50.0 µl

The reaction mixture was incubated at 37 °C for 45 min. Subsequently, RNA was re-extracted from the mixture by TRI reagent following the same protocol

TH-1245_08610607

described in previous section. DNA free RNA samples were dissolved in nuclease-free water and estimated by spectrophotometer for cDNA synthesis.

3.13 Reverse Transcription for cDNA synthesis:

Around 1 µg of total RNA was used for reverse transcription using H Minus reverse transcriptase (RT) (Fermentas) and random hexamer (Fermentas). For a 20 µl of reaction mix, following protocol was followed:

A sample mix was prepared:

RNA	1.00 µg
Random Hexamer (Fermentas) (100 pmol/ µl)	1.00 µl
Nuclease-free water to final volume	10.00 µl

The sample mix was incubated at 65 °C for 5 min to break RNA secondary structures and immediately chilled on ice. 8 µl of reaction mix was added to the heat-treated sample mix. A reaction mix was prepared as:

5 X Reaction Buffer RT (Fermentas)	4.00 µl
dNTP mix (10 mM each) (1 mM final concentration)	2.00 µl
H Minus reverse transcriptase (Fermentas) (200 units/µl)	1.00 µl
Nuclease-free water	3.00 µl

Reverse transcription was carried out at 37 °C for 60 min. The reaction was stopped by heating at 70 °C for 10 min followed by chilling on ice. 1 µl of RT products were used as template for downstream PCR amplification steps.

TH-1245_08610607

3.14 Polymerase Chain Reaction (PCR):

Taq DNA polymerase (Genei, Bangalore) was used for all PCR reactions. 25-50 ng of DNA sample was used in 20 µl reaction mixture. The composition of reaction mix was as follows:

10 X Taq Assay buffer A (10 mM Tris-HCl (pH 9), 1.5 mM MgCl2, 50 mM KCl, 0.01% gelatin)	2.00 µl
dNTP (10 mM each)	0.50 µl
Taq DNA polymerase (3U/µl)	0.30 µl
5'primer (20 pmole/µl)	1.00 µl
3'primer (20 pmole/µl)	1.00 µl
DNA	25.00 ng
Nuclease-free water to final volume	20.00 µl

PCR amplification was performed by thermal cycling (Palm Cycler, Genetix Biotech. Asia Pvt. Ltd.). A typical thermal cycling involved initial denaturation for 5 min at 94 °C, followed by 40 cycles as follows: 1 min at 94 °C, 1 min at 60 °C, 1 min at 72 °C and the final extension was performed for 10 min at 72 °C. Sequence of primers and reaction conditions used are given in appendix (Table A7).

3.15 Preparation of Competent Cells:

Competent *E. coli* cells were prepared by $CaCl_2$ method. A single colony was inoculated in 5 ml LB media and incubated overnight at 37 °C with shaking. 500 µl of the primary culture was inoculated in 25 ml of LB media and grown till its OD_{600} reached 0.4-0.5. The culture was kept on ice for 10 min and centrifuged at 3000 g for 10 min at 4 °C. The pellet was resuspended uniformly in 12.5 ml of ice-cold sterile 50 mM $CaCl_2$ and kept on ice for 45 min. The cells

TH-1245_08610607

were harvested at 1000 g for 10 min at 4 °C and the pellet was re-suspended in 2 ml chilled 50 mM $CaCl_2$. Sterile glycerol (20% of final volume) was added to the cell suspension and aliquots of 200 µl each were made in sterile vials and stored at -70 °C for further use.

3.16 Transformation in Bacterial Cells:

Recombinant plasmids were transformed in chemically competent *E.coli* cells by heat shock method [106]. Plasmid/ligation mixtures (usually 10-20 µl) were mixed with 200 µl of competent cells and placed on ice for 45 min without any disturbances. The cells were subjected to heat shock at 42 °C in a water bath for 90 s and chilled on ice immediately afterwards. 800 µl of pre-warmed LB media was added and the cells were incubated for 1 hr at 37 °C with shaking. Cells were harvested by centrifugation at 3000 g for 10 min at 4 °C and re-suspended in 100 µl of LB media. Re-suspended cells were plated on TYA plates containing the appropriate antibiotic followed by incubation at 37 °C for 12-16 hr. Subsequently, the colonies were picked, gridded on a TYA plate containing appropriate antibiotic and screened by colony PCR and restriction digestions.

3.17 Digestion of DNA by Restriction Enzyme:

Plasmids or PCR amplified DNA fragments were subjected to digestion by restriction endonuclease. An aliquot of plasmid DNA (~5 µg) was digested overnight with the required amount of restriction endonuclease according to the conditions specified by the manufacturer. The reaction was terminated by heating at 68 °C for 10 min. An aliquot was loaded on an agarose gel for analysis and resolved by electrophoresis. Whenever needed, RNase (0.25 µl/20 µl reaction) was added to the reaction mix to remove RNA.

TH-1245_08610607

The digestion mix:

10 X Buffer 3	2.00 µl
BamH I (NEB, 20 U/µl)	0.50 µl
Xho I (NEB, 20 U/µl)	0.50 µl
BSA (100 X)	0.20 µl
DNA	5 µg
Nuclease-free water to final volume	20.00 µl

3.18 Ligation reaction:

The restriction digested vector and insert were resolved by agarose gel electrophoresis and the digested DNA fragments were eluted out using QIAquick Gel Extraction Kit. The gel-eluted products were ligated using T4 DNA ligase. For ligation reaction, linearized vector and insert fragment were mixed in 1:3 molar ratios respectively and incubated with 1 X ligation buffer and 2 units of T4 DNA ligase enzyme. The ligation reaction was carried out at 4 °C for 12-16 hr and terminated by incubating at 65 °C for 10 min.

The ligation mix:

Insert DNA	25.0 ng
pET-22b vector (Novagen)	50.0 ng
2 X rapid ligation buffer	5.00 µl
T4 DNA ligase	1.00 µl
Nuclease-free water to final volume	10.0 µl

The reaction mix was incubated at 4 °C in ice-water bath overnight and the ligated mix was transformed in *E. coli* DH5α cells by standard chemical transformation method. Transformed cells were plated over TYA/Amp plate.

TH-1245_08610607

After overnight growth at 37 °C, colonies were picked and checked by colony PCR. Plasmids were isolated from positive clones and digested with *BamH I* & *Xho I* and checked on agarose gel. Clones with proper insert were grown in LB media and stored at –70 °C with 20% glycerol.

3.19 Sequencing of RDT cloned in pET-22b vector:

Insert in various clones were sequenced. Sequencing was done by dideoxy method using universal T7 Forward and Reverse primers (Appendix Table A7). Sequencing was performed by Xcleris Genomics (Ahmedabad).

3.20 Expression of His- tagged full-length DT in *E.coli* BL21 (DE3):

The recombinant plasmid of the clone of DT in DH5α procured from Addgene (pET-22b DT 51E/148K, Plasmid 11081) was isolated using Alkaline Lysis and checked by restriction digestion and confirmed by DNA sequencing by dideoxy method. The recombinant construct of DT was transformed in chemically competent *E.Coli* BL21 (DE3) using standard heat shock method. Transformed cells were plated on TYA/Amp plate. After 16 hr of incubation at 37 °C, bacterial colonies were picked and gridded in another TYA/Amp plate. A Single colony of the BL21 cells having pET-22b DT construct was inoculated in 5 ml 2xTY medium containing ampicillin (100 μg/ml). This was incubated with shaking at 37 °C for overnight. 500 μl of this overnight culture was sub-cultured into 100 ml 2xTY medium containing same concentration of ampicillin and incubated with shaking (180 rpm) at 28 °C till OD_{600} reached ~ 0.6. The recombinant protein expression was induced by addition of IPTG (1 mM) for 8 hr at 28 °C with shaking (180 rpm). Cells from culture media were harvested by centrifugation and re-suspended uniformly in PBS (pH 7.4) and periplasmic extract were extracted as follows: the pelleted cells were re-suspended in a sensitization buffer (20% sucrose / 1 mM EDTA / 30 mM Tris-HCl, pH 8.0) and incubated at room temperature for 10 min with gently

TH-1245_08610607

stirring. Subsequently, the mixture was centrifuged and the cell pellets were re-suspended in 10 ml of ice-cold 5 mM $MgSO_4$ and incubated on ice for 10 min with intermittent slow pipetting. The mixture was centrifugation for 10 min at 11,000 g, 4 °C. The supernatant periplasmic extract was collected and stored at 4 °C or -20 °C for further processing.

3.21 Cloning of N-terminal truncated DT (RDT) into bacterial expression vector:

The plasmid DNA containing mutated Diphtheria toxin cloned in pET-22b vector was procured from Addgene (pET-22b DT 51E/148K; Plasmid 11081) and was used as the template for amplifying the receptor-binding domain of DT (corresponding to 382^{nd} – 535^{th} amino acids) using specific primers (Appendix Table. A7). The primer set which was used for amplification contains restriction enzyme sites for *BamH I* and *Xho I* at 5′ and 3′ end respectively. The PCR product as well as the plasmid pET-22b (Novagen) was double digested separately with *BamH I* and *Xho I* (NEB) and the double digested PCR product was ligated to doubly digested pET-22b RDT. An aliquot of this ligated product, pET-22b RDT, was subsequently used to transform in chemically competent *E. coli* DH5*α* using the standard heat shock method mentioned earlier. Transformed cells were plated on TYA/Amp plate. After 16 hr of incubation at 37 °C, bacterial colonies were picked and gridded in another TYA/Amp plate and recombinant clones were checked by colony PCR. Recombinant clones were selected and plasmid DNA isolated using Alkaline Lysis and checked by restriction digestion. The selected clones were stored as glycerol stocks at -80 °C. One selected clone was confirmed by DNA sequencing by dideoxy method. The recombinant pET-22b RDT from this clone was further transformed to *E.coli* BL21 (DE3) for protein expression.

TH-1245_08610607

3.22 Expression of His- tagged RDT in *E.coli* BL21 (DE3):

A fresh single colony of *E.coli* BL21 with pET-22b RDT construct was inoculated in 5 ml 2xTY medium containing ampicillin (100 mg/L), and 1% glucose. This was incubated with shaking at 37 °C for overnight. This was further sub-cultured (1:200 dilution) into 100 ml 2xTY containing the same concentration of antibiotics and glucose. This was incubated with shaking (180 rpm) at 37 °C till its OD_{600} reached ~ 0.6-0.8. Subsequently, cells were pelleted down by centrifugation (5000 rpm, 15 min, and 4 °C) and re-suspended in fresh media with antibiotics to remove glucose. Expression of the recombinant protein was induced by Isopropyl β-D-thiogalactopyranoside (IPTG) (0.5 mM) for 8 hr at 28 °C with shaking (180 rpm). Cells were harvested by centrifugation and re-suspended uniformly in PBS (pH 7.4), and whole cell lysate in PBS was prepared by sonication for 6 cycles, each of 10 s, at 25% amplitude using Ultrasonic processor (Hielscher). Homogenate formed after sonication was clarified by centrifugation for 10 min at 11,000 g, 4 °C. The supernatant was collected and stored at 4 °C or -20 °C for further processing.

3.23 Purification of His- tagged DT & RDT:

The pET-22b vector carries C-terminal His-Tag downstream to the MCS. The recombinant Histidine-tagged proteins (DT & RDT) were purified by immobilized metal ion (Ni^{++} chelate) affinity chromatography on His Trap FF affinity column (GE Healthcare) as per the manufacturer's protocol. Briefly, the protein sample for purification was prepared by diluting the whole cell lysate (1:10 dilution) with binding (equilibration) buffer, pH 7.4 containing imidazole (40 mM). The diluted protein sample with imidazole, pH 7.4, was allowed to pass through the column at a flow rate of 2 ml/min. Subsequently, the column was thoroughly washed with wash buffer (binding buffer) having imidazole (40 mM). Elution was done using Elution buffer containing 300 mM imidazole and the residual imidazole was removed by dialysis against PBS or

TH-1245_08610607

water for 8 hours at 4 °C with slow stirring. The detailed composition of the buffers is given in Table A5 of the appendix. The Bradford assay was used to determine the concentration of purified proteins.

3.24 Protein Extraction from mammalian cells:

Isolation of total protein from mammalian cell lines was done using RIPA buffer (Appendix Table. A5). Media was discarded from culture plate and cells were washed with ice cold PBS to remove the residual media. Keeping the culture plate on ice, required amount of RIPA buffer containing the protease inhibitor, PMSF (1 mM), phosphatase inhibitor sodium fluoride (50 mM) and sodium orthovanadate (1 mM) was added to the cells. After 5 min of incubation on ice, cells were scrapped and sonicated for 10 s. Cell lysate was clarified by centrifugation for 10 min at 10,000 rpm, 4 °C. The supernatant was collected and mixed with required amount of SDS-PAGE sample loading buffer, boiled for 3 min at 100 °C and stored at -80 °C. Concentrations of proteins were estimated by Lowry's method prior to addition of SDS-PAGE sample loading buffer.

3.25 Sodium dodecyl sulfate polyacrylamide gel electrophoresis (SDS-PAGE) of protein:

SDS-PAGE was performed to analyze the expression of recombinant proteins for western blot. Required amount of purified protein or cell lysates were mixed with 4 X SDS-PAGE gel loading buffer with reducing agent (2-mercaptoethanol) and heated in boiling water bath for 3 min. The denatured protein samples along with standard SDS-PAGE protein markers were subjected to SDS-PAGE following the method of Laemmli [167]. Gels may be run at either constant current or constant voltage. The electrophoresis was carried out using 5% stacking and 15% separating gels of thickness 0.75 mm at constant voltage of 120 V for both stacking and separating gel, respectively, in

TH-1245_08610607

a MiniVE vertical electrophoresis system (G.E Healthcare). The progress was checked by monitoring the position of the tracking dye. The run is complete when the tracking dye reached the bottom of the gel. After the completion of electrophoresis, the gels were stained with the coomassie brilliant blue or silver staining method (Appendix Table. A5).

3.26 Western Blot:

Western blot was performed to analyze the recombinant protein expression in bacterial system as well as to study the expression level of cell signaling molecules. Protein samples were resolved by SDS-PAGE using 15% gel in the mini vertical electrophoresis module (Amersham Biosciences) at 120 V, and the gel was placed in the electro-blotting module in Towbin buffer and run at 25 V, 300 mA for 4 hr in 4 ^{o}C to transfer the proteins to PVDF membrane using standard semi-dry electro-blotting technique. Subsequently, the membrane was carefully taken out of the electro-blotting module and transfer of proteins on membrane was confirmed by Ponceau S staining. Membranes were washed with phosphate-buffered saline (PBS; pH 7.4) with 0.1% Tween 20 on a shaker for 10 min to remove Ponceau S stain. The buffer was discarded and washed again with PBS with 20% methanol for 5 min on a rocking shaker and again washed with PBS on a shaker. After discarding the wash buffer, the membrane was blocked to prevent non-specific adsorption with blocking buffer MPBST (2% skimmed milk in PBS with 0.1% Tween 20) for 2 hr at room temperature with slow shaking. After blocking, the membrane was washed three times with wash buffer (0.1% PBST), each washing for 5 min accompanied by shaking. The wash buffer was discarded and primary antibody appropriately diluted in blocking buffer (2% skimmed milk in PBS with 0.1% Tween 20) was added to the membrane and incubated for required duration with slow shaking. Again, the membrane was washed three times with wash buffer (0.1% PBST), each washing for 5 min accompanied by shaking. This was followed by

TH-1245_08610607

incubation with secondary antibody appropriately diluted in blocking buffer for 1 hr at room temperature with slow shaking. Thereafter, the membrane was washed thoroughly three times with wash buffer (0.1% PBST) and then 2-3 times with PBS while shaking. Finally, the blot was developed using chemi-luminescence (Super Signal West Dura, Thermo Scientific) and imaged using gel documentation system (Gel logic 1500, Kodak). Details of reagents used are given in Table A5 and A6 in appendix.

3.27 Solid-Phase ELISA:

The binding of recombinant proteins (DT or RDT) as well as Complex of RDT with Curcumin (Curcumin-RDT complex) to HB-EGF was checked by solid phase ELISA in 96-well plate. An ELISA plate was coated with 100 ng per well of recombinant human HB-EGF (R & D Systems) and incubated overnight at room temperature. Subsequently, the plate was washed once with PBS (pH 7.4). All wells were blocked to prevent nonspecific binding by adding 300 µl/well with blocking solution (1% BSA in PBS) and incubated for 2 hr at RT. Thereafter, the plate was washed thrice with PBS. Recombinant protein or protein complexes in blocking solution were added to HB-EGF coated wells and incubated for 2 hr at RT. Subsequently, the plate was washed three times with PBS. Anti-His antibody (Calbiochem; 1:1000 dilution) in 1% BSA in PBS, was added and incubated for 2 hr at RT. The plate was washed three times with PBS. Goat anti-mouse-HRP conjugated antibody (Sigma-Aldrich; 1:1000 dilution) in 1% BSA in PBS was added to each well to detect bound antibody. After 1 hr of incubation at room temperature, the plate was washed 5 times with PBS. The assay was developed using OPD (O-phenylenediamine dihydrochloride). OPD (4 mg) was dissolved in 10 ml of OPD substrate buffer (0.66 M Na_2HPO_4 / 0.347 M Citric acid, pH 5.0). 10 µl of H_2O_2 (Hydrogen peroxide) was added and mixed well before adding to each well of the ELISA Plate (100 µl/well). After development of color, 50 µl of stop solution (8N

TH-1245_08610607

Sulphuric acid) was added to each well. The absorbance of the colorimetric reaction was measured at 492 nm in Teccan Multimode ELISA plate reader (Infinite M200, Tecan, Switzerland).

3.28 ELISA to detect Shedding of soluble HB-EGF by Chemotherapeutic agents:

The ecto-domain shedding of soluble HB-EGF by different chemotherapeutic agents was detected in U-87 MG and MCF-7 cells, using solid phase ELISA. Briefly, cells were seeded in serum media for 24 hr and treated with different chemotherapeutic agents, Paclitaxel (1 μM), Etoposide (100 μM), Irinotecan (100 μM), Doxorubicin (0.2 μM), and Cisplatin (50 μM) respectively for 48 hr in serum free media. Subsequently, conditioned media were collected and clarified by centrifugation. The media was coated (100 μl) on a 96-well plate for overnight at 4 ^{o}C. Following incubation, the plate was washed once with PBS and blocked with blocking buffer for 2 hr at room temperature. After washing three times with PBS, the amount of HB-EGF was detected by using mouse anti-HB-EGF antibody (1:1000 dilution, 2 hr, and room temperature) and subsequent development of the assay was done using the general protocol for ELISA as described earlier.

3.29 Chemotherapeutic Treatments and Measurement of IC_{50}:

The cytotoxic effect of several anti-cancer drugs namely, Paclitaxel, Etoposide, Irinotecan, Doxorubicin and Cisplatin alone and in combination with RDT was analyzed in two cell lines, U-87 MG and MCF-7. Both the cell lines were treated with various doses of these drugs in combination with RDT in serum free condition for 48 hr and the cell viability was measured by MTT assay as described earlier.

The IC_{50} of Etoposide or Irinotecan in combination with RDT was measured in U-87 MG and MCF-7 cells. Briefly, cells were cultured in 96-well culture plate

TH-1245_08610607

for 24 hr and treated with different doses ranging from (0 μM to 100 μM) of Etoposide or Irinotecan in combination with various doses of RDT ranging from (0 μM to 0.20 μM) and the cell viability were measured by MTT assay. Data of these MTT experiments were used to calculate % inhibition in cell viability for each treatment. The % inhibition data were fitted to a power equation, $y = mx^n + c$, where y = % inhibition and x = dose of the drug, to calculate the IC_{50} values in each case of these drugs in combination with RDT.

Calculation of IC_{50} of drugs for each treatment using data fitted to power equation:

$$y = mx^n + C$$

(Power equation; where, y = % inhibition in cell viability and, x= Dose of drug.)

IC_{50} value was calculated as;

$$IC_{50} = \sqrt[n]{\frac{(50 - C)}{m}}$$

3.30 Cell-Based ELISA:

Binding of recombinant RDT to cell surface HB-EGF was detected using cell-based ELISA as described by Brown et al. [168]. The experiment was performed on formalin-fixed U-87 MG glioma cell line. The general protocol was same as solid phase ELISA with the following modifications. A 96-well sterile plate was seeded at 1×10^4 cells per well in DMEM with 10% FBS. After overnight incubation at 37 °C in 5% CO_2, the media was removed and the cells were fixed in a 10% formalin solution for 45 min at 4 °C. The monolayer was washed three times with phosphate-buffered saline containing 0.05% Tween 20 (PBST). The monolayer was incubated with blocking solution (1% BSA in PBST) for 1 hr at 4 °C to prevent nonspecific binding. The plate was washed once with PBST and then incubated with RDT in blocking solution for 2 hr at 4

TH-1245_08610607

°C. The plate was washed once with PBST and then incubated for 2 hr at 4 °C with mouse anti-His antibody in blocking solution (1:1000 dilution) to respective wells. Following three additional washes with PBST, bound antibody was detected using anti-mouse antibody-HRP (1:1000 dilution, 4 °C, and 1 hr). The assay was developed using OPD as stated earlier and absorbance was measured at 492 nm.

A similar cell-based experiment was performed to check the binding of recombinant DT-FITC to cell surface HB-EGF. Briefly, DT was conjugated with a fluorescent probe, FITC, using FITC Labelling Kit (Bangalore Genei) to form DT-FITC conjugate. The conjugation and purification of DT-FITC was done and as per the manufacturer's protocol. BSA-FITC conjugate was similarly prepared to act as a negative control. HeLa cells were seeded in a 96-well culture plate. After 24 hr, cells were treated with DT-FITC (1:25 dilution) and BSA-FITC (1:10 dilution) in DMEM containing 0.05% BSA respectively for 2 hr at 37 °C. Subsequently, cells were fixed with 3.7% formaldehyde in PBS for 10 min. After fixation, cells were thoroughly washed with PBS and the bound conjugate was measured by a fluorescence spectrophotometer for the fluorescence signal of FITC at 525 nm (Excitation wavelength used = 495 nm).

3.31 Surface Plasmon Resonance (SPR):

We have utilized Surface Plasmon Resonance to study the kinetics of interaction of DT and RDT with recombinant HB-EGF. The experiment was performed using Biacore X100 instrument (Biacore, GE Healthcare). We immobilized recombinant HB-EGF on CM5 chip. The immobilization involves activation of carboxymethyl groups on a dextran-coated chip by reaction with N-hydroxysuccinimide, followed by covalent bonding of the ligands to the chip surface via amide linkages and blockage of excess activated carboxyls with ethanolamine. Reactions were performed using manufacturer's protocol.

TH-1245_08610607

Reference surface was prepared in the same manner, except that all carboxyls are blocked and no ligand was added.

The sensor chip was equilibrated with 10 mM phosphate buffer (pH 7.4) with 0.05% Tween 20. The surface was activated by passing 1:1 mix of 0.4 M EDC & 0.1 M NHS, at a flow rate of 10 µl/min for 7 min. Recombinant HB-EGF in PBS was added to 10 mM sodium acetate coupling buffer (final conc. of protein = 25 µg/ml, pH = 6.0). The protein was passed over the chip at a flow rate of 10 µl/min with RU target set to 200 RU. Approximately 400 RU of HB-EGF immobilization was achieved by this experiment. Excess activated groups were blocked using a 7 min injection of 1 M ethanolamine, pH 8.5, at a flow rate of 10 µl/min.

Binding to immobilized HB-EGF was detected using Single Cycle protocol. DT or RDT was dissolved in running buffer (10 mM phosphate buffer with 0.05% Tween 20, pH 7.4) at various concentrations. These analytes were injected sequentially at a rate of 30 µl/min at 25 °C. An association phase of 120 s, while dissociation phase of 600 s was used for each sample. Resulting sensograms were fitted to 1:1 ligand binding model using BIAevaluation software (version 2.0) to calculate association (K_a) and dissociation (K_d) rate constants.

3.32 Molecular Docking:

Automated molecular docking was performed to detect possible binding of Curcumin to RDT. Web-based docking server SwissDock (http://swissdock.vital-it.ch/) was used for this purpose [169]. Structure of RDT was derived from the crystal structure of wild-type DT (PDB ID: 1F0L, resolution: 1.55 Å, R-value: 0.188) after trimming C and T-domains. The resulting structure corresponds to Ser381 to Ser535 of 1F0L. Four structures of Curcumin collected from ZINC database [170] was used for docking (ZINC ID: 00899824, 17255287, 20230445 and 31261437). Docking runs were performed as blind, covering the entire protein surface, with default parameters values in

TH-1245_08610607

'Accurate' mode with no flexibility for the protein. Clusters were ranked based on Fullfitness score and top ten docked clusters of each docking experiments were considered for further analysis. Clusters where Curcumin was docked on the receptor binding face of RDT were rejected. Docking data was visualized and analyzed using Chimera [171].

3.33 Formation of Curcumin-Protein complexes:

Curcumin (MF=$C_{12}H_{20}O_6$; MW=368.37g/mol) was purchased from Hi-Media (RM-1449-5G). Bovine Serum Albumin (BSA; MW = 66,000 Dalton) of analytical grade was purchased from SRL. The Curcumin stock solution (1 mg/ml) was prepared in ethanol. Whenever required, the stock solution was further diluted in ethanol. Required amount of Curcumin in ethanol was added to required amount of protein (RDT or BSA) solution in PBS (pH 7.4) to achieve desired molar ratios as mentioned in results section. Subsequently, these solutions were incubated for 2 hr at 4 °C to allow complexation. After incubation, samples were used immediately for different assays. In all experiments, the control used was Curcumin diluted in PBS, having required concentration and solvent ratio, which was incubated accordingly.

3.34 UV-Visible Absorption Spectroscopy:

UV-visible absorption spectra of Curcumin alone or in complex with proteins were measured using a UV-Visible spectrophotometer (Perkin Elmer). The spectra were recorded from 350 nm to 900 nm using a 10 mm path length quartz cell.

3.35 Fluorescence Spectroscopy of Curcumin-RDT:

The binding of Curcumin to RDT or BSA was quantified by fluorescence spectrophotometry. The fluorescence spectra were recorded on a single beam Fluorescence spectrometer (Perkin Elmer, LS55), using a 10 mm path length

TH-1245_08610607

quartz cell. The emission spectra were recorded from 450 nm to 700 nm with an excitation wavelength of 430 nm. The excitation and emission slit widths used were 2.5 nm and 15 nm respectively.

3.36 Time-Resolved Fluorescence Spectroscopy:

Time-resolved fluorescence decay of Curcumin, both in absence and presence of RDT were recorded using a Life Spec II spectrofluorimeter (Edinburgh Instruments). The sample was excited by PicoQuant 405 nm LED source. The path length of quartz cell used in the experiment was 10 mm and the decay was measured in a time scale of ns/channel using emission wavelength fixed at 510 nm and slit width at 22 nm. A total of 5000 fluorescent counts were measured for a fixed time period of 20 ns. The decay curves were analyzed using FAST, version 3.4.1 (Edinburgh Instruments). Exponential component analysis (with tail fitting) was used to calculate fluorescence life time. Each data was fitted sequentially to 1, 2, 3 & 4 component models and fitting with the best χ^2 value was considered. Average life time was calculated as

$$\langle \tau \rangle = \frac{\sum_i \beta_i \tau_i^2}{\sum_i \beta_i \tau_i},$$

here, β_i = i th pre-exponential factor.
τ_i = i th characteristic factor.

3.37 Immuno-Fluorescence Microscopy:

U-87 MG glioma cells (5×10^3 cells/well) were seeded in a sterile, black 96-well plate in DMEM with 10% FBS and incubated at 37 °C in 5% CO_2. After the 48 hr incubation, the culture media was removed and cells were fixed by adding 100 µl per well of a 3.7% formaldehyde solution made in PBS that has been pre-warmed to 37 °C. The cells were incubated in 3.7 % formaldehyde solution at 37 °C for 30 min. Fixed cells were washed once by adding 100 µl per well of PBS and blocked by incubating with 1% bovine serum albumin (BSA) in PBS at 37 °C for 45 min. Subsequently, RDT diluted in blocking solution at a

TH-1245_08610607

concentration of 500 ng/well was added to the cells and incubated at 37 °C for 2 hr. The cells were washed thrice with PBS and 100 µl of diluted mouse anti-His antibody (Calbiochem, 1:1000 dilution) was added. After 2 hr of incubation at 37 °C, cells were washed by PBS. Subsequently, 100 µl of anti-mouse-FITC (BD Biosciences, 1:1000 dilution) was added and incubated for 2 hr at 37 °C. All dilutions of antibody were made in blocking solution. After 2 hr of incubation with the FITC labeled antibody, cells were washed 4-5 times with PBS. These cells were counter stained with DAPI (Sigma-Aldrich) by incubating with 400 nM DAPI in PBS for 5 min in dark at room temperature. Double stained cells were washed 3 times by PBS and imaged using an inverted epi-fluorescence microscope (Nikon, Eclipse TiU). A filter for green fluorescence (B-2E/C) was used for FITC and DAPI was detected using UV-2E/C filter. Similar protocol was used to detect cell surface HB-EGF, by using mouse anti-HB-EGF antibody (R & D Systems; 1:1000 dilution) in place of anti-His antibody.

3.38 Fluorescence Imaging of Curcumin in cell:

U-87 MG cells were seeded in a sterile, 6-well plate (5×10^4 cells/well) and incubated at 37 °C in 5% CO_2 for 24 hr. Subsequently, cells were incubated with Curcumin (2 µM), Curcumin-protein complexes (molar ration 10:1) in media with serum for 4 hr at 37 °C. Subsequently, cells were fixed by 3.7% formaldehyde in PBS at 37 °C for 30 min. After the incubation, the formaldehyde solution was removed. The fixed cells were washed with PBS. Cells were stained with DAPI to counter-stain the nuclei of fixed cells. After washing witn PBS, cells were imaged using inverted epi-fluorescence microscope (Eclipse TiU, Nikon). Curcumin was detected using filter for green fluorescence (B-2E/C, Nikon) and DAPI using (UV-2E/C (Nikon).

TH-1245_08610607

3.39 HPLC to measure Cellular uptake of Curcumin:

Cellular uptake of Curcumin was measured using HPLC as per the protocol of Kunwar et al [172] as described below. U-87 MG cells were seeded in 6 well plate (1×10^5 cells/well). After 24 hr, cells were treated with Curcumin (1 μM) or Curcumin-protein complexes (molar ratio 10:1) for 2 hr at 37 °C. Subsequently, cells were washed thrice with PBS and trpsinized. Cells were harvested by centrifugation (2000 rpm, 5 min) and the cell pellet was washed with cold PBS. The pellet was air dried and suspended in to 0.1 ml of methanol and sonicated for 3 cycles, each of 10 s, at 25% amplitude using Ultrasonic Processor (Hielscher). The lysate was centrifuged at 10,000 rpm for 5 min and the Curcumin content in the supernatant was determined by HPLC. Total cellular uptake was estimated from the data.

HPLC was performed as per the protocol described by Cooper et. al [173] using Jasco liquid chromatograph (Perkin Elmer Series 200) equipped with Brownlee Analytical Silica-based C18 column (250 × 4.6 mm, 5-μm particle size; cat. # N9303514). The mobile phase consisted of 40% THF and 60% water containing 1% citric acid, adjusted to pH 3.0, with concentrated KOH solution (v/v). The system was run isocratically at a flow rate of 1 ml/min. Sample detection was achieved at 420 nm, and injection volumes were 20 μl. A calibration curve to quantify Curcumin was generated by analyzing methanolic solution of pure Curcumin in the concentration range of 10 to 1000 nM. Conc. of Curcumin in methanolic cell extracts was determined using this calibration curve.

3.40 Flow Cytometry to analyze Cell cycle:

Flow cytometric analysis of cells stained with propidium iodide (PI) was used to determine % of cells in different phases of the cell cycle. U-87 MG cells were seeded in 6 well plates (1×10^5 cells/well). After 24 hr, cells were then exposed to specific treatment in serum free culture medium and incubated for 48 hr in a

TH-1245_08610607

CO_2 atmosphere incubator at 37 °C. After 48 hr incubation, the cells were detached from the culture plate by trypsinization, harvested, fixed and stained with PI as per the protocol of Riccardi and Nicoletti [174]. In brief, after trypisinization, cells were harvested by centrifugation. Harvested cells were re-suspended at a concentration of 1×10^6 cells/ml in DMEM and pelleted down by centrifugation. Cells were washed by re-suspending in ice-cold PBS and centrifuged. Finally the cells were re-suspended in 500 µl of ice cold PBS and fixed with 4.5 ml of pre-chilled 70% ethanol added to the re-suspended cells slowly with intermittent vortexing and keeping the cells on ice. Fixed cells were stored at 4 °C for 24 hr. Cells were then re-pelleted and re-suspended in 0.5 ml of PBS, 0.5 ml of DNA extraction buffer was added and incubated at room temperature for 5 min. Supernatant was removed by centrifugation and cells were re-suspended in 1 ml of DNA staining solution (Appendix Table. A5) incubated at 4 °C in dark for at least 1 hr. Cell cycle distribution of the cells was determined by analyzing 20,000 cells using a FACSCalibur flow cytometer and the Cell Quest software (FACS Calibur, Becton-Dickinson Biosciences). Stained cells were analyzed by flow cytometry and cell cycle analysis was performed using Modfit LT (Verity Software). Fluorescence intensities of PI stained cells were measured in FL2 channel in log mode and doublet discrimination was achieved using FL2 as DDM parameter.

3.41 Flow Cytometry to detect apoptotic cells:

Extent of apoptosis was estimated by flow cytometry using Annexin V-FITC Apoptosis Detection Kit I (BD Biosciences) as per the manufacturer's protocol. Briefly, U-87 MG cells were seeded in 6 well plates (1×10^5 cells/well) and after 24 hr of seeding, cells were treated as per requirement. At specified time point cells were detached from the culture plates by trypsinization and harvested by centrifugation at 400 g for 5 min. Cells were washed in PBS and re-suspended in 100 µl of 1 X Binding Buffer (provided by manufacturer). Cells were then

TH-1245_08610607

stained with 5 µl Annexin V-FITC and 5 µl propidium iodide (PI) in the dark for 15 min at room temperature. After adding the 400 µl of 1 X binding buffer to each tube samples were analyzed by flow cytometry with a FACSCalibur instrument (FACS Calibur, Becton-Dickinson Biosciences). Fluorescence intensity of FITC and PI stained cells was measured in FL1 and FL3 channel in log mode, respectively.

3.42 Data Analysis:

Two-way ANOVA or one-way ANOVA followed by pairwise multiple comparisons, was used depending upon the type of experiment. SigmaPlot (Systat Software, Inc.), was used for all statistical analysis and to generate graphs. Means of multiple data points were plotted. Error bars represent standard deviations if not otherwise mentioned.

TH-1245_08610607

4 Results & Discussion

Cell surface molecules like receptors, are often good therapeutic targets. Many such molecules are over-expressed in diseased condition. These molecules can be used for two therapeutic purposes as shown in Figure 4.1. They can be used as targets for homing drugs to specific cells expressing these molecules. Antibody tagged drugs are often used for this purpose. Recombinant antibodies or ligands to such cell surface molecules can also be used to block signaling through those molecules. Cell surface Heparin-binding epidermal growth factor (HB-EGF) is a promising target for cancer therapeutics [74, 157]. It is expressed as a membrane-bound molecule that subsequently gets released by ectodomain shedding. It is over-expressed in many types of cancers and induces oncogenic signals. An antibody against HB-EGF or a ligand of HB-EGF can be used to block HB-EGF mediated downstream signaling as well as for homing drugs to cells expressing HB-EGF.

Interestingly, Diphtheria Toxin (DT) is a natural ligand of HB-EGF and can be utilized for these purposes. DT binds HB-EGF, gets internalized via receptor-mediated endocytosis and causes cytotoxicity through its catalytic domain. In this work, we have used the HB-EGF binding domain of DT to target HB-EGF. At first, we have expressed a mutated non-toxic DT and used it to standardize our experiments. We have also used this protein as a control in some of the subsequent experiments. Then, this clone was used to generate recombinant receptor- binding domain of DT (RDT). Subsequently, we have used the recombinant RDT to enhance cellular uptake of curcumin to cells expressing HB-EGF. At the end, we show that RDT can also potentiate cytotoxicity of some common therapeutic agents possibly through blocking HB-EGF.

TH-1245_08610607

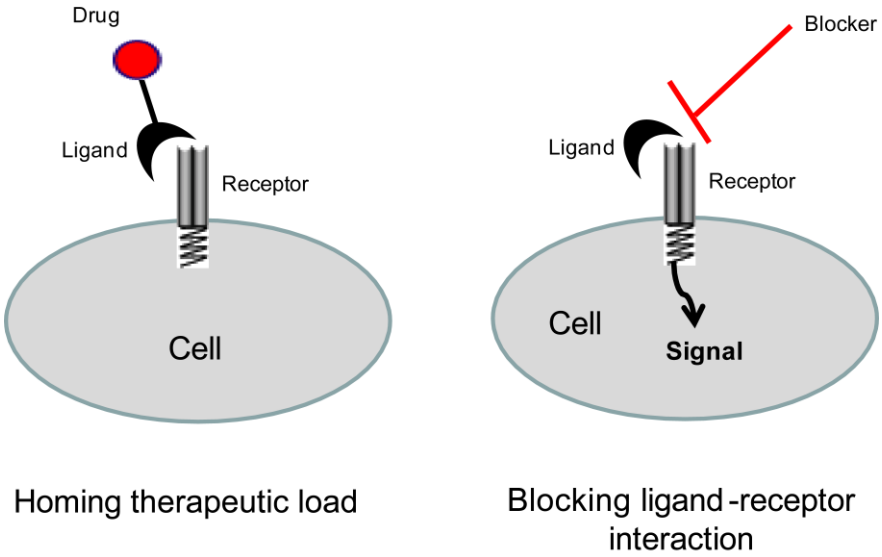

Figure 4.1: Cell surface molecule as therapeutic target. A ligand of cell surface molecule may be conjugated with a drug and can be used for homing of the drug to cells expressing the molecule. A blocker may be used to block the ligand-receptor interaction and thereby attenuating the signaling pathway.

4.1 Recombinant Mutated Diphtheria Toxin (DT):

4.1.1 Recombinant construct for Mutated Non-toxic DT:

Mutated non-toxic DT cloned in pET-22b vector was procured from Addgene (pET-22b DT 51E/148K, Plasmid 11081). It has mutations at two sites in the catalytic domain making it non-toxic. pET-22b has pel-B leader sequence and His-tag which enable expression in the bacteria periplasm and purification of the protein by affinity chromatography respectively. The design of the recombinant construct is shown in Figure 4.2a.

The recombinant construct was transformed in chemically competent *E.Coli* BL21 (DE3) using standard heat shock method. Recombinant clones were checked by restriction digestion (Figure 4.2b). Subsequently, the sequence of the insert in a selected clone was confirmed by DNA sequencing by dideoxy

TH-1245_08610607

method. It was confirmed that the insert is in the right frame with Pel B leader sequence as well as with His-tag at the C-terminal. The sequence of the cloned DT is identical with the wild type DT sequence (NCBI RefSeq: GI: 56068038) except having mutations at 51st and 148th amino acids (Lys51→Glu and Glu148 →Lys). The annotated sequence with color coding is shown in Figure 4.3.

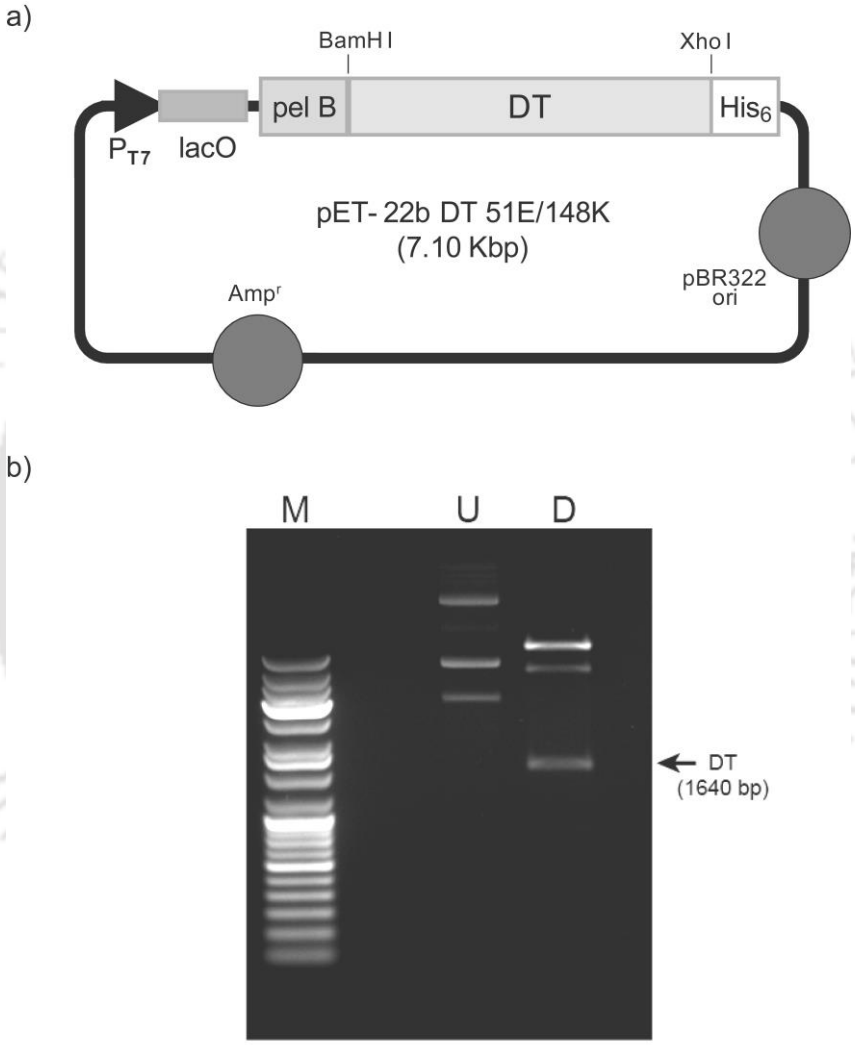

Figure 4.2: Recombinant construct for mutated non-toxic Diphtheria Toxin (DT). (a) Design of the construct of pET-22b DT. Full-length mutated DT (1.640 Kbp) is cloned into *BamH I – Xho I* site of the expression vector. Amp^r: Ampicillin resistance gene; P_{T7}: T7 Promoter; lacO: lac operator; pel B: Pel B leader sequence; His_6: Histidine tag. (b) Restriction digestion by *BamH I* and *Xho I* of the recombinant plasmid of DT to confirm the presence of the insert. M: DNA ladder, U: Undigested plasmid, D: Double digested plasmid.

TH-1245_08610607

a)

ATGAAATACCTGCTGCCGACCGCTGCTGCTGGTCTGCTGCTCCTCGCTGCCCAGCCGGCGATGGCCATGG
ATATCGGAATTAATTC*GGATCC*GGGCGCTGATGATGTTGTTGATTCTTCTAAATCTTTTGTGATGGAAAACT
TTTCTTCGTACCACGGGACTAAACCTGGTTATGTAGATTCCATTCAAAAAGGTATACAAAAGCCAAAATCT
GGTACACAAGGAAATTATGACGATGATTGGGAGGGGTTTTATAGTACCGACAATAAATACGACGCTGCGG
GATACTCTGTAGATAATGAAAACCCGCTCTCTGGAAAAGCTGGAGGCGTGGTCAAAGTGACGTATCCAGG
ACTGACGAAGGTTCTCGCACTAAAAGTGGATAATGCCGAAACTATTAAGAAAGAGTTAGGTTTAAGTCTC
ACTGAACCGTTGATGGAGCAAGTCGGAACGGAAGAGTTTATCAAAAGGTTCGGTGATGGTGCTTCGCGTG
TAGTGCTCAGCCTTCCCTTCGCTGAGGGGAGTTCTAGCGTTAAGTATATTAATAACTGGGAACAGGCGAA
AGCGTTAAGCGTAGAACTTGAGATTAATTTTGAAACCCGTGGAAAACGTGGCCAAGATGCGATGTATGAG
TATATGGCTCAAGCCTGTGCAGGAAATCGTGTCACGCGATCAGTAAGTAGCTCATTGTCATGCATAAATCT
TGATTGGGATGTCATAAGGGATAAAACTAAGACAAAGATAGAGTCTTTGAAAGAGCATGGCCCTATCAAA
AATAAAATGAGCGAAAGTCCCAATAAAACAGTATCTGAGGAAAAAGCTAAACAATACCTAGAAGAATTTC
ATCAAACGGCATTAGAGCATCCTGAATTGTCAGAACTTAAAACCGTTACTGGGACCAATCCTGTATTCGCT
GGGGCTAACTATGCGGCGTGGGCAGTAAACGTTGCGCAAGTTATCGATAGCGAAACAGCTGATAATTTGG
AAAAGACAACTGCTGCTCTTTCGATACTTCCTGGTATCGGTAGCGTAATGGGCATTGCAGACGGTGCCGTT
CACCACAATACAGAAGAGATAGTGGCACAATCAATAGCTTTATCGTCTTTAATGGTTGCTCAAGCTATTCC
ATTGGTAGGAGAGCTAGTTGATATTGGTTTCGCTGCATATAATTTTGTAGAGAGTATTATCAATTTATTTCA
AGTAGTTCATAATTCGTATAATCGTCCCGCGTATTCTCCGGGGCATAAAACGCAACCATTTCTTCATGACG
GGTATGCTGTCAGTTGGAACACTGTTGAAGATTCGATAATCCGAACTGGTTTTCAAGGGGAGAGTGGGCA
CGACATAAAAATTACTGCTGAAAATACCCCGCTTCCAATCGCGGGTGTCCTACTACCGACTATTCCTGGAA
AGCTGGACGTTAATAAGTCCAAGACTCATATTTCCGTAAATGGTCGGAAAATAAGGATGCGTTGCAGAGC
TATAGACGGTGATGTAACTTTTTGTCGCCCTAAATCTCCTGTTTATGTTGGTAATGGTGTGCATGCGAATCT
TCACGTGGCATTTCACAGAAGCAGCTCGGAGAAAATTCATTCTAATGAAATTTCGTCGGATTCCATAGGCG
TTCTTGGGTACCAGAAAACAGTAGATCACACCAAGGTTAATTCTAAGCTATCGCTATTTTTTGAAATCAAA
AAC*CTCGAG*CACCACCACCACCACCACTGA

b)

MKYLLPTAAAGLLLLAAQPAMAMDIGINSDPGADDVVDSSKSFVMENFSSYHGTKPGYVDSIQKGIQKPKSGT
QGNYDDDWEGFYSTDNKYDAAGYSVDNENPLSGKAGGVVKVTYPGLTKVLALKVDNAETIKKELGLSLTEPL
MEQVGTEEFIKRFGDGASRVVLSLPFAEGSSSVKYINNWEQAKALSVELEINFETRGKRGQDAMYEYMAQACA
GNRVTRSVSSSLSCINLDWDVIRDKTKTKIESLKEHGPIKNKMSESPNKTVSEEKAKQYLEEFHQTALEHPELSE
LKTVTGTNPVFAGANYAAWAVNVAQVIDSETADNLEKTTAALSILPGIGSVMGIADGAVHHNTEEIVAQSIALSS
LMVAQAIPLVGELVDIGFAAYNFVESIINLFQVVHNSYNRPAYSPGHKTQPFLHDGYAVSWNTVEDSIIRTGFQG
ESGHDIKITAENTPLPIAGVLLPTIPGKLDVNKSKTHISVNGRKIRMRCRAIDGDVTFCRPKSPVYVGNGVHANLH
VAFHRSSSEKIHSNEISSDSIGVLGYQKTVDHTKVNSKLSLFFEIKNLEHHHHHH

Figure 4.3: Annotation of the sequence of mutated recombinant DT. (a) The DNA sequence. Green: Start codon, Pink: Pel B leader sequence, Blue: The full-length DT in our clone, Orange: His-tag, Red: Stop codon, Red underlined: Mutated codons at 153rd & 444th codon. First italics in brown: *BamH I* site, Last italics in brown: *Xho I* site. (b) The amino acid sequence. Same color coding used. The mutated His-tagged DT has 575 amino acids including the leader sequence.

TH-1245_08610607

4.1.2 Expression & characterization of full-length DT:

The protein expression was induced by addition of IPTG (1 mM) for 8 hr at 28 °C. Periplasmic extract was prepared and checked by SDS-PAGE (Figure 4.4a). The recombinant DT expressed in periplasm was purified by affinity chromatography, using Nickel-column (His-Trap column). The calculated molecular weight of this protein is ~60 kDa. The purified recombinant product was characterized by SDS-PAGE (Figure 4.4b). It was further characterized by Western Blot using anti-His antibody (Figure 4.4c). The results of these SDS-PAGE and western blot experiments confirmed that the expressed His-tagged DT is in proper reading frame.

4.1.3 Functional characterization of full-length DT:

We further investigated the function of recombinant mutated full-length DT. Solid-phase ELISA was performed to check the binding to HB-EGF. Recombinant human HB-EGF was immobilized on an ELISA plate. After blocking, DT was allowed to bind. Bound DT was detected by anti-His antibody followed by HRP-labeled anti-mouse antibody. As evident from the ELISA data in Figure 4.5a, recombinant DT showed binding to immobilized HB-EGF. A similar result was obtained in another ELISA experiment where recombinant full-length DT was immobilized and HB-EGF was allowed to bind. Bound HB-EGF was detected by anti-HB-EGF antibody followed by HRP-labeled anti-mouse antibody (Figure 4.5b). Both these experimental results showed that recombinant mutated full-length DT binds to HB-EGF.

4.1.4 Selection of suitable system for cell-based assays:

We were interested to explore binding of this recombinant DT or its fragment to cell surface HB-EGF. We screened several cell lines to identify cells that can be used for cell based assays. To begin with, we performed Reverse Transcription-PCR to check the status of HB-EG expression in different cell lines. The results

TH-1245_08610607

of this experiment are shown in Figure 4.6. As shown in the figure, all the cell lines tested by us, namely U-87 MG, U-373, HEK-293, HeLa, MCF-7 and HT-29 express HB-EGF.

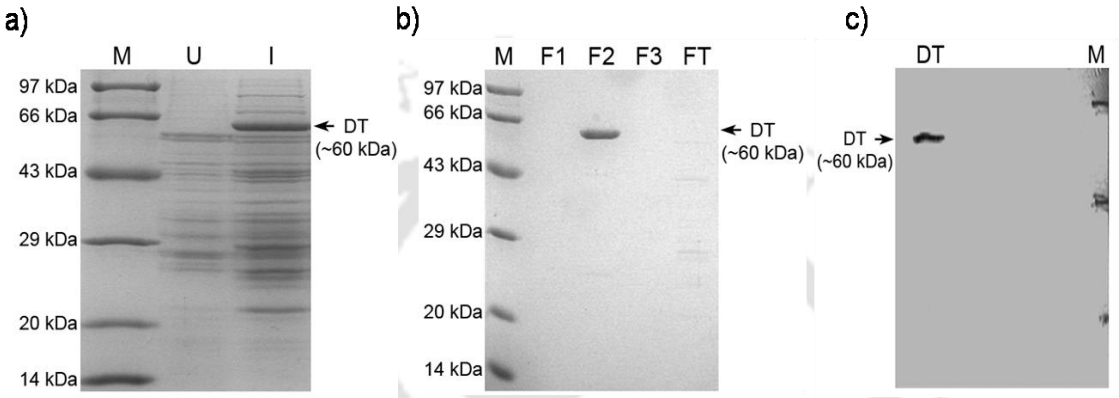

Figure 4.4: Expression of recombinant His-tagged full-length DT in *E.Coli* BL21 (DE3). (a) SDS-PAGE to detect expression of full-length DT. The clone having pET-22b DT was induced with 1 mM IPTG at 28 °C for 8 hr. The periplasmic extract was prepared and resolved by SDS-PAGE. (b) SDS-PAGE to detect purified DT. It was purified by affinity chromatography and was detected in the 2nd eluted fraction. (c) Western Blot to detect His-tagged DT. The protein was detected by anti-His antibody, followed by anti-mouse HRP antibody. 12% polyacrylamide gels were used and gels were stained by coomassie brilliant blue. M: Protein molecular weight marker, U: Periplasmic extract of un-induced clone, I: Periplasmic extract of induced clone, F1, F2 & F3: Eluted fractions, FT: Flow-through.

TH-1245_08610607

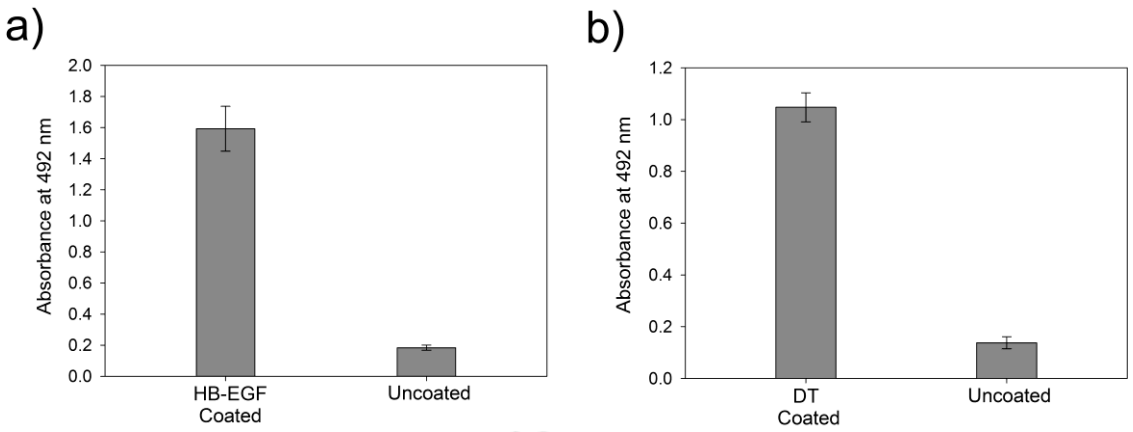

Figure 4.5: Solid-phase ELISA to detect binding of DT to HB-EGF. (a) Recombinant human HB-EGF (100 ng/well) was coated on an ELISA plate and DT was allowed to bind to it. (b) Recombinant DT (200 ng/well) was coated an ELISA plate and HB-EGF was allowed to bind to it. Bound DT or bound HB-EGF was detected using mouse anti-His antibody or anti-HB-EGF antibody respectively, followed by goat-anti-mouse-HRP conjugated antibody. ELISA was developed using OPD and absorbance was measured at 492 nm. Each bar represents mean of four different wells.

Subsequently, we investigated whether our recombinant DT could bind to cell surface HB-EGF or not. We did a preliminary experiment with HeLa cells to check the binding of DT to HB-EGF expressed on its surface. In this experiment, we conjugated DT with a fluorescent probe, FITC. BSA was also conjugated with the same fluorescent probe to act as a negative control. We treated HeLa cells with DT-FITC and BSA-FITC separately in a 96-well culture plate for 2 hr. Cells were thoroughly washed with PBS and the bound DT-FITC or BSA-FITC was measured by a fluorescence spectrophotometer for the fluorescence signal of FITC at 525 nm. As evident from the Figure 4.7, cells treated with DT-FITC gave higher fluorescence compared to untreated or BSA-FITC treated cells. This result confirmed that DT binds to HB-EGF expressed on the surface of these cells.

All the cells screened express HB-EGF at different levels. The fluorescence based experiment confirmed that our recombinant DT binds to HB-EGF expressed on

TH-1245_08610607

HeLa cells. However, we have used U-87 MG, a human glioblastoma cell line in most of the subsequent studies. This cell line expresses HB-EGF (Figure 4.6). It has been earlier shown that HB-EGF is over-expressed in several gliomas and induces proliferation of glioma cell lines in vitro [75]. Therefore, HB-EGF is a potential biomarker for glioblastoma and can serve as a target for therapeutic intervention in glioblastoma multiforme (GBM). Considering these, we decided to use the U-87 MG cell line for our further studies.

We confirmed the expression of HB-EGF on the surface of U-87 MG cells using the immuno-fluorescence imaging. In this experiment, U-87 MG cells were seeded in 96-well plate. The cells were fixed by formalin, blocked with BSA and then treated with mouse anti-HB-EGF antibody. The bound antibody was then detected with FITC tagged goat anti-mouse antibody. Nuclei of cells were counter stained with DAPI. Double stained cells were then imaged using an epi-fluorescence microscope. We observed extensive green fluorescence in cells treated with mouse anti-HB-EGF antibody (Figure 4.8, upper panel) compared to negative control cells (Figure 4.8, lower panel). This experiment confirmed the expression of HB-EGF on the cell surface of U-87 MG cells.

TH-1245_08610607

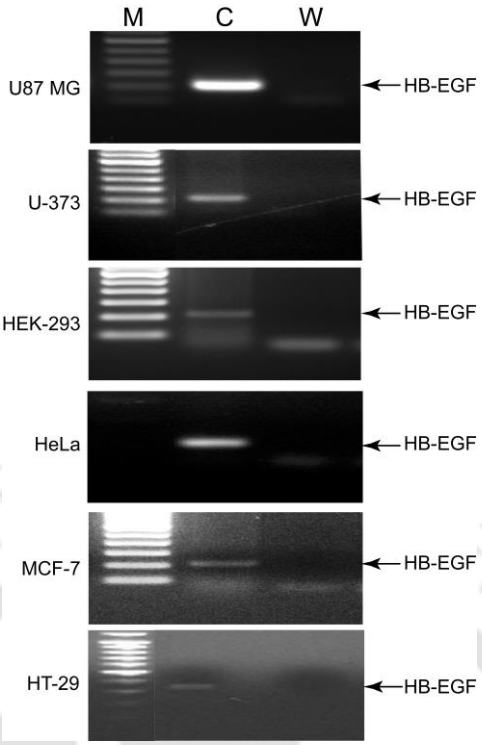

Figure 4.6: Expression of HB-EGF in different cell lines. Reverse Transcription-PCR was performed to check the expression of HB-EGF in different cell lines using HB-EGF specific primers. M: DNA marker, C: cDNA, and W: Water. Size of the PCR product was 210 bp.

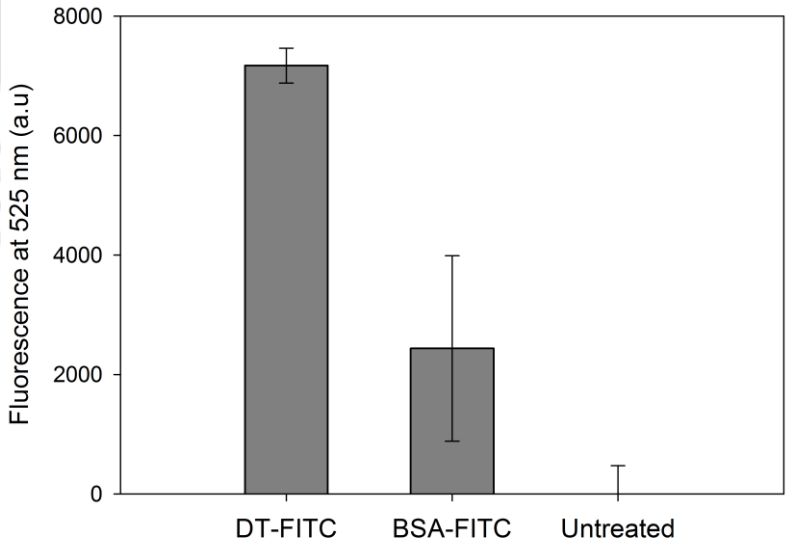

Figure 4.7: DT binds to cell surface HB-EGF in HeLa cells. HeLa cells in 96-well culture plate were treated with DT-FITC or BSA-FITC for 2 hr. The cells were thoroughly washed with PBS and the bound DT-FITC or BSA-FITC was measured by a fluorescence spectrophotometer at 525 nm. Each bar represents mean of four different wells.

TH-1245_08610607

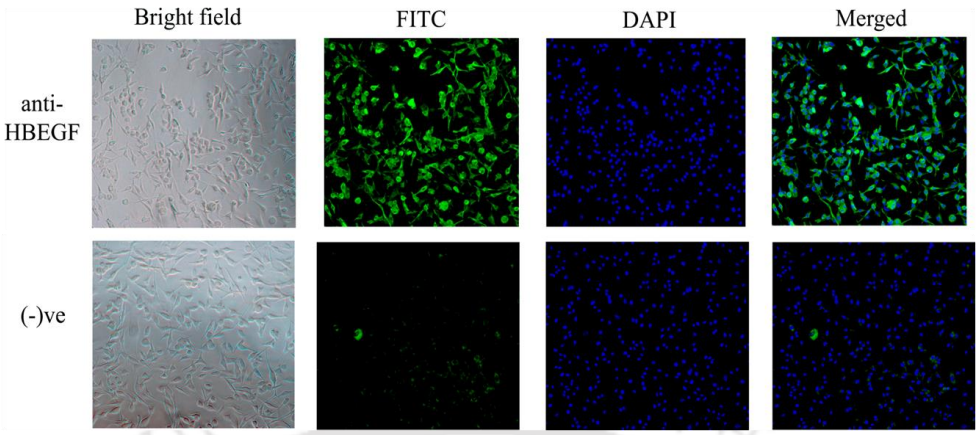

Figure 4.8: HB-EGF is expressed on the surface of U-87 MG cells. Immuno-fluorescence imaging to detect HB-EGF on the surface of U-87 MG cells. Cell surface HB-EGF was detected using mouse anti-HB-EGF antibody followed by goat anti-mouse-FITC conjugate. Cells stained without anti-HB-EGF antibody but with mouse anti-His antibody followed by goat anti-mouse-FITC was used as (-) ve control. Images were taken at 10× magnification.

4.2 Recombinant Receptor-Binding Domain of DT (RDT):

DT is a Y-shaped molecule with three independent domains as shown in the 3-dimensional ribbon diagram of full-length DT (Figure 4.9a). DT binds to HB-EGF, through its receptor-binding domain present at the C-terminal end (NCBI CDD: 65145). This domain corresponds to 382^{nd}-535^{th} amino acid residues of full-length DT. A smaller protein elicits less immunogenicity and has better tissue penetration [175, 176]. Therefore, we planned to express and use recombinant receptor-binding domain of DT (RDT) as a therapeutic ligand of HB-EGF.

At first, we investigated if this domain would be functional and work independently when rest of the domains are missing. A structure based analysis was performed. X-ray crystallographic structures of free DT and DT bound to HB-EGF are available. We overlapped the R-domain of free DT (PDB ID: 1F0L)

TH-1245_08610607

with the R-domain of DT bound to HB-EGF (PDB ID: 1XDT). We observed that R-domain undergoes very little structural change upon binding to the receptor as shown in the Figure 4.9b. This indicated that probably this domain is structurally rigid and may be expressed independently without change in structure and loss of function.

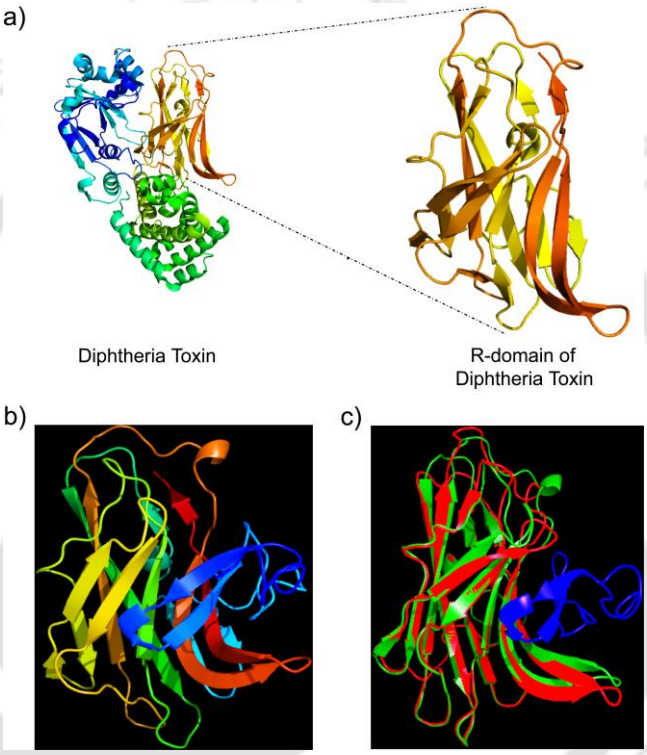

Figure 4.9: (a) Three-dimensional ribbon diagram of DT. The receptor-binding domain to be sub-cloned has been enlarged. Blue: N-terminal catalytic domain; Green: Trans-membrane domain; Yellow-orange: C-terminal receptor-binding domain of DT. Based on the X-ray crystallographic structure (PDB ID: 1 F0L). (b) Interaction of R-domain of DT with the EGF-like domain of HB-EGF (PDB ID: 1XDT). EGF-like domain of HB-EGF is shown in blue. (c) R-domain of free DT (PDB ID: 1F0L) overlapped with R-domain of DT bound to HB-EGF (PDB ID: 1XDT). Blue: EGF-like domain of HB-EGF, Green: R-domain of free DT and Red: R-domain of DT bound to HB-EGF. Overall rms < 1.1 Å.

TH-1245_08610607

4.2.1 Cloning of Recombinant RDT:

The receptor binding domain of DT (RDT) was sub-cloned from pET-22b DT in the pET-22b expression vector and expressed in *E.Coli*. Our cloning strategy is shown in Figure 4.10. The mutated non-toxic DT (pET-22b DT 51E/148K, Plasmid 11081) was used as a template. The DNA fragment corresponding to 382^{nd} – 536^{th} amino acid (155 amino acids) of DT was amplified by PCR using specific primers for the fragment (Figure 4.11a). This amplified fragment (RDT) was cloned into the *BamH I - Xho I* sites of pET-22b expression vector. The recombinant construct (pET-22b RDT) was transformed in chemically competent *E.Coli* DH5α by standard heat shock method. The recombinant clones were checked by restriction digestion. One representative clone is shown in Figure 4.11b. Subsequently, the sequence of the insert in one selected clone was confirmed by DNA sequencing by dideoxy method. It was confirmed that the nucleotide sequence of the insert is in proper reading frame with Pel B leader sequence and His-tag and the sequence of the cloned RDT is identical with the DT sequence from 1144 to 1608 base position (NCBI RefSeq: GI: 56068038) available in GenBank, NCBI. The annotated sequence is shown in Figure 4.12.

4.2.2 Expression of Recombinant RDT in *E.Coli*:

This recombinant construct was further used for expression of His-tagged RDT in *E.Coli* BL21 (DE3). Expression of the recombinant RDT was induced with IPTG (0.5 mM) at 28 °C temperature for 8 hr. Subsequently, the cells were harvested by centrifugation and whole cell lysate was prepared by sonication and checked by SDS-PAGE (Figure 4.13a). The recombinant protein was purified from clarified cell lysate in a single step using affinity chromatography with His-Trap FF affinity column. Elution buffer having imidazole was used for elution of RDT and the residual Imidazole was removed by dialysis against PBS (pH 7.4). The purified protein was analyzed by SDS-PAGE (Figure 4.13b). The

TH-1245_08610607

calculated molecular weight of this protein is ~20 kDa having His-tag at the C-terminal and some additional amino acids at the N-terminal originating from the vector. The recombinant RDT was further characterized by Western Blot analysis with mouse anti-His antibody followed by anti-mouse HRP antibody (Figure 4.13c). The yield of the purified recombinant RDT expressed in *E. coli* BL21 (DE3) varied from 350 to 450 µg/L of culture as estimated by Bradford assay.

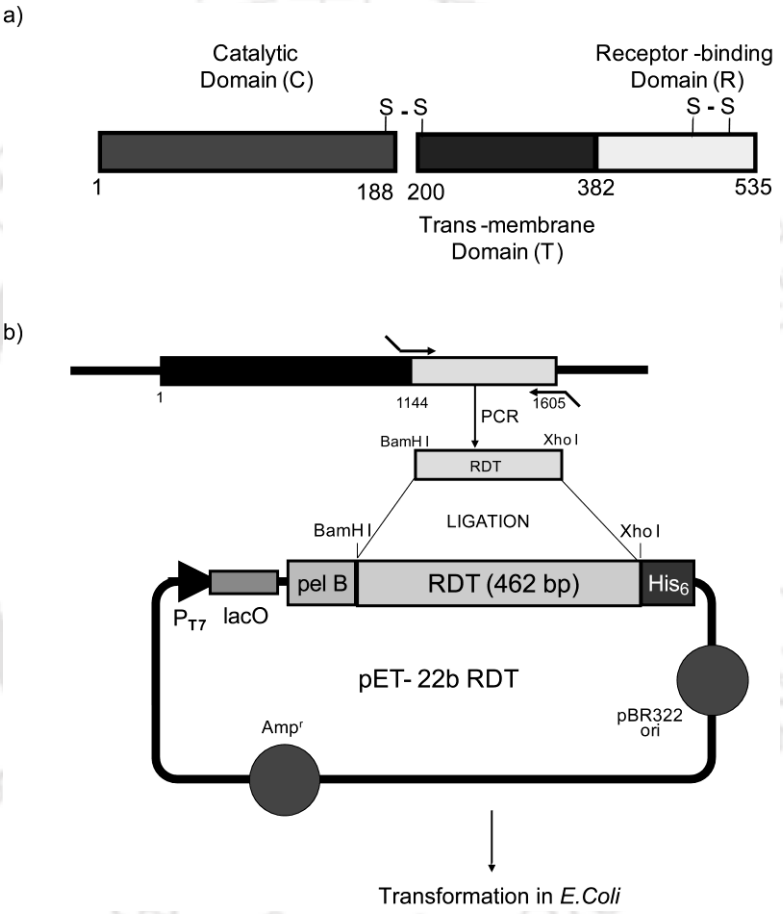

Figure 4.10. Strategy for cloning and expression of recombinant RDT in *E.coli*. a) Schematic diagram showing the domains with amino-acid number. Catalytic domain (1-188 a.a), Trans-membrane domain (200-382 a.a) and Receptor-binding domain (382-535 a.a). b) Plan for cloning of recombinant RDT in pET-22b. RDT was amplified by PCR using the primers having *BamH I* and *Xho I* overhangs. Amplified product was cloned into pET-22b. Amp^r: ampicillin resistance gene; P_{T7}: T7 Promoter; lacO: lac operator; pel B: Pel B leader sequence; His_6: Histidine tag.

TH-1245_08610607

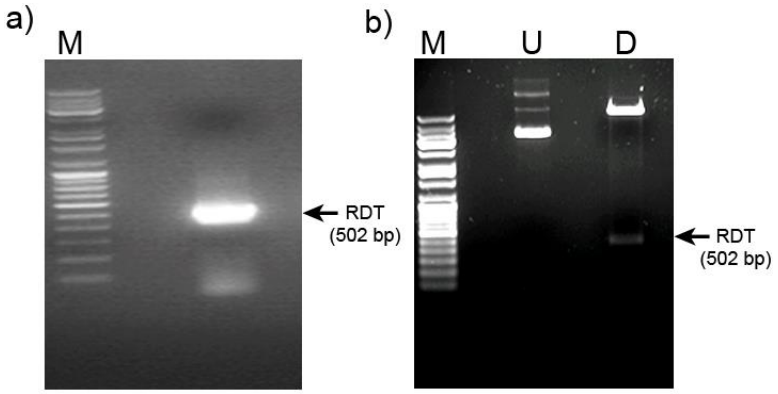

Figure 4.11. Cloning of receptor-binding domain of DT (RDT) into pET-22b vector. a) RDT was amplified by PCR using pET-22b DT as template. The amplified product was resolved in agarose gel. M: DNA molecular weight marker. This amplified product was eluted out and cloned in pET-22b vector. b) Restriction digestion of one positive clone with *BamH I* and *Xho I*. Digested products were resolved in agarose gel. U and D indicate undigested and digested plasmid respectively. Lane M: DNA molecular weight marker.

a)

ATGAAATACCTGCTGCCGACCGCTGCTGCTGGTCTGCTGCTCCTCGCTGCCCAGCCGGCGATGGCCATGG
ATATCGGAATTAATTC*GGATCC*GTCTCCGGGGCATAAAACGCAACCATTTCTTCATGACGGGTATGCTGTC
AGTTGGAACACTGTTGAAGATTCGATAATCCGAACTGGTTTTCAAGGGGAGAGTGGGCACGACATAAAAA
TTACTGCTGAAAATACCCCGCTTCCAATCGCGGGTGTCCTACTACCGACTATTCCTGGAAAGCTGGACGTT
AATAAGTCCAAGACTCATATTTCCGTAAATGGTCGGAAAATAAGGATGCGTTGCAGAGCTATAGACGGTG
ATGTAACTTTTTGTCGCCCTAAATCTCCTGTTTATGTTGGTAATGGTGTGCATGCGAATCTTCACGTGGCAT
TTCACAGAAGCAGCTCGGAGAAAATTCATTCTAATGAAATTTCGTCGGATTCCATAGGCGTTCTTGGGTAC
CAGAAAACAGTAGATCACACCAAGGTTAATTCTAAGCTATCGCTATTTTTTGAAATCAAAAGC*CTCGAG*CA
CCACCACCACCACCACTGA

b)

MKYLLPTAAAGLLLLAAQPAMAMDIGINSDPSPGHKTQPFLHDGYAVSWNTV
EDSIIRTGFQQGESGHDIKITAENTPLPIAGVLLPTIPGKLDVNKSKTHISVNGRK
IRMRCRAIDGDVTFCRPKSPVYVGNGVHANLHVAFHRSSSEKIHSNEISSDSI
GVLGYQKTVDHTKVNSKLSLFFEIKSLEHHHHHH

Figure 4.12: Annotation of the sequence of recombinant RDT. (a) The DNA sequence. Green Region: Start codon, Pink: Pel B leader sequence, Blue: The cloned receptor-binding domain of DT (RDT), Orange: His-tag, Red: Stop codon, First italics in brown: *BamH I* site, Last italics in brown: *Xho I* site. (b) The amino acid sequence. Identical color coding used. The matured His-tagged RDT has 195 amino acids including the leader sequence.

TH-1245_08610607

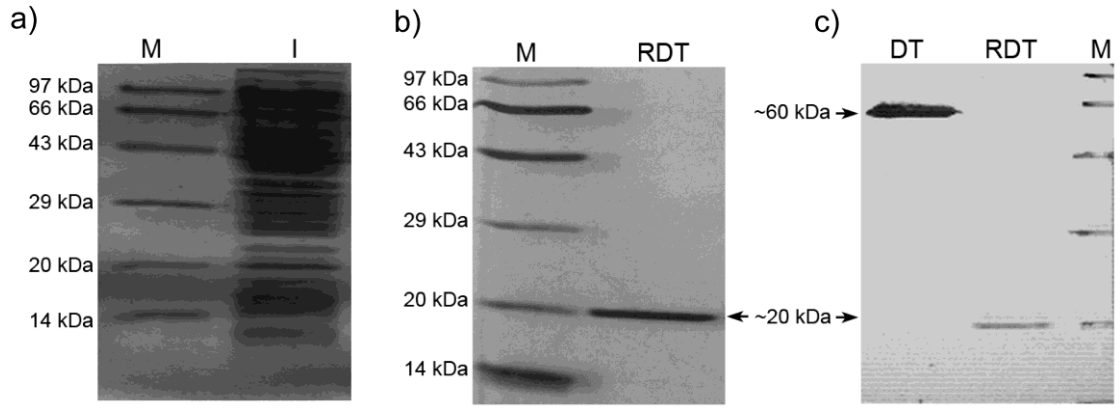

Figure 4.13: Expression, purification and characterization of recombinant receptor binding domain of DT (RDT). (a) SDS-PAGE to detect expression of recombinant RDT. The clone having pET-22b RDT was induced at 28 °C with 0.5 mM IPTG for 8 hr. Proteins in clarified cell lysate were resolved by SDS-PAGE and stained by coomassie brilliant blue. The recombinant protein (~20 kDa) was purified by affinity chromatography using His Trap FF affinity column. (b) The purified protein was resolved and stained by silver staining in SDS-PAGE. (c) Western Blot to detect recombinant RDT. The protein was detected by mouse anti-His antibody followed by anti-mouse HRP antibody. Recombinant full length mutated DT (~60 kDa) expressed & purified in the same fashion was used as a control in the Western Blot experiment. 15% Polyacrylamide gels were used.

4.2.3 Characterization of Recombinant RDT:

After successful expression and purification of the recombinant RDT, we performed experiments to check the binding ability of this protein to HB-EGF. To check binding, we performed a solid-phase ELISA. The microplate was coated with recombinant human HB-EGF (100 ng/well). After blocking, RDT of different concentrations were added and incubated for 2 hr at room temperature. Thereafter, the bound RDT was detected using mouse anti-His antibody followed by goat anti-mouse-HRP conjugated antibody. We observed that RDT binds to recombinant HB-EGF in a dose-dependent fashion (Figure 4.14).

TH-1245_08610607

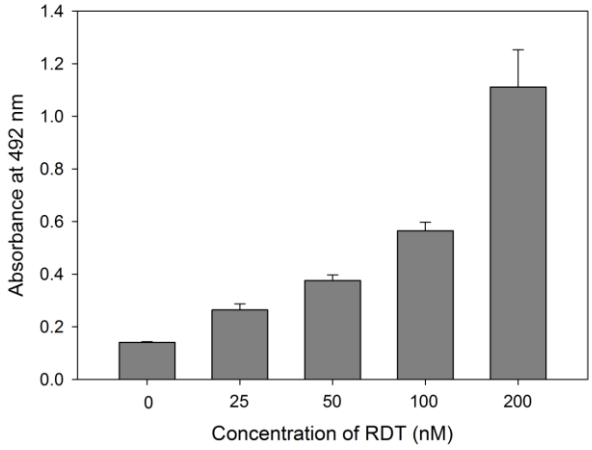

Figure 4.14: Recombinant RDT binds HB-EGF in a dose-dependent fashion. Solid phase ELISA to detect binding of RDT to HB-EGF. Recombinant human HB-EGF (100 ng/well) was coated on 96-well plate. RDT of different concentrations were added and incubated for 2 hr at room temperature. Bound RDT was detected using mouse anti-His antibody followed by goat-anti-mouse-HRP conjugated antibody. ELISA was developed using OPD and absorbance measured at 492 nm. Each bar represents mean of four different wells.

Subsequently, we explored the kinetics of interaction of RDT with HB-EGF. We performed the SPR experiment to measure the kinetic parameters of RDT binding to HB-EGF using Biacore X100 (GE Healthcare). Recombinant human HB-EGF was immobilized on CM5 sensor chip. Binding of RDT was measured using single-cycle kinetics, with sequential injection of RDT as analyte in increasing order of concentration (from 400 nM to 1000 nM) at 25 °C with a flow rate of 30 µl/ml. The binding of full length DT to HB-EGF was also measured in the same fashion. The data for both RDT and DT were analyzed and fitted to 1:1 binding model using BIA evaluation Software (version 2.0) to calculate association (k_a), dissociation (k_d) rate constants and the affinity in terms of dissociation constant ($K_D = k_d/k_a$). The sensograms of one representative SPR experiment each for DT and RDT are shown in Figure 4.15. The experiment was repeated thrice for RDT and DT and the average values for k_{on} , k_{off} and K_D for RDT and DT binding to immobilized recombinant HB-EGF calculated from

TH-1245_08610607

these three independent experiments (Table 4.1). We observed that RDT has binding affinity equivalent to that of the full-length DT and close to the value that has been earlier reported for full-length DT [177]. However, kinetic parameters, association and dissociation rate constants, for RDT vary by one order from those of DT. RDT binds with a higher association rate constant (k_a), but dissociates faster than DT. RDT is smaller in size and this may be the reason for the faster kinetics.

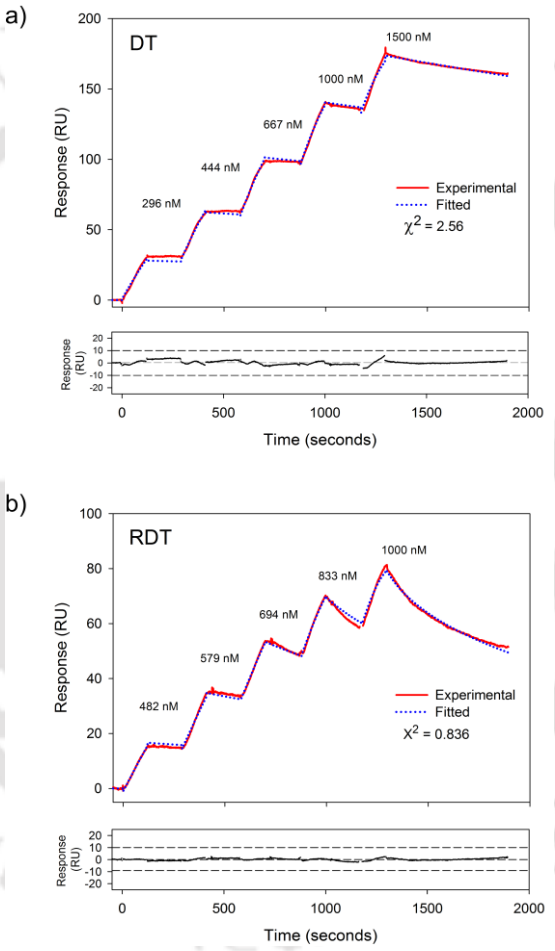

Figure 4.15: Kinetic analysis by SPR. (a) Sensogram of one representative SPR experiment for DT. (b) Sensogram of one representative SPR experiment for RDT. Recombinant human HB-EGF was immobilized on CM5 sensor chip (~400 RU). Binding was measured using single-cycle kinetics (25 °C, flow rate of 30 µl/min) using five samples of each analyte (from ~300 nM to 1500 nM for DT and from to ~400 nM to 1000 nM for RDT). Data was analyzed and fitted to 1:1 binding model using BIAevaluation Software (version 2.0). Residual values are shown in lower panels.

TH-1245_08610607

Table 4.1: Comparative data of SPR

	k_{on} (1/M.1/s)	k_{off} (1/s)	K_D (M)
RDT	4.434×10^{4}	3.073×10^{-4}	7.348×10^{-8}
DT	3.975×10^{3}	1.575×10^{-4}	4.045×10^{-8}
DT(Reported*)	7.900×10^{4}	2.000×10^{-3}	2.600×10^{-8}

Calculated from three independent experiments.

* Reference [177]

Once it was confirmed that RDT binds to recombinant HB-EGF on solid-phase, we further investigated whether RDT can bind to HB-EGF expressed on the cell surface. As shown earlier, HB-EGF is highly expressed in U-87 MG glioma cell line (Figure 4.6 and 4.8). Therefore, we performed a cell-based ELISA using U-87 MG to check if RDT can bind to HB-EGF present on cell surface. For cell based ELISA, cells in 96-well plate were fixed with formalin in PBS for 45 minutes at 4 °C. After blocking, RDT was added and incubated for 2 hr. Bound RDT was detected using mouse anti-His antibody followed by goat anti-mouse-HRP conjugated antibody. We observed that RDT binds to U-87 MG cells expressing HB-EGF in a dose dependent fashion (Figure 4.16).

Subsequently, we re-confirmed that recombinant RDT binds to cell surface HB-EGF on U-87 MG cells using the immuno-fluorescence imaging. U-87 MG cells were seeded in 96-well plates. The cells were fixed by formalin and blocked with BSA and then allowed RDT (200 ng/well) to bind to cell surface HB-EGF in U-87 MG cells for 2 hr at 37 °C. The bound RDT was detected with mouse anti-His antibody followed by FITC tagged goat anti-mouse antibody. Nuclei of cells in all the cases were counter-stained with DAPI. Double stained cells were imaged under an epi-fluorescence microscope. We observed green fluorescence

TH-1245_08610607

in cells treated with RDT (Figure 4.17, upper panel). No such fluorescence was observed in the negative control (Figure 4.17, lower panel).

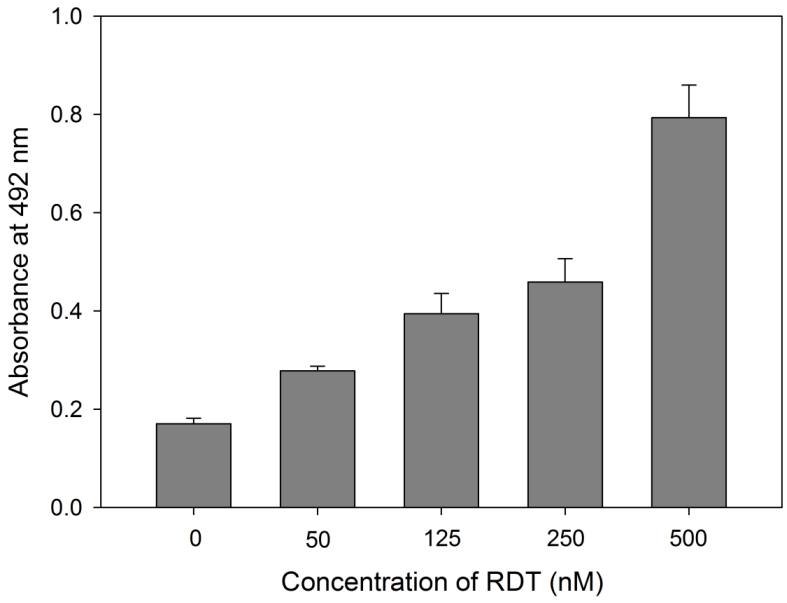

Figure 4.16: Recombinant RDT binds to cell surface HB-EGF in a dose-dependent fashion. Cell ELISA to detect binding of RDT to HB-EGF expressed on the surface of U-87 MG cells. Cells in a 96-well culture plate were fixed and RDT of different concentrations were added. Bound RDT was detected using mouse anti-His antibody followed by goat-anti-mouse-HRP conjugated antibody. ELISA was developed using OPD and absorbance measured at 492 nm. Each bar represents mean of four different wells.

TH-1245_08610607

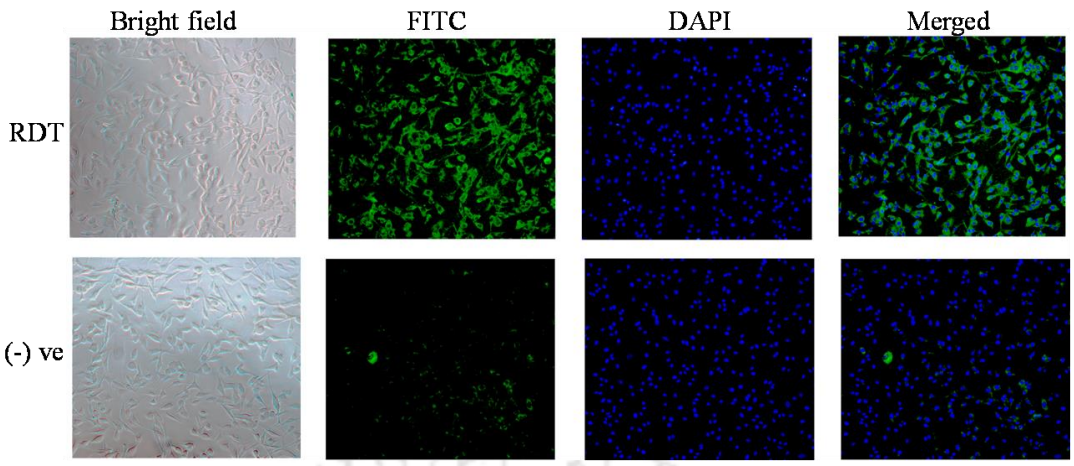

Figure 4.17: RDT binds to cell surface HB-EGF on U-87 MG cells. Immuno-fluorescence imaging to show binding of RDT to U-87 MG cells. RDT bound to cell surface HB-EGF was detected using mouse anti-His antibody followed by goat anti-mouse-FITC conjugate. Cells without RDT treatment but stained with mouse anti-His antibody followed by goat anti-mouse-FITC conjugated antibody was used as (-) ve control. Images were taken at 10X magnification.

4.3 RDT for drug delivery:

Proteins are utilised in a number of ways to enhance potency of therapeutic agents. Proteins like serum albumin, and peptides like cell penetrating peptides, have been used to enhance cellular uptake of drugs [178-180]. Nanoparticles made up of human serum albumin, casein, collagen, β-lactoglobulin have also been used as molecular carriers [14, 15, 181]. Virus-like particles (VLPs) has also been used as drug carrier [182]. Ligand-receptor system like Transferrin and its receptor has also been explored to enhance cellular uptake and potency of drugs [183].

RDT binds to cell surface HB-EGF. Therefore, we investigated if recombinant RDT can be utilized for drug delivery. A drug may be attached with RDT through covalent or non-covalent interactions. Then RDT would be carry and deliver the drug to cells expressing HB-EGF. Drug loaded nano-carriers or

TH-1245_08610607

liposomes may be crowned with RDT on their surface. RDT will home these carrier to cells expressing HB-EGF.

Many drugs, including chemotherapeutic agents are hydrophobic. Hydrophobicity limits their bioavailability, and delivery to target cells [184]. Some proteins bind to such molecules by hydrophobic interactions, forming protein-drug complexes [16, 17]. If such a protein is a ligand for a cell surface receptor, we may use the protein-drug complex for cell specific drug delivery. We investigated whether a drug can bind to RDT. RDT has an immunoglobulin fold with beta sheeted structure forming a cage at its core as shown in the ribbon diagram of RDT (Figure 4.18a). Being a cage like structure, one can expect that a small molecule could go and reside in that cage. But, as shown in Figure 4.18b, the core of the cage is filled with amino acid side chain. Therefore, the cage will not be accessible to a drug. Although majority of the hydrophobic residues are inside the beta sheeted structure, there are several hydrophobic residues also on the surface. We analyzed the surface of the protein in different orientations. We observed several hydrophobic patches on the surface of the protein as shown in Figure 4.19. The abundance of hydrophobic patches over the surface of RDT prompted us to investigate if a hydrophobic drug can bind to RDT through hydrophobic interactions and be delivered to HB-EGF expressing cells.

Curcumin is a hydrophobic molecule that binds to many proteins [185-187]. It is a potential chemotherapeutic agent and has been shown to be involved in multiple pathways. Its utilities in many cancers and in several other diseases have been explored [188]. However, hydrophobicity, poor stability, poor bioavailability and low cellular uptake of this molecule limits its utilities [184]. Further, curcumin is a good probe to investigate novel delivery systems for hydrophobic drugs. It is a fluorochrome and the fluorescence spectrum of curcumin depends upon the polarity of the environment with substantially pronounced fluorescence yield in non-polar environment than in aqueous

TH-1245_08610607

environment [185]. Therefore, we selected curcumin to investigate the drug binding ability of RDT.

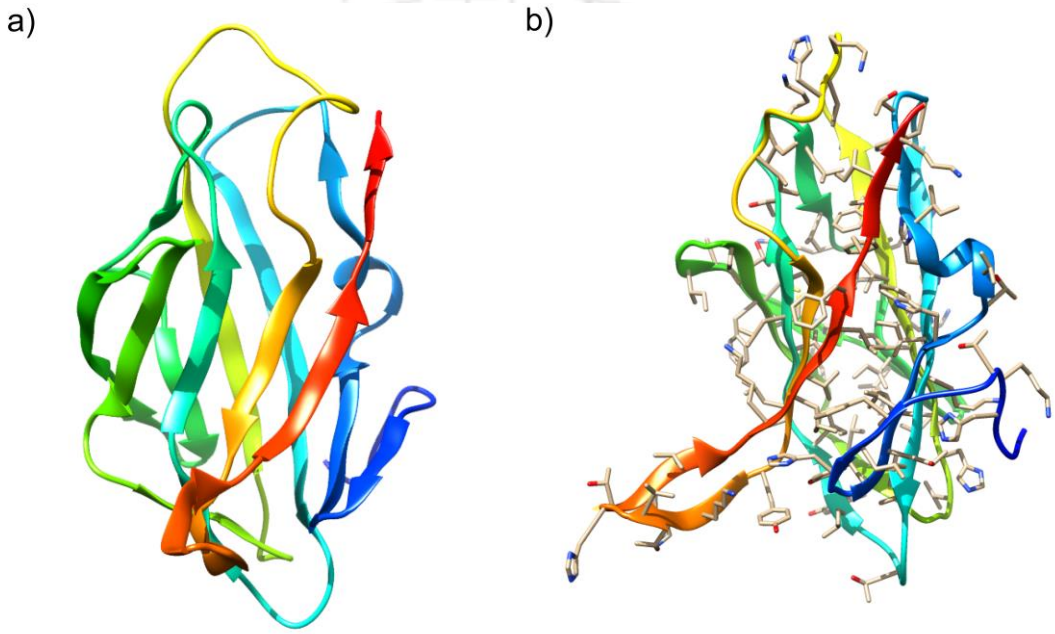

Figure 4.18: Cage like structure of RDT. The ribbon diagram (a) shows that RDT has an immunoglobulin fold with beta sheeted structure. (b) The ribbon diagram with hydrophobic residues shows that the core of the β-sheeted structure is filled with hydrophobic residues and possibly not accessible for external molecule.

TH-1245_08610607

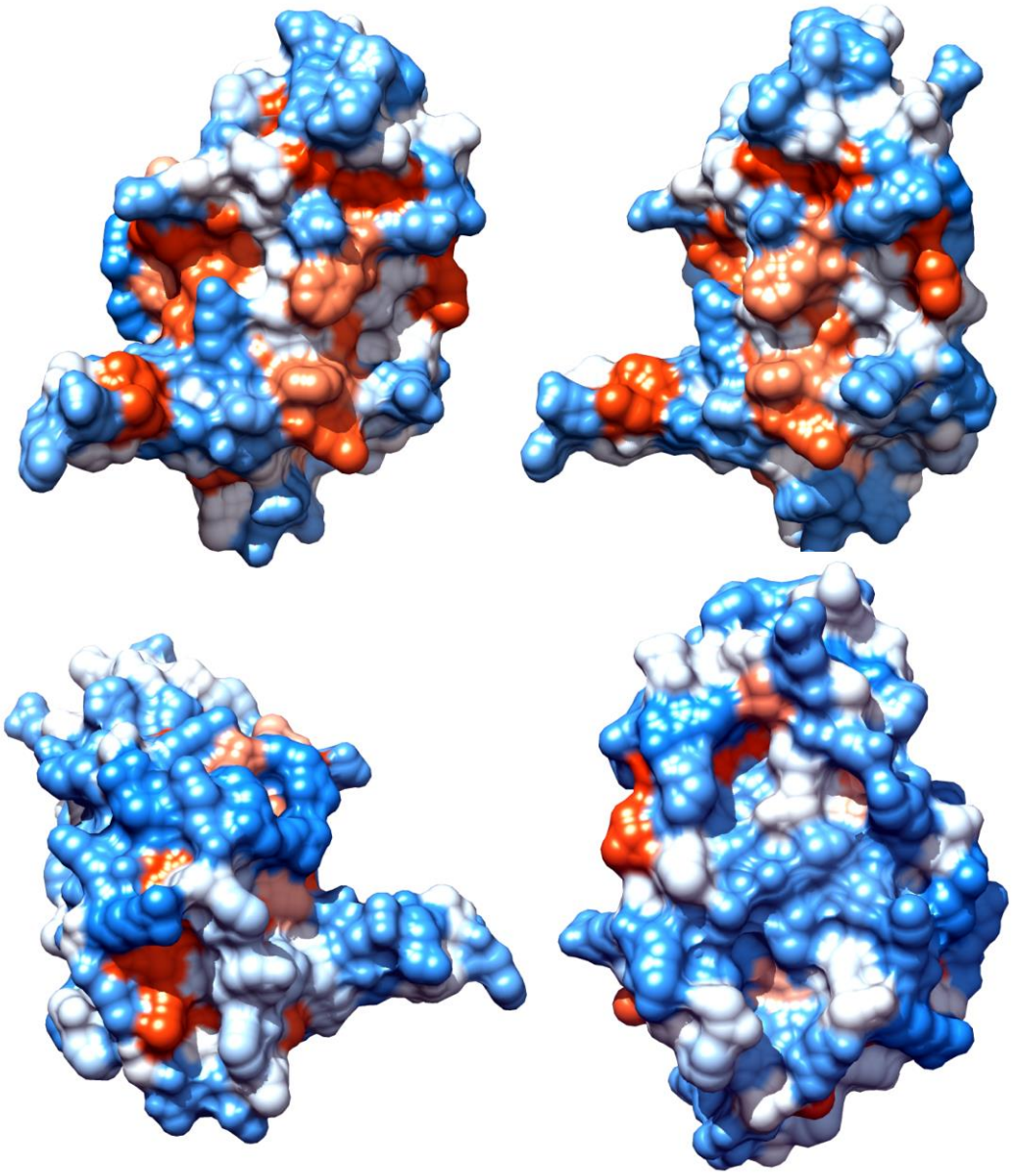

Figure 4.19: RDT has hydrophobic patches on surface. The Surface diagram of RDT in four different orientations shows the hydrophobic as well as hydrophilic regions present on the surface of the protein. Color code for protein surface: blue = hydrophilic and orange red = hydrophobic.

TH-1245_08610607

4.3.1 Docking of Curcumin on RDT:

We explored the possibility of binding of curcumin to RDT using an automated Molecular docking. The web-based Swiss docking server ((http://swissdock.vital-it.ch/) [169] was used for docking. Structure of RDT was derived from X-ray crystal structure of DT (PDB ID: 1F0L), after trimming its C- and T-domains (Figure 4.20a). Structure of curcumin in four different conformations (ZINC ID: 00899824, 17255287, 20230445 and 31261437) were collected from Zinc database [170] (Figure 4.20b). Each of the four curcumin structures was allowed to bind to RDT separately. Docking was performed as blind, with default parameter values in 'Accurate' mode with no flexibility for RDT. The server gave an exhaustive list of binding poses for each docking with fullfitness scores that represent how well the molecules have docked. We selected the top ten best docked poses for each of the four docking experiment. The data for docking of four different curcumin ligands to RDT is shown in Table 4.2.

RDT binds to HB-EGF through a hydrophobic face. Therefore, we screened the docking results based on score and considered only those binding sites which are away from the receptor binding face of RDT. This would ensure simultaneous binding of curcumin and HB-EGF to RDT. RDT has several patches of hydrophobic regions on the surface. Multiple potential binding sites for curcumin were observed in our docking experiments. One such potential binding site is shown in Figure 4.21a. In this pose, curcumin remains in an extended conformation and binds to a hydrophobic groove (Figure 4.21b). This binding site is made up of 11 amino acids, five of which are hydrophobic and three have aromatic side chain (T386, Q387, P388, F389, L390, W398, V401, S404, L529, F530, and E532 of 1F0L).

Interaction of curcumin with hydrophobic and aromatic residues of proteins has been reported in several studies [189]. Extended conjugated aromatic ring of the curcumin at one end rests on a hydrophobic patch provided by P388, F389, and

TH-1245_08610607

L390 as shown in the ball and stick model on the left side of Figure 4.22. Binding of curcumin in this pose is further facilitated via formation of a hydrogen bond between a keto group and the side chain of Q387 as shown in the upper ball and stick model of Figure 4.22. Such hydrogen bond between keto-enol group of curcumin and side chains of proteins has been reported in other docking studies also [189].

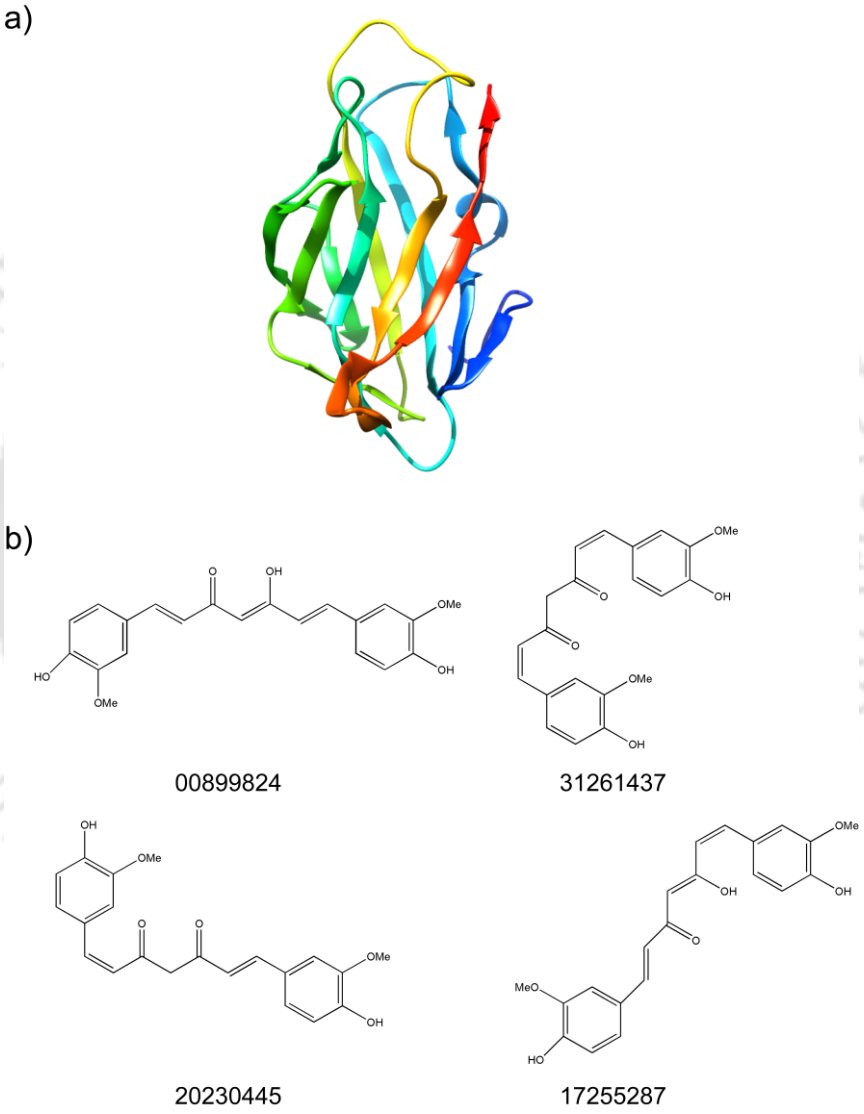

Figure 4.20: Structure of RDT and Curcumin used for docking. (a) The ribbon diagram shows the structure of RDT used in molecular docking. The structure was derived from X-ray crystal structure of DT (PDB ID: 1F0L, resolution: 1.55 Å, R-value: 0.188) after trimming its C-and T-domains. This corresponds to Ser381 to Ser535 of 1F0L. (b) Structures of curcumin in four conformations, collected from Zinc database (ZINC ID: 00899824, 17255287, 20230445 and 31261437).

TH-1245_08610607

Table 4.2: Result of Docking of Curcumin on RDT

Curcumin (Zinc ID)	Number of clusters in HB-EGF binding face*	Number of clusters on other sites*	Full Fitness Scores†
899824	4	6	-964.9938 to -959.78375
17255287	8	2	-963.4402 to -960.60020
20230445	10	0	–
31261437	8	2	-972.2258 to -970.3016

* Top ten clusters of each docking experiment are considered.

† The range of Full Fitness score of clusters away from HB-EGF binding sites.

4.3.2 Curcumin binds to RDT:

Our preliminary investigations using molecular docking indicates that curcumin may bind to RDT. Curcumin is a fluorochrome and is known to bind proteins like bovine serum albumin (BSA), and human serum albumin (HSA) at hydrophobic sites [185]. When incubated with these proteins, curcumin forms curcumin-protein complexes and shows enhanced fluorescence in these complexes [186, 187]. Therefore, protein-curcumin interaction can be easily monitored using fluorescence spectroscopy. We have also used fluorescence spectroscopy to investigate possible binding of curcumin to RDT.

TH-1245_08610607

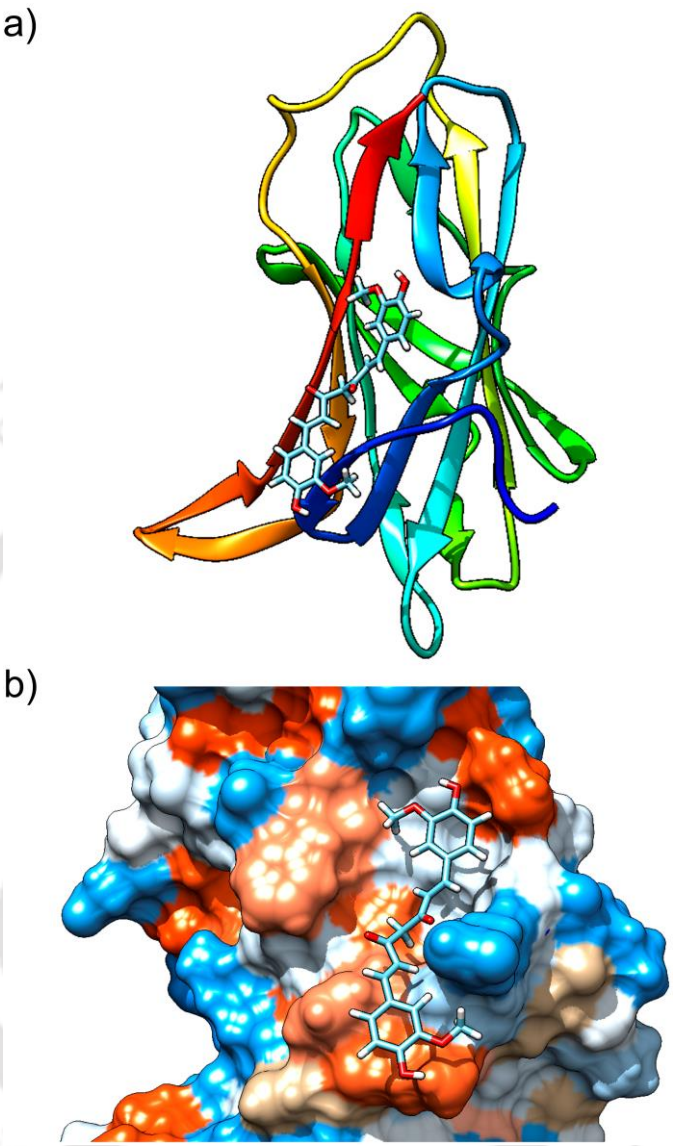

Figure 4.21: Docking of curcumin to RDT. (a) The ribbon diagram shows the orientation of a potential binding pose (score = -970.3). (b) Surface rendering of the same binding site. In this pose, curcumin remains in an extended conformation and binds to a hydrophobic groove. This binding site is made up of 11 amino acids, five of which are hydrophobic and three have aromatic side chain (T386, Q387, P388, F389, L390, W398, V401, S404, L529, F530, and E532 of 1F0L). Color code for protein surface: blue = hydrophilic and orange red = hydrophobic.

TH-1245_08610607

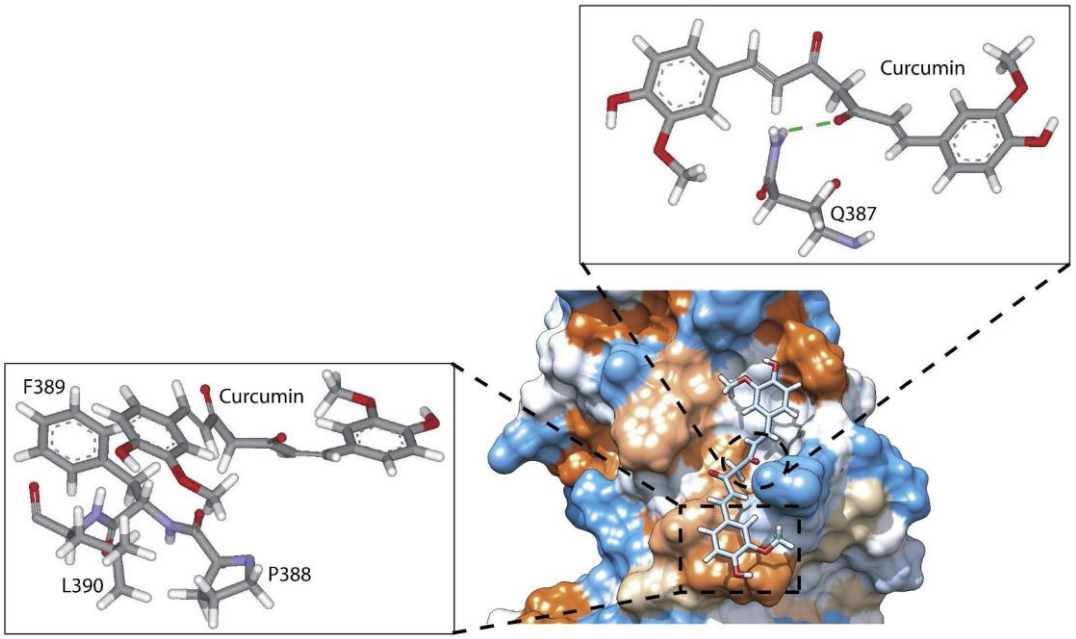

Figure 4.22: Interaction of different residues of RDT with Curcumin. In this pose, curcumin binds to an extended groove of the protein that has several hydrophobic residues. One aromatic ring of curcumin rest on a hydrophobic patch provided by P388, F389 and L390 as shown in the ball and stick model on the left. Hydrogen bond (in green) between keto oxygen of curcumin and 5-N of Q387 is shown in the upper ball and stick model. Numbering of amino acids as in the PDB file 1F0L was followed. Color code for protein surface: blue = hydrophilic and orange red= hydrophobic.

Curcumin (10 μM) was incubated with RDT (1 μM) in PBS at 4 °C for 2 hr to generate curcumin-RDT complex and fluorescence spectroscopy was used to detect formation of curcumin-RDT complex. The absorption spectrum of Curcumin (10 μM) in PBS (pH 7.4) was measured and absorption maximum was observed at 430 nm as shown in Figure 4.23. In our experiments, when excited at 430 nm, curcumin in PBS showed two low-intensity broad peaks near 510 nm and 570 nm. However, when incubated with RDT, the fluorescence emission of curcumin increased almost four fold with maximum at 510 nm (Figure 4.24a). RDT in itself does not have any significant fluorescence in this

TH-1245_08610607

range when excited at 430 nm (Figure 4.24b). We have also observed similar change in fluorescence emission when Curcumin (10 μM) was incubated with BSA (1 μM) (Figure 4.24a). Fluorescence emission spectrum shown in Figure 4.24a indicates that Curcumin binds to RDT that provides a hydrophobic environment, thereby enhancing the fluorescence of curcumin.

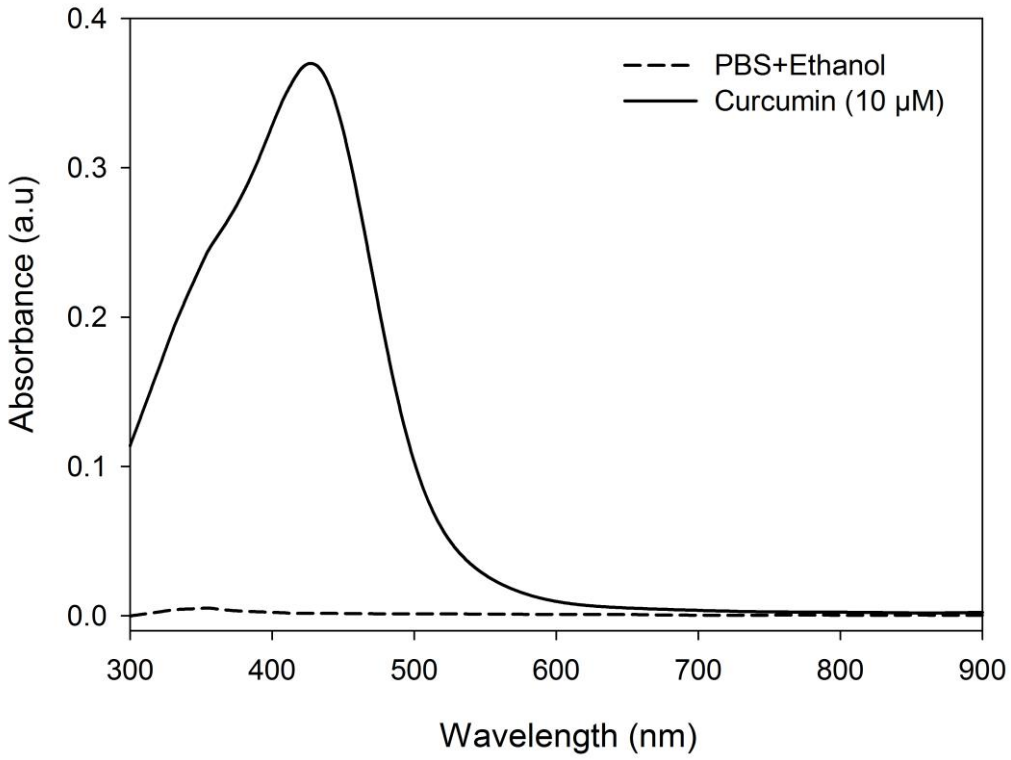

Figure 4.23: UV-Visible absorption spectrum of Curcumin. A 10 μM curcumin solution in PBS (pH 7.4) was used. The absorption maximum (λ_{max}) was observed to be 430 nm. PBS with equivalent amount of ethanol was used as control.

TH-1245_08610607

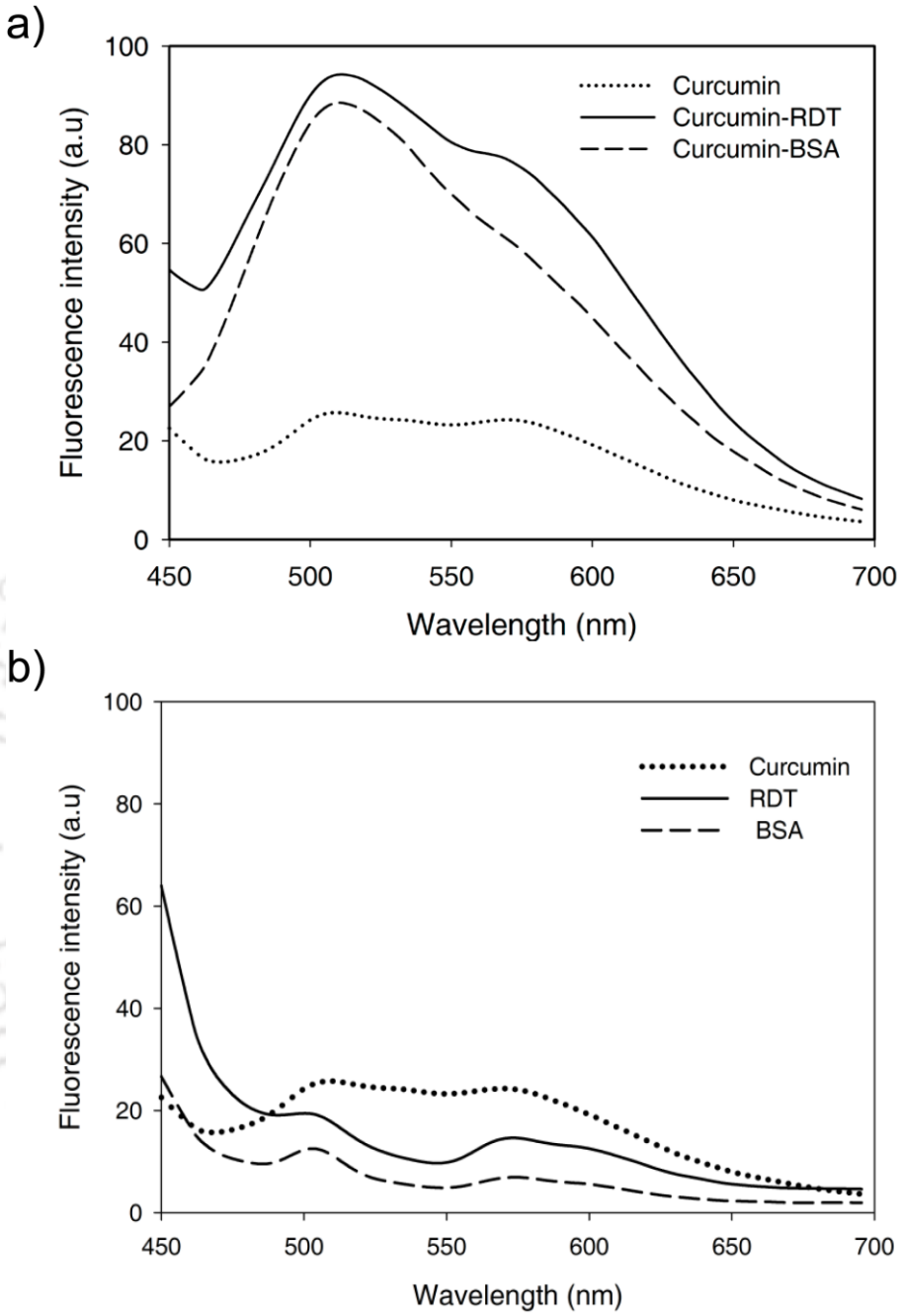

Figure 4.24: Fluorescence spectroscopy to detect binding of curcumin to RDT. a) Fluorescence emission spectra of curcumin alone or in complex with RDT or BSA in PBS. Concentration of curcumin was 10 μM. The molar ratio of curcumin to protein was 10 μM:1 μM. b) Fluorescence emission spectra of curcumin, RDT and BSA in PBS. Concentration of curcumin was 10 μM. Concentration of both the proteins was 1 μM. λ_{Ex} = 430 nm.

TH-1245_08610607

Curcumin-RDT complex formation was further investigated by incubating curcumin (10 μM) with RDT in different molar ratios (RDT: Curcumin = 0 μM:10 μM to 2 μM:10 μM). We observed that fluorescence of curcumin changes with change in concentration of RDT (Figure 4.25a). As shown in Figure 4.25b, intensity of fluorescence emission of curcumin at 510 nm increases with increase in amount of RDT, as more and more curcumin moves from aqueous environment to the hydrophobic environment provided by RDT.

Formation of curcumin-RDT complex was further substantiated by time-resolved fluorescence analysis. As shown in Figure 4.26, fluorescence decay of curcumin in curcumin-RDT complex is slower than that of curcumin alone in PBS. The data was fitted to multi-component exponential models (with tail fitting) and the fittings with best χ^2 values are reported. As per the model fitting, average lifetimes of fluorescence decay of curcumin are 0.86 ns and 1.04 ns for curcumin alone and for curcumin-RDT complex respectively. It is well known that solvent can quench the fluorescence of a fluorophore and complexation with a protein can reduce such quenching, thereby increasing the fluorescence lifetime [190]. Water quenches fluorescence of curcumin [191]. Therefore, complexation with RDT may have reduced such quenching and increased the fluorescence lifetime of curcumin.

TH-1245_08610607

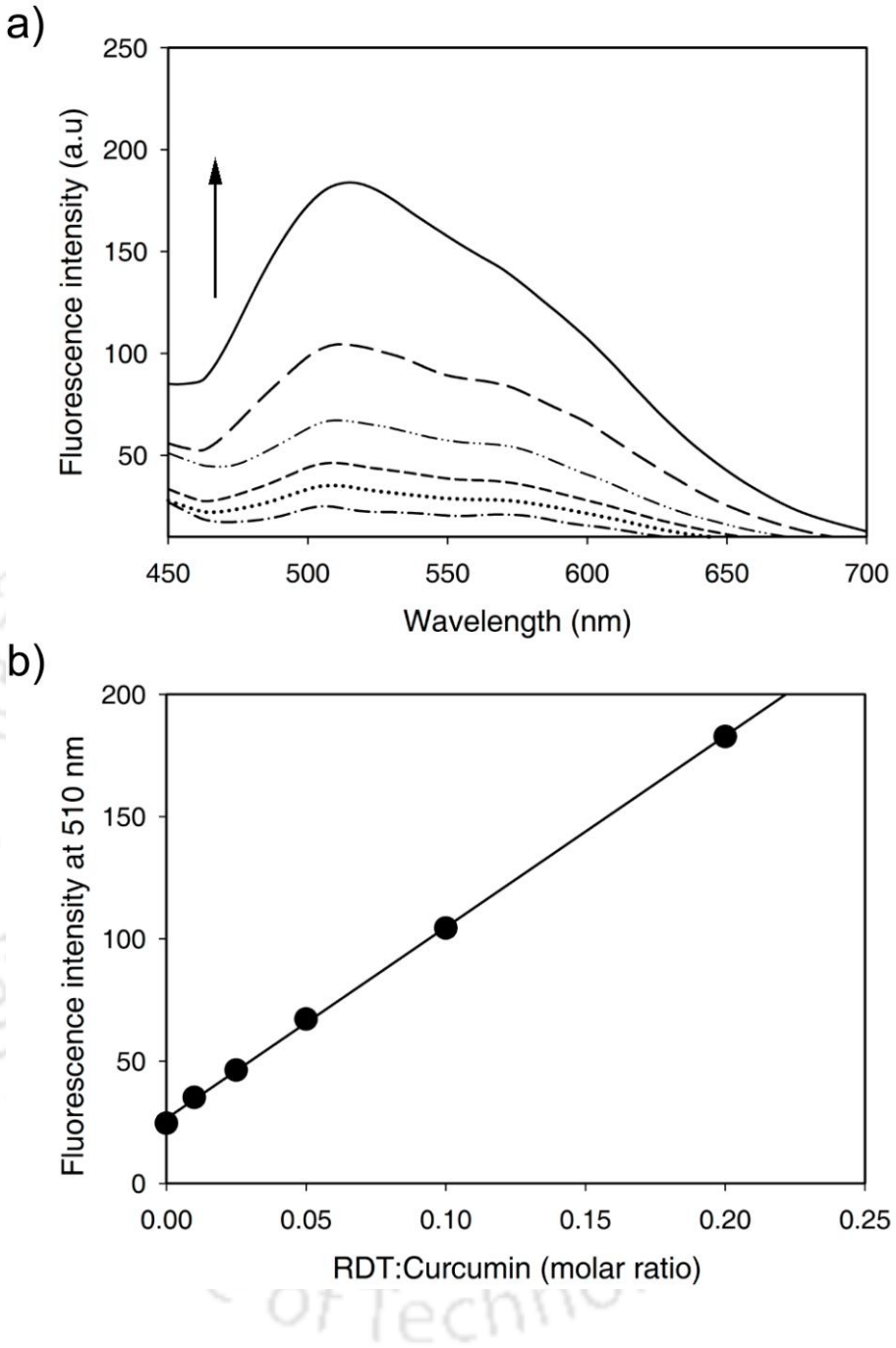

Figure 4.25: Fluorescence spectroscopy to show dose-dependent binding of curcumin to RDT. a) Fluorescence emission spectra of curcumin-RDT complexes with different molar ratios of curcumin and RDT. Concentration of curcumin was 10 μM and the amount of RDT was varied (0 μM, 0.1 μM, 0.25 μM, 0.5 μM, 1 μM, and 2 μM). The arrow indicates increasing amount of RDT. b) Shows linear enhancement of fluorescence intensity at 510 nm with increase in amount of RDT as observed in the spectra in (a).

TH-1245_08610607

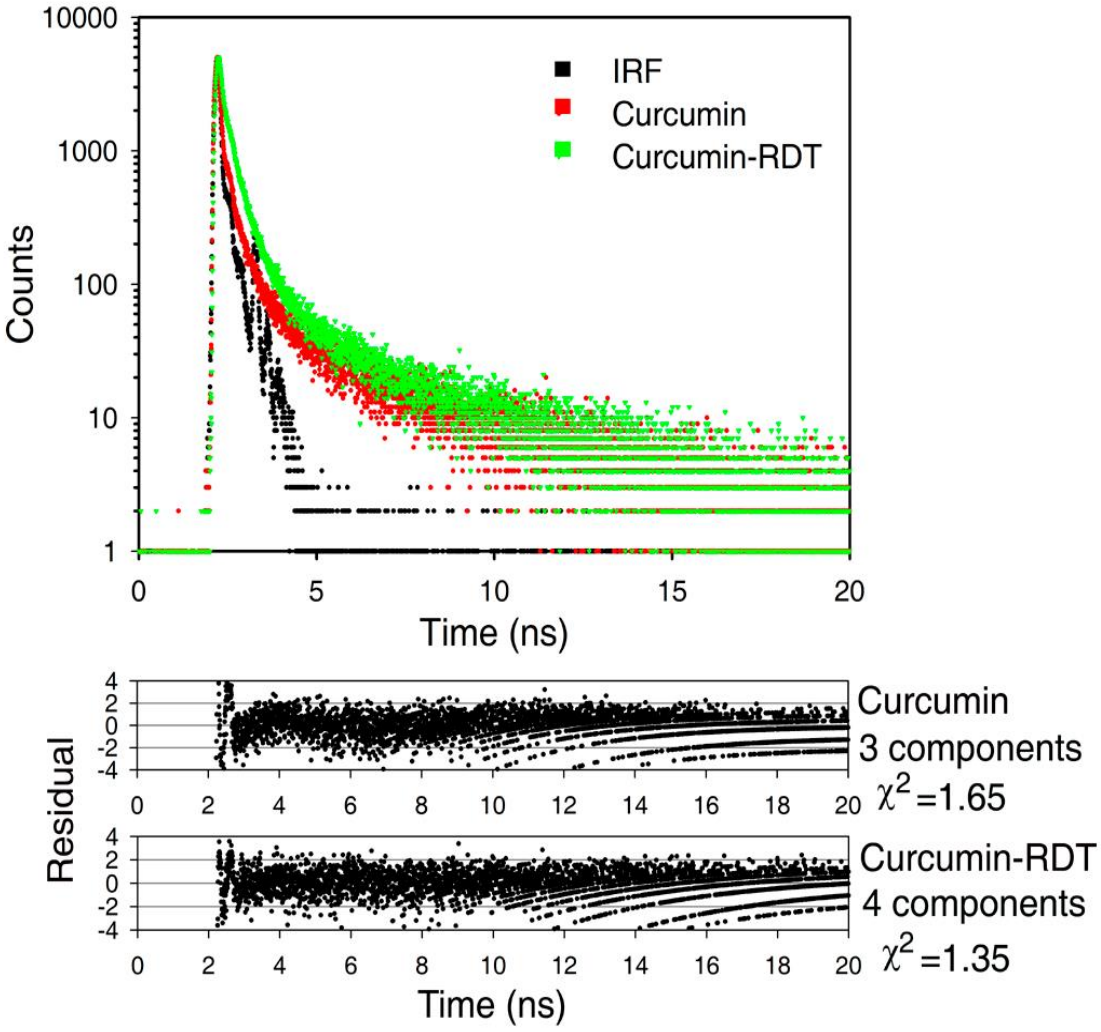

Figure 4.26: Time-resolved fluorescence spectroscopy for curcumin-RDT complex. Concentration of curcumin was 10 μM. The molar ratio of curcumin to protein was 10 μM:1 μM. The average lifetimes of fluorescence decay of curcumin increased from 0.86 ns for curcumin alone to 1.04 ns for curcumin-RDT complex. The data was fitted to multi-component exponential models (with tail fitting) and the fittings with best χ^2 values are reported.

TH-1245_08610607

4.3.3 Stability of Curcumin-RDT complex:

Curcumin is poorly stable in water [191, 192]. We, therefore, investigated the stability of curcumin-RDT complex. We performed an experiment where curcumin-RDT and curcumin-BSA complexes were formed by incubating curcumin (10 μM) with respective proteins (1 μM) in PBS (pH 7.4) at 4 °C for 2 hr and the samples were incubated for various duration both at 4 °C or at 37 °C. Subsequently, the absorption spectrum of curcumin was measured. Change in absorbance at 430 nm was used to measure the relative stability of curcumin at 4 °C (Figure 4.27a) and at 37 °C (Figure 4.27b). At 4 °C, both the protein increases relative stability of curcumin. However, at 37 °C, complexation with BSA or RDT does not affect curcumin stability and by 24 hr 20% of curcumin gets degraded. These two experiments confirmed that curcumin is moderately stable in aqueous environment. Most of our subsequent experiments were performed at 37 °C. As per the data shown in Figure 4.27b, complexation with protein would not affect stability of curcumin in our experiments. In most of our subsequent experiments, except phenotypic assays like cell viability assay, treatment duration was 2 - 4 hr. From data shown in Figure 4.27, one can be assured that stability of curcumin would not be a major issue in these experiments.

4.3.4 Curcumin-RDT complex binds to HB-EGF:

After confirming the stability of curcumin-RDT complex, we enquired whether this complex would bind HB-EGF. Complexation of RDT with curcumin may affect the receptor binding ability of RDT. Therefore, we investigated the binding ability of curcumin-RDT complex with HB-EGF using a solid phase ELISA. Recombinant human HB-EGF was coated on an ELISA plate. After blocking, RDT (1 μM) or curcumin-RDT complexes with two different molar ratios (1 μM:1 μM and 10 μM:1 μM) was added and incubated for 2 hr at room temperature. Bound RDT was detected using mouse anti-His antibody followed

TH-1245_08610607

by goat anti-mouse-HRP conjugated antibody and ELISA was developed by using OPD and the absorbance was measured at 492 nm. We observed that Curcumin-RDT complex binds to HB-EGF coated on ELISA plate (Figure 4.28). This confirmed that complexation of RDT with curcumin does not affect the receptor-binding ability of RDT.

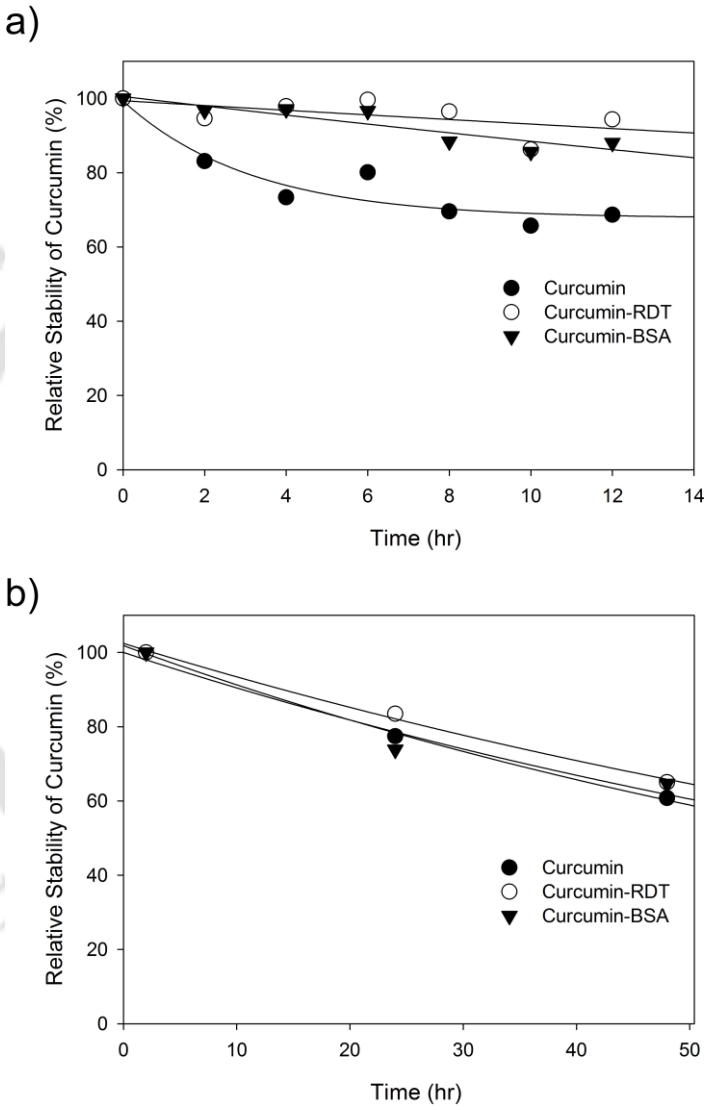

Figure 4.27: Stability of Curcumin in curcumin-protein complex. Relative stability of curcumin alone and in complex with RDT or BSA in PBS (pH 7.4) at (a) 4 °C, and (b) 37 °C. Curcumin (10 μM) alone and curcumin-protein complex (molar ratios 10 μM:1 μM) in PBS (pH 7.4) were incubated at 4 °C or 37 °C for various durations and absorption spectrum of curcumin was measured. Change in absorbance at 430 nm was used to measure the stability of curcumin.

TH-1245_08610607

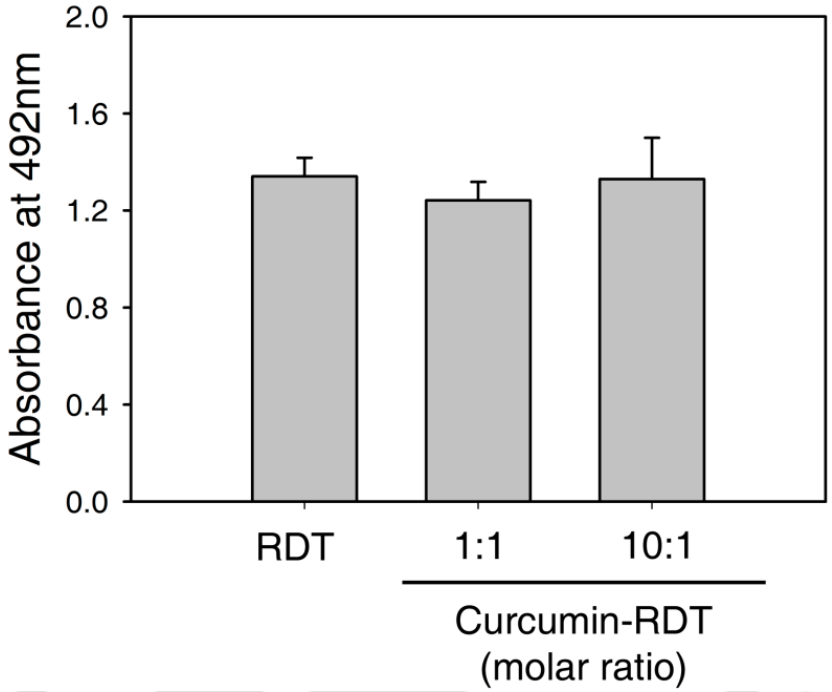

Figure 4.28: Solid phase ELISA to show that curcumin-RDT complex binds to HB-EGF. Recombinant human HB-EGF was coated on a microplate. After blocking, RDT (1 μM) or curcumin-RDT complexes with two different molar ratios (1 μM:1 μM and 10 μM:1 μM) was added and incubated for 2 hr at room temperature. Bound RDT was detected using mouse anti-His antibody followed by goat anti-mouse-HRP conjugated antibody and ELISA was developed by using OPD and the absorbance was measured at 492 nm. Each bar represent mean of three wells. One-way ANOVA: no significant difference between these three samples ($p = 0.454$).

4.3.5 Curcumin-RDT enhances cellular uptake of curcumin:

We have observed that curcumin-RDT complex binds to HB-EGF. Subsequently, we enquired whether this complex could bind to cell surface HB-EGF and deliver curcumin to human glioblastoma U-87 MG cells that expresses HB-EGF. Mishima et al. [75] have shown that HB-EGF is overexpressed in gliomas and induces proliferation of glioma cell lines *in vitro*. It has been shown that mutated DT, CRM197, increases permeability of blood-brain barrier and crosses the barrier [163, 165]. Therefore, DT or its derivatives like RDT can have potential

TH-1245_08610607

use in HB-EGF-targeted delivery in glioma. We used fluorescence microscopy to visualize delivery of curcumin to these cells. We incubated U-87 MG cells with curcumin, curcumin-RDT and curcumin-BSA complexes. After thorough washing, fluorescence microscopy was used to detect presence of curcumin. We did not observe green fluorescence of curcumin in these cells treated with curcumin alone (Figure 4.29, lower panel). This was expected as we have used very low concentration of curcumin (2 μM) and it is also known that curcumin has very low fluorescence in aqueous environment due to the quenching effect of water. Further, curcumin does not bind specifically to cell membrane and most of the curcumin must have got washed-off. As a control, we used curcumin-BSA complex in our experiment. Curcumin in complex with BSA has high and detectable fluorescence (as shown in Figure 4.24a). However, fluorescence signature of curcumin was not observed in cells treated with this complex (Figure 4.29, middle panel). This indicated that curcumin-BSA complex does not get attached to U-87 MG cells and may have got removed by washing. This is expected as BSA does not have any known specific binding to U-87 MG cells. Therefore, any curcumin-BSA complex bound to cells would get removed by washing. Like curcumin alone, curcumin-BSA complex can also get internalized through non-specific fluid phase endocytosis. However, as the concentration of the complex was low, this process will not lead to any detectable signal in the imaging experiment. On the other hand, fluorescence of curcumin was detected and found to be co-localized with U-87 MG cells when provided as curcumin-RDT complex (upper panel of Figure 4.29). Two aspects can be concluded from this observation: 1) the curcumin-RDT complex was retained even after washing as RDT has specific interactions with cell surface HB-EGF, and 2) a substantial portion of curcumin remains as curcumin-RDT complex that provides the required environment for enhanced and detectable fluorescence of curcumin. This imaging based experiment substantiated our expectation that curcumin-RDT complex would be able to deliver curcumin to

TH-1245_08610607

U-87 MG cells that express HB-EGF. However, this epi-fluorescence based experiment does not confirm uptake of curcumin by these cells. Curcumin attached to cell surface would also give rise to similar images. Therefore, we used HPLC to measure internalized curcumin.

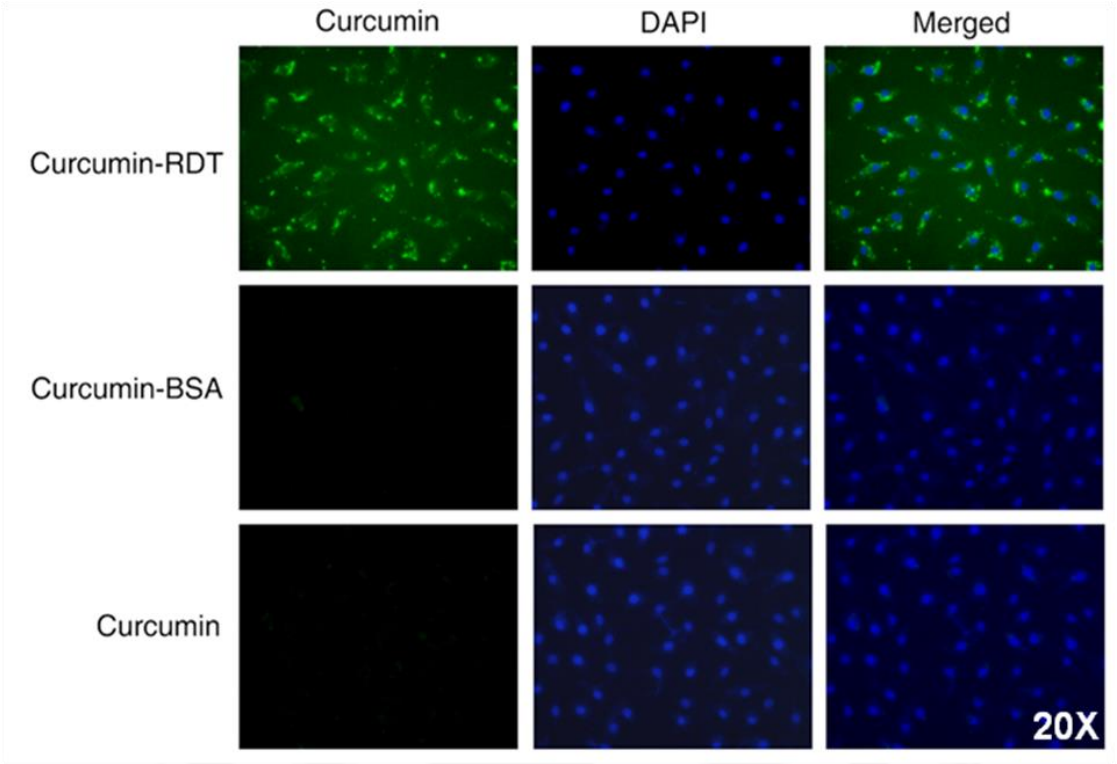

Figure 4.29: Curcumin-RDT enhances accumulation of curcumin in U-87 MG cells. U-87 MG cells in 6-well plates were incubated with curcumin (2 μM) and curcumin-protein complexes (molar ratio 10 μM:1 μM) for 4 hr in presence of serum at 37 °C. Subsequently, cells were washed with PBS and fixed. In all cases, nucleus was counter-stained with DAPI. Double-stained cells were imaged using a fluorescence microscope (Nikon Eclipse TiU). Filter for green fluorescence (B-2E/C, Nikon) was used for curcumin. DAPI was detected using UV-2E/C filter (Nikon). Fluorescence microscopy was done at 20× magnification.

TH-1245_08610607

U-87 MG cells were incubated with curcumin or curcumin-RDT/BSA complexes for 2 hr in presence of serum at 37 °C. Concentration of curcumin was 1 μM. Molar ratio of curcumin to proteins was 10 μM:1 μM. Subsequently, cells were washed thoroughly with PBS, harvested by trypsinization and internalized curcumin was extracted with methanol as described in the methods section. Both RDT and BSA have multiple cutting sites for trypsin. Therefore, repeated washes with PBS followed by trypsinization would remove curcumin of curcumin-protein complex bound to the cell surface. Subsequent methanolic extract will have curcumin that was present inside the cell. Contamination from cell surface bound curcumin will be nil or minimal. The methanolic extract was analyzed by HPLC to quantify the amount of curcumin present. Pure Curcumin in methanol was used as standard and quantification was achieved using a standard curve generated using this (Figure 4.30). We observed that when given as a complex with RDT, internalization of curcumin in U-87 MG cells was substantially higher than when given alone or in complex with BSA (Figure 4.31).

Fluorescence imaging followed by HPLC confirmed that cellular uptake of curcumin is higher when provided as curcumin-RDT complex. U-87 MG cells express HB-EGF on cell surface. Curcumin-RDT would bind to cell surface HB-EGF. Once bound, this complex may enter through receptor-mediated endocytosis. However, we do not have specific evidence for the same. DT is internalized through receptor-mediated endocytosis. It is not known whether RDT will have the same fate as rest of the domains are absent. Even then, it can be expected that internalization of curcumin will be higher when cells are treated with curcumin-RDT complex. Binding to cell surface HB-EGF would lead to accumulation of curcumin around the cell thereby increasing effective concentration. This will lead to enhanced internalization even by fluid-phase endocytosis.

TH-1245_08610607

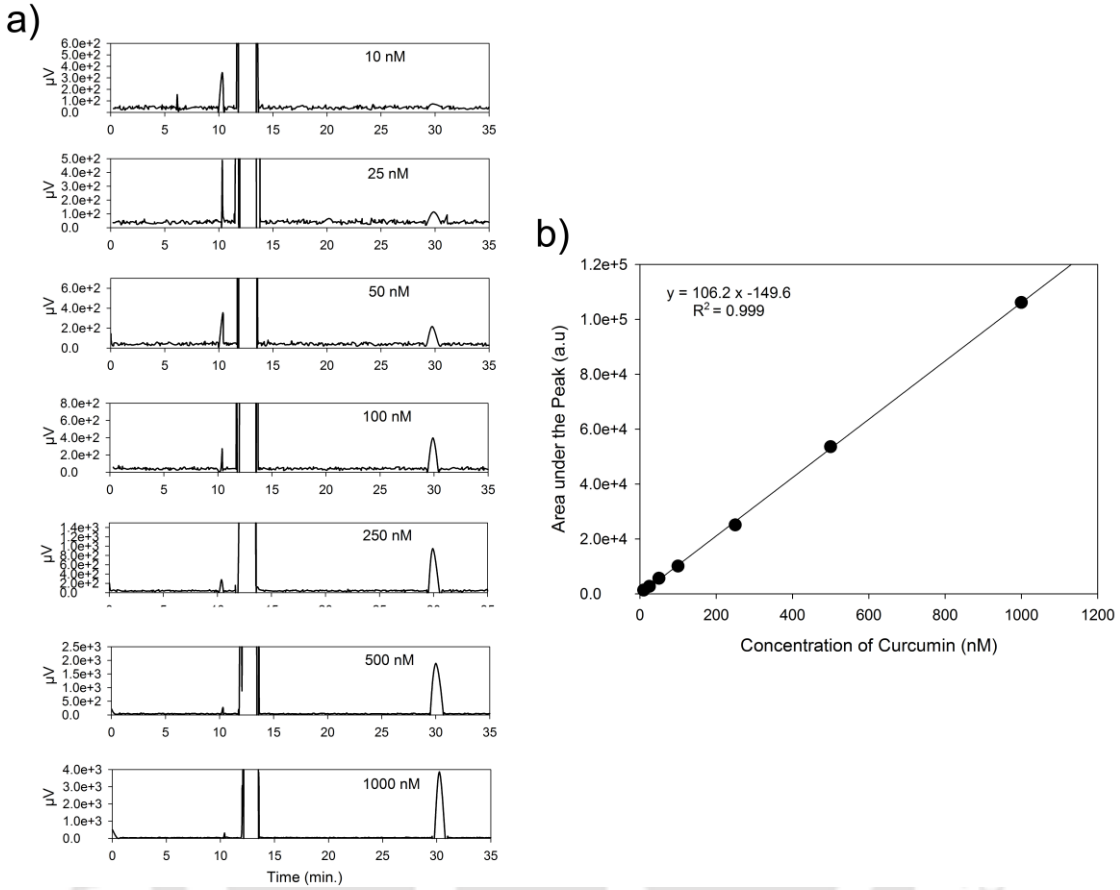

Figure 4.30: Standard curve for detection of curcumin in methanol by HPLC. (a) HPLC chromatograms of various conc. of curcumin in methanol. The peak around 30 min. corresponds to curcumin. (b) A standard curve for measuring conc. of curcumin in methanol. HPLC was performed using C18 column with 40% THF and 60% water containing 1% citric acid (pH 3.0) as mobile phase.

TH-1245_08610607

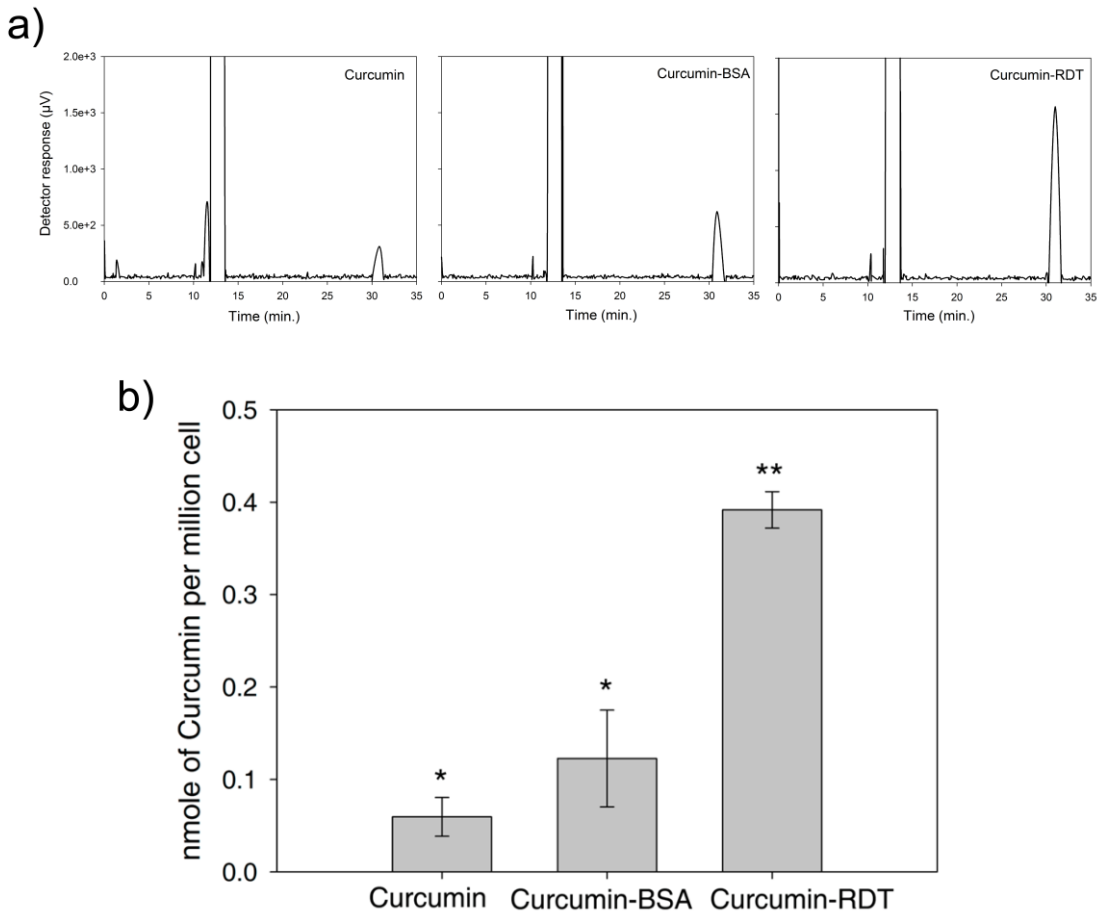

Figure 4.31: HPLC to detect enhanced cellular uptake of curcumin in U-87 MG cells. a) HPLC chromatograms of methanolic extracts of cells in different treatment groups. The peak around 30 min corresponds to curcumin. Data of a representative experiment is shown here. b) Bar plot showing the amount of internalized curcumin in cells in different treatment groups, as measured by HPLC. Each bas represent mean of three independent experiments. Cells were treated with curcumin (1 μM) or curcumin-protein complex (molar ratio 10 μM:1 μM) for 2 hr. One-way ANOVA with pair wise comparison: * no significant difference between these two ($p = 0.143$), ** significantly different from others ($p < 0.001$).

TH-1245_08610607

4.3.6 Curcumin-RDT complex has higher potency than curcumin:

We have observed that RDT binds curcumin and delivers to cells expressing HB-EGF, thereby enhancing cellular uptake. Enhanced delivery of curcumin should eventually lead to increased potency of curcumin. Curcumin is known to inhibit proliferation of wide varieties of cancer cells. It inhibits multiple pathways, including NF-κB and AP-1 pathways, leading to inhibition of cell proliferation and often triggers apoptosis [188, 193]. However, the IC_{50} for curcumin is usually high. Poor solubility in water and low uptake by cells may be the causes of such high IC_{50}.

Therefore, we investigated the effect of enhanced cellular uptake of curcumin via curcumin-RDT complex on human glioblastoma U-87 MG cells. We treated these cells with various amount of curcumin either alone or in complex with RDT and measured the viability of these cells after 72 hr of treatment using MTT. Although, the IC_{50} of curcumin for U-87 MG cells is high (40 μM [194]), we have used it at suboptimal doses. We observed that curcumin, in the concentration range of 1 – 20 μM, does not have considerable effect on the viability of U-87 MG cells (Figure 4.32). However, when used as curcumin-RDT complex, the viability of U-87 MG cells was reduced to ~65% in a dose-dependent fashion. The extent of inhibition was much higher than what was achieved by curcumin alone (Figure 4.32). This experiment strengthens our idea that increase in uptake of curcumin by RDT would increase its potency.

4.3.7 Effect of Curcumin-RDT is not synergistic:

The increase in the potency of curcumin may also happen due to the synergistic effect of RDT. Mutated DT, (CRM197) is known to block signaling through HB-EGF [118, 154]. Though not investigated, RDT should also be able to block signaling through HB-EGF. That may lead to down regulation of MAPK and PI3K pathways, thereby damping the canonical survival signals. Curcumin

TH-1245_08610607

modulates signaling through these two pathways [193] and blocking of HB-EGF by RDT may have potentiated that effect.

Therefore, an MTT assay was performed where curcumin and RDT were added sequentially. RDT was added first, so that it can bind and downregulate the signaling of HB-EGF and curcumin was added subsequently after one hour. As shown in Figure 4.33, sequential addition of RDT and curcumin does not increase the effect of curcumin. This ruled out the possible synergistic effect of RDT when given with curcumin.

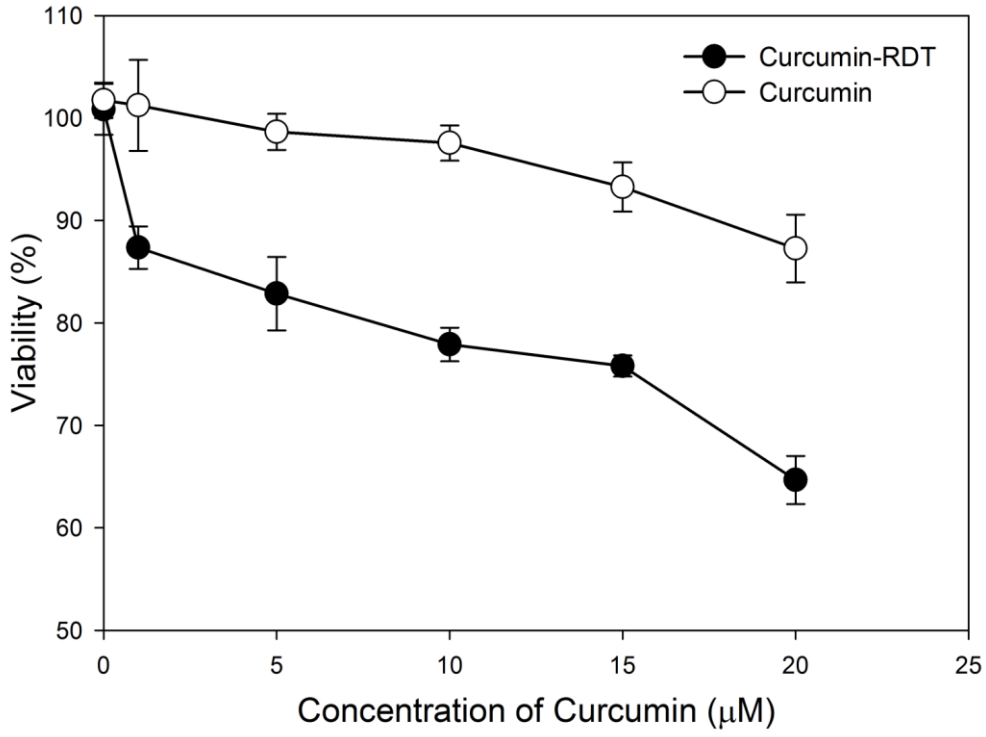

Figure 4.32: Effect of curcumin-RDT on viability of U-87 MG cells. Viability of cells was measured by MTT assay after 72 hr treatment in absence of serum. Concentration of RDT was 0.1 μM and concentration of curcumin was varied. Percentage of cell viability was calculated relative to cells treated with equivalent amount of ethanol in PBS. Each data point in the plot represents mean of four different wells. Two-way ANOVA with pair wise comparison indicates that there is significant difference in the viability of cells treated with curcumin and curcumin-RDT complex ($p<0.001$)

TH-1245_08610607

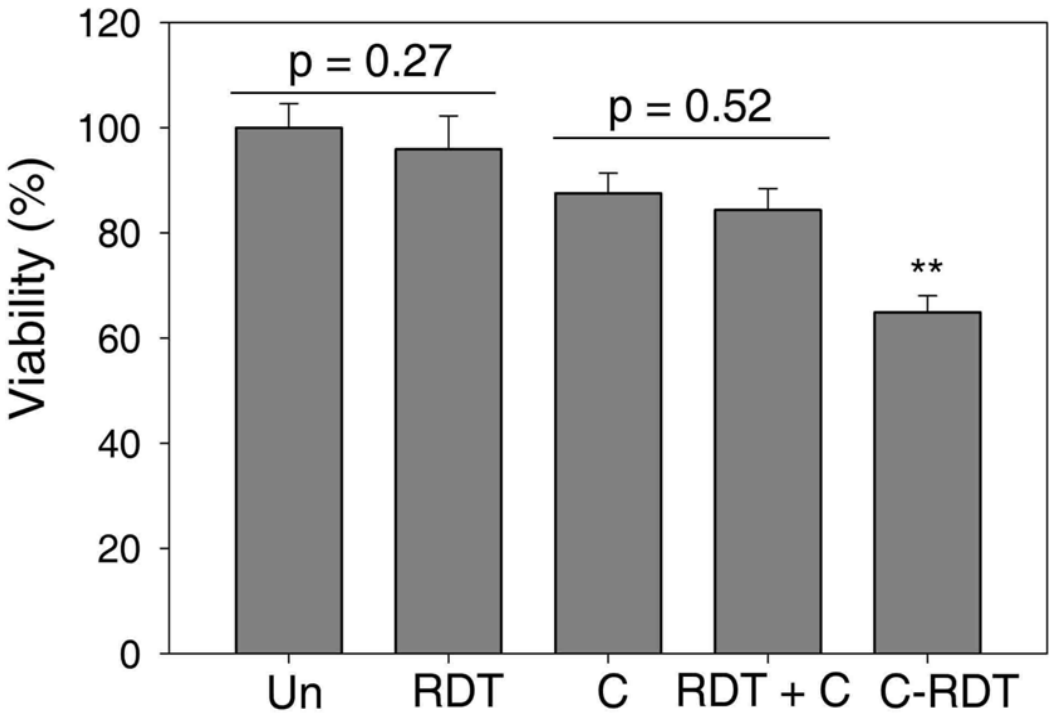

Figure 4.33: Effect of Curcumin-RDT is not synergistic. Viability of cells was measured by MTT assay after 72 hr treatment in absence of serum. Here, C: curcumin (20 μM), C-RDT: curcumin-RDT complex (20 μM:0.1 μM), RDT+ C: RDT (0.1 μM) followed by curcumin (20 μM), RDT: RDT (0.1 μM), Un: untreated. Each data point in the plot represents mean of four different wells. One way ANOVA with pair wise comparison was used. ** Significantly different from other treatment groups ($p < 0.001$).

4.3.8 Curcumin-RDT complex induces cell cycle arrest in U-87 MG cells:

Subsequently, we looked into the mechanism behind the anti-proliferating effect of curcumin-RDT complex. Curcumin is known to induce cell cycle arrest [188]. We performed a flow cytometry based experiment to understand the effect of curcumin-RDT on the cell cycle of U-87 MG cells. Distribution of cells in different phases of cell cycle was measured by flow cytometry after staining with PI. PI is a fluorogenic compound that binds to DNA by intercalating between the bases. PI binds stoichiometrically to nucleic acids so that fluorescence emission is proportional to the DNA content of a cell. U87

TH-1245_08610607

MG cells were treated in absence of serum, with Curcumin-RDT complex for 48 hr. After staining with PI, cell cycle analysis was done by flow cytometry. Result of one particular experiment is shown in Figure 4.34. It is evident from the histograms that treatment with curcumin-RDT complex reduced cells in G1 phase of the cell cycle and increased population in sub-G0/G1 (Figure 4.34a). The experiment was repeated and percentage of cells in different phases of cell cycle in different treatment groups is shown in Figure 4.34b. Treatment with curcumin-RDT leads to decrease in G1 phase with similar increase in cells in sub-G0/G1 phase. Apoptotic and necrotic cells constitute sub-G0/G1 phase. Curcumin is known to block cells at G1 phase [188]. Treatment with curcumin-RDT may be blocking cells at G1 phase and those cells are undergoing apoptosis, thereby increasing sub-G0/G1 population. A marginal increase in percentage of cells in S and G2/M phase was also observed for Curcumin-RDT treated cells (Figure 4.34a) but the change was not statistically significant.

4.3.9 Curcumin-RDT complex induces apoptosis in U-87 MG cells:

To identify apoptotic population in our experiment, we have used a Flow cytometry based assay. Loss of plasma membrane integrity is one of the earliest features of apoptosis. In apoptotic cells phosphatidylserine (PS) gets translocated from the inner to the outer leaflet of the plasma membrane, thereby exposing PS to the outer part of the cell membrane. Annexin V is a phospholipid-binding protein that has high affinity for PS, and binds to cells with exposed PS. Since externalization of PS occurs in the earlier stages of apoptosis, FITC Annexin V staining can identify apoptosis at an earlier stage. Extensive disruption of cell membrane happens at the late phase of apoptosis. Cells with compromised cell membrane, like in late phase of apoptosis or in necrosis, can be stained with propidium iodide (PI). Viable cells with intact membranes exclude PI. To differentiate the apoptotic and necrotic death,

TH-1245_08610607

staining with FITC Annexin V is used in conjunction with PI to identify early apoptotic cells (PI negative, FITC Annexin V positive) and late apoptotic cells (PI positive, FITC Annexin V positive).

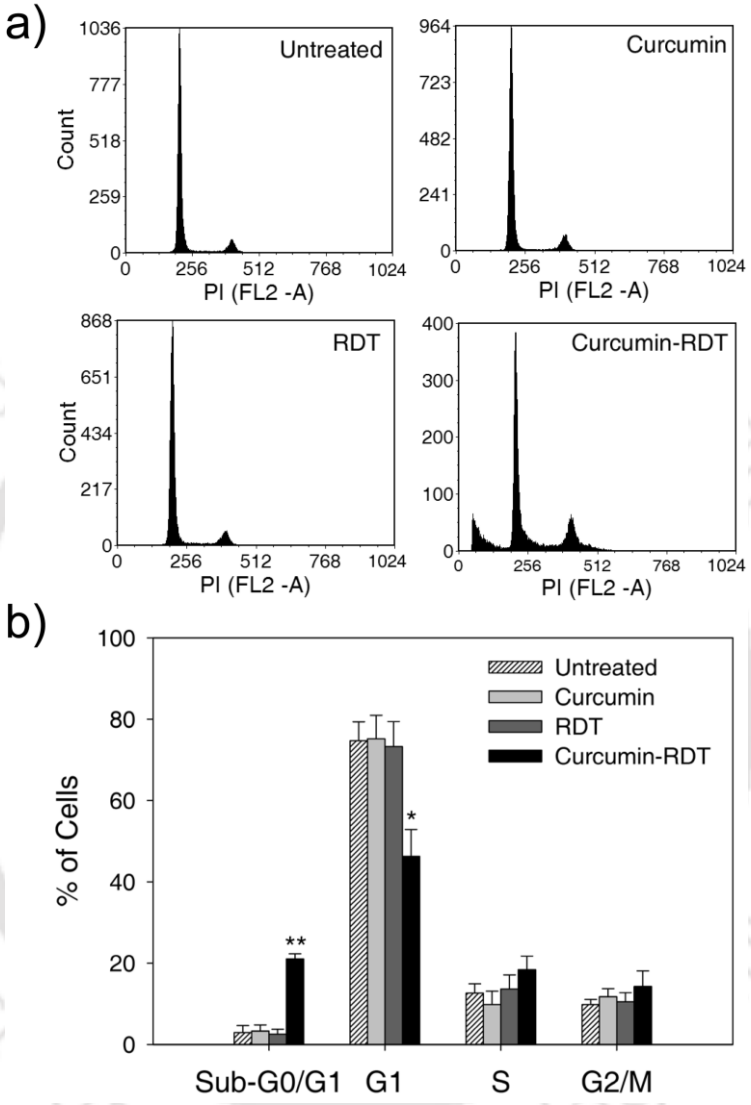

Figure 4.34: Effect of curcumin-RDT on distribution of cells in different stages of cell cycle. U-87 MG cells were treated with either curcumin (20 μM) or RDT (0.1 μM) or curcumin-RDT complex (20 μM:0.1 μM) or left untreated for 48 hr in absence of serum, were stained with PI and analyzed by flow cytometry. a) Histograms for PI intensity in different treatment groups in a representative experiment. b) Bar plot showing percentage of cells in different phases of cell cycle in different treatment groups. Each bar represents mean of three independent experiments. One way ANOVA with pairwise comparison: ** $p < 0.001$, * $p = 0.002$.

TH-1245_08610607

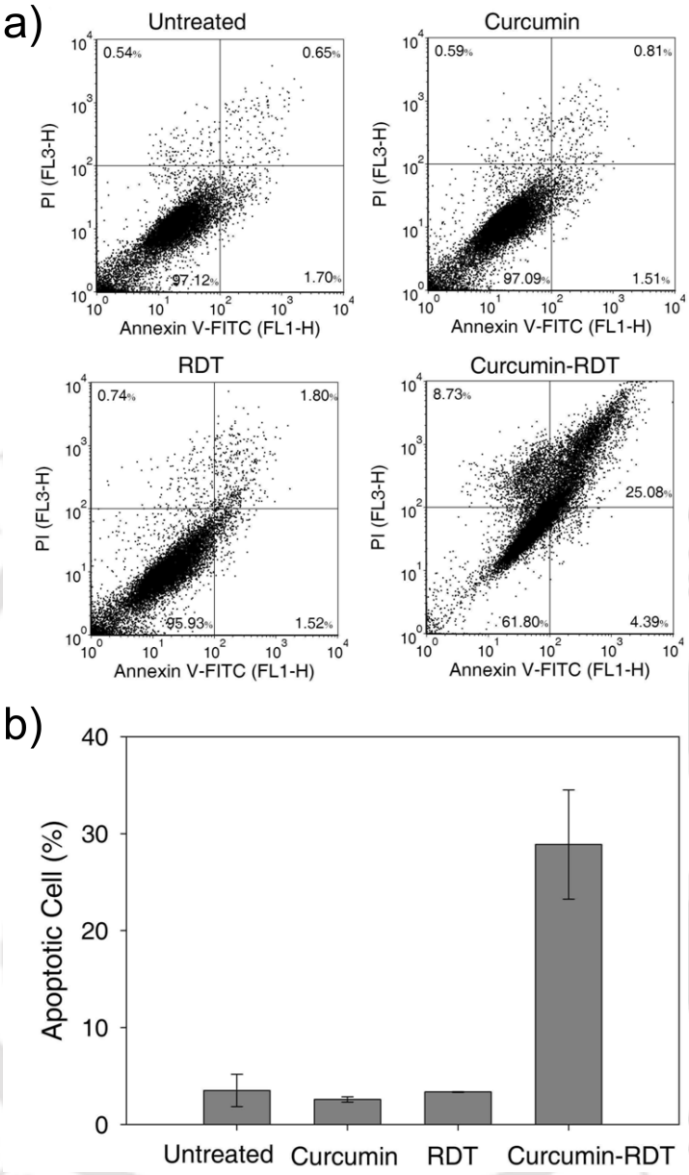

Figure 4.35: Curcumin-RDT complex induces apoptosis in U-87 MG cells. U-87 MG cells were treated with either curcumin (20 μM) or RDT (0.1 μM) or curcumin-RDT complex (20 μM:0.1 μM) or left untreated for 48 hr and analyzed by flow cytometry after double staining with PI and Annexin-V-FITC. a) Dot plots showing the flow cytometric data of a representative experiment. Cells present in lower and upper quadrants represent cells in early and late apoptosis respectively. b) Bar plot showing percentage of apoptotic cells in different treatment groups. Each bar represents mean of three independent experiments.

TH-1245_08610607

These experiments proved that cellular uptake and potency of curcumin increases when it is provided as curcumin-RDT complex. As shown in Figure 4.36, we have cloned, expressed and purified the R-domain of DT. This recombinant protein retains its HB-EGF binding. One can easily generate curcumin-RDT complex by incubating these two in required concentration. When cells expressing HB-EGF are treated with this complex, RDT facilitates enhanced uptake of curcumin. This enhancement in cellular uptake leads to potentiation of the cytotoxic effects of curcumin.

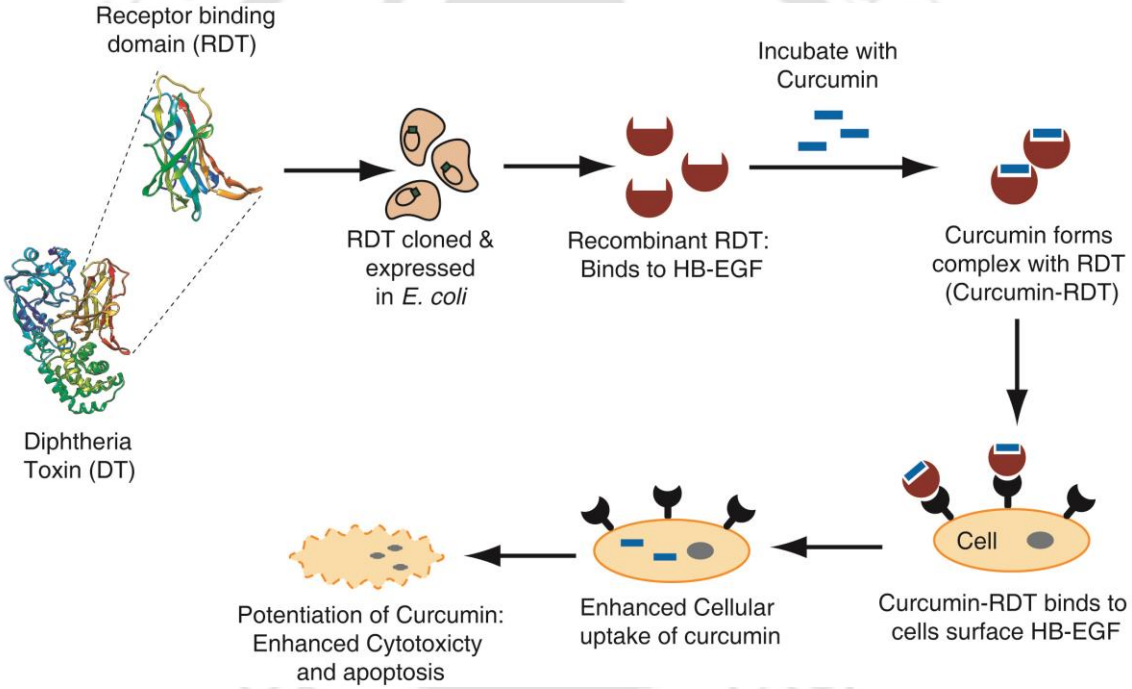

Figure 4.36: Using recombinant receptor-binding domain of Diphtheria toxin to enhance drug delivery.

TH-1245_08610607

4.4 Using RDT to increase potency of some chemotherapeutic agents:

Chemotherapeutic agents like Paclitaxel, Etoposide and Irinotecan, increase expression and ectodomain shedding of HB-EGF [117, 120, 123, 125]. Increase in soluble HB-EGF activates pro-survival and pro-proliferation signalling pathways by EGFR transactivation, thereby counteracting the effect of these chemotherapeutic agents. A ligand of HB-EGF may be used to block or sequester HB-EGF. When used in combination, such a molecule will potentiate chemotherapeutic agent. As shown earlier, RDT binds to recombinant HB-EGF as well as to HB-EGF on the surface of U-87 MG cells. Therefore, we hypothesized that RDT would also act as a specific inhibitor of HB-EGF and may enhance cytotoxicity of chemotherapeutic agents (Figure 4.37).

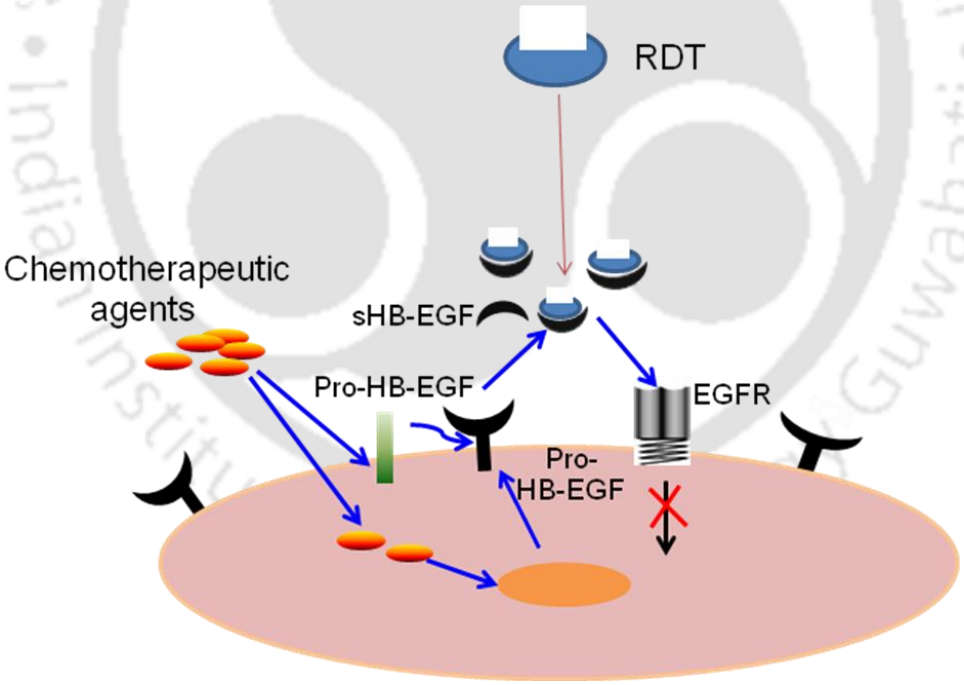

Figure 4.37: RDT may potentiate action of chemotherapeutics. Chemotherapeutic agents like Paclitaxel, Etoposide and Irinotecan, increase expression and shedding of HB-EGF. Increase in soluble HB-EGF promote pro-survival and pro-proliferation signaling, thereby counteracting the effect of these chemotherapeutic agents. RDT binds to HB-EGF and may be used to block or sequester HB-EGF. This will potentiate those chemotherapeutic agents.

TH-1245_08610607

4.4.1 Certain chemotherapeutic agents increase HB-EGF:

Chemotherapeutic agents like Paclitaxel (Taxol), Etoposide, Irinotecan, Doxorubicin and Cisplatin are known to increase the expression of HB-EGF. Therefore, we checked the expression of HB-EGF in cells following treatment with these agents. We performed reverse transcriptase-polymerase chain reaction (RT-PCR) to check the expression level of HB-EGF in cells treated with these anticancer drugs. U-87 MG and MCF-7 cells were treated with the drugs for 48 hr, respectively and expression of HB-EGF was measured. We observed that these chemotherapeutic agents induced HB-EGF expression in both the cell lines (Figure 4.38).

Chemotherapeutic agents are known to induce the ectodomain shedding of HB-EGF. Therefore, we treated U-87 MG cells and MCF-7 cells with these drugs and analyzed the shedding of soluble HB-EGF by measuring soluble HB-EGF in the culture medium by ELISA. As shown in Figure 4.39, the soluble HB-EGF in culture medium increased after treatment with different chemotherapeutic agents in both the cell lines.

TH-1245_08610607

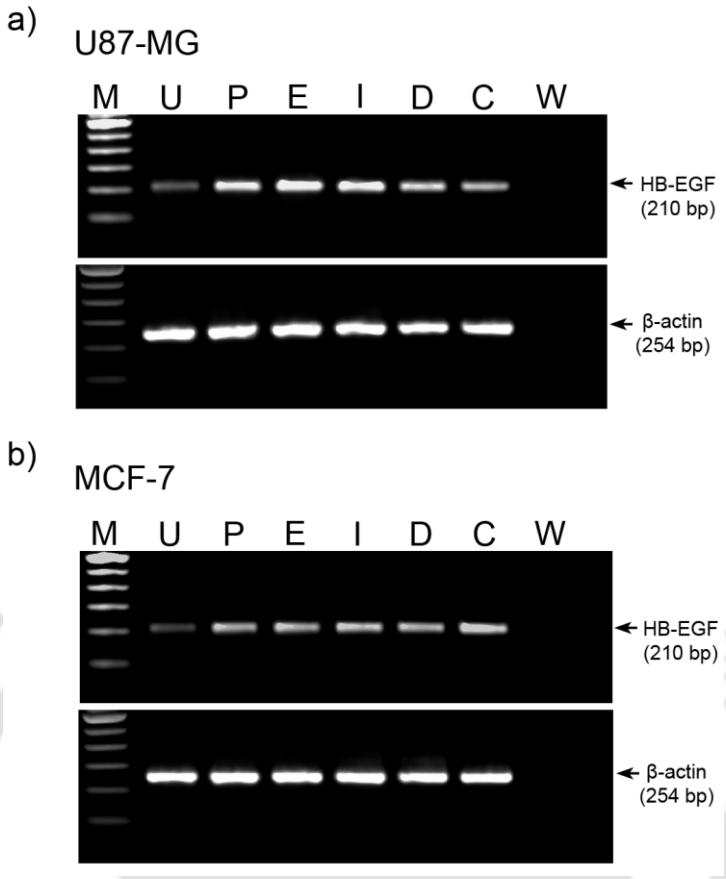

Figure 4.38: Chemotherapeutic agents increase expression of HB-EGF. RT-PCR to detect the expression of HB-EGF in (a) U-87 MG cells, and (b) MCF-7 cells, treated with different chemotherapeutic agents. β-actin was used as endogenous control. Drugs used were: P: Paclitaxel (1 μM), E: Etoposide (100 μM), I: Irinotecan (100 μM), D: Doxorubicin (0.2 μM), and C: Cisplatin (50 μM). U: Untreated cells and W: water, were used as controls. Cells were treated for 48 hr in serum free media.

TH-1245_08610607

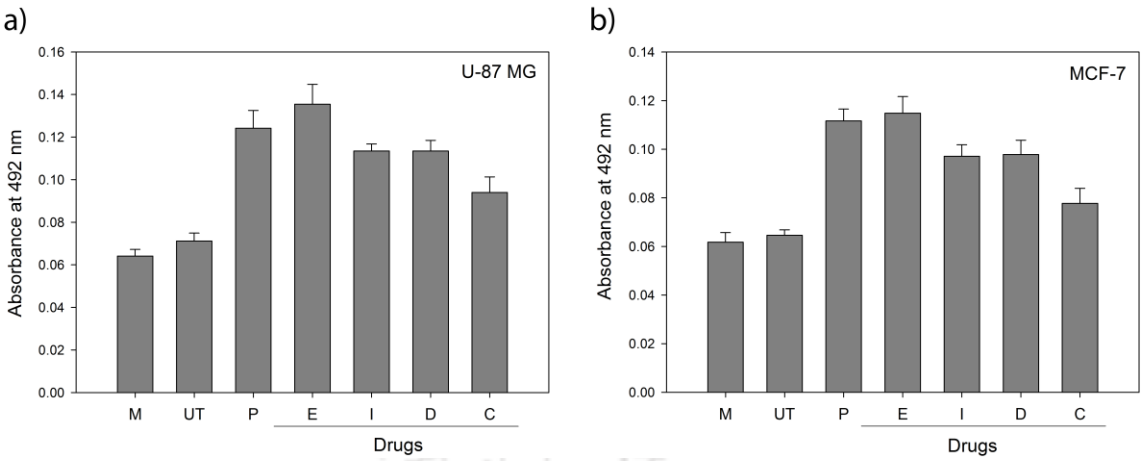

Figure 4.39: Chemotherapeutic agents increase soluble HB-EGF. ELISA to detect the soluble HB-EGF in the culture media for (a) U-87 MG cells, and (b) MCF-7 cells, treated with different chemotherapeutic agents. The soluble HB-EGF was detected by anti-HB-EGF antibody followed by HRP-conjugated mouse antibody. Drugs used were: P: Paclitaxel (1 μM), E: Etoposide (100 μM), I: Irinotecan (100 μM), D: Doxorubicin (0.2 μM), and C: Cisplatin (50 μM). M: Serum free media; UT: Untreated U-87 MG or MCF-7 cells. Cells were treated for 48 hr in serum free media.

4.4.2 RDT potentiates chemotherapeutic agents:

It has been reported earlier that co-administration of mutated DT, CRM197, with conventional chemotherapeutic agents resulted in synergistic antitumor effects [120, 122, 126, 195]. We anticipated having similar results with RDT. Therefore, we investigated the cytotoxic effects of several anti-cancer drugs namely, Paclitaxel (Taxol), Etoposide, Irinotecan, and Cisplatin in combination with RDT in two cell lines, U-87 MG and MCF-7. Both the cell lines were treated with various doses of these drugs in combination with RDT and the cell viability was measured by MTT assay. In our work on curcumin with RDT, we have prepared curcumin-RDT complex and then treated cells with that complex. But here in these assays, drugs and RDT were added simultaneously to the cells without any prior complexation. We observed that RDT significantly enhanced the cytotoxic effect of these drugs in both the cell lines (Figure 4.40 for U-87 MG

TH-1245_08610607

& Figure 4.41 for MCF-7). However, RDT alone does not have any effect on cell viability.

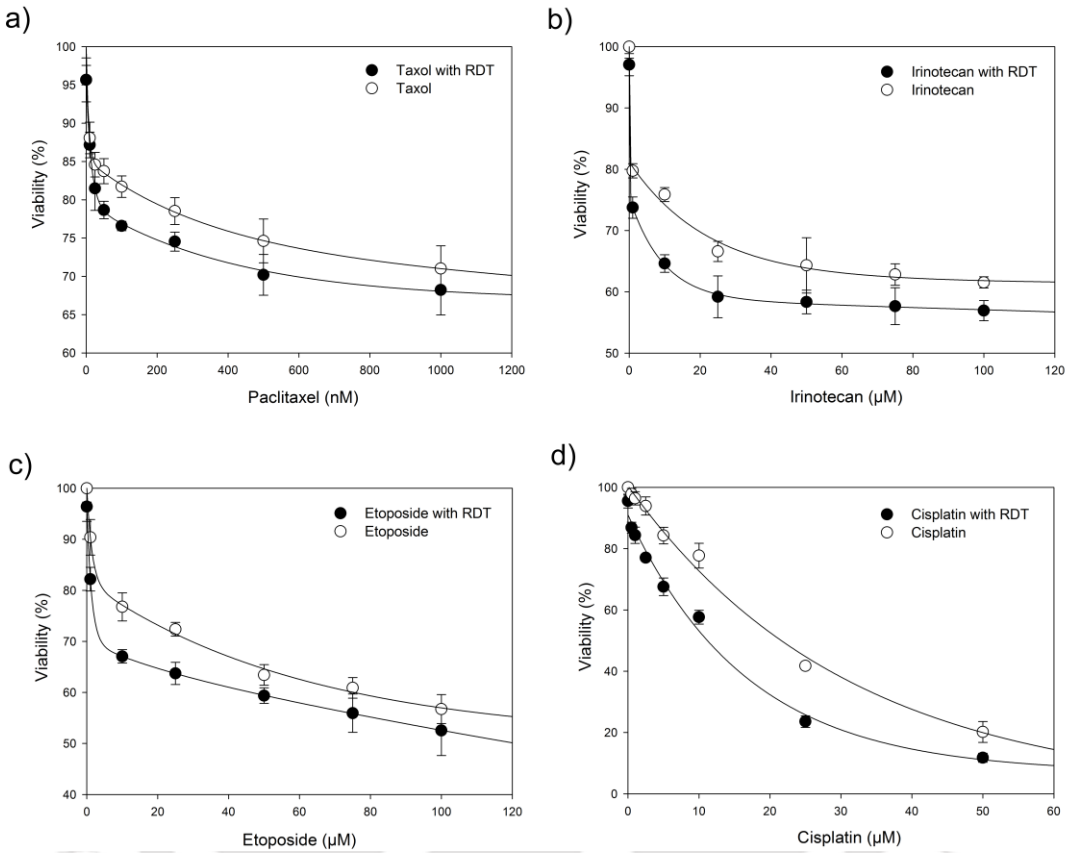

Figure 4.40: RDT potentiates chemotherapeutic agents in U-87 MG cells. Cell viability was measured by MTT assay after 48 hr of treatment with different concentrations of (a) Paclitaxel (Taxol), (b) Irinotecan, (c) Etoposide, and (d) Cisplatin in absence or presence of RDT (0.1 μM). Each data point in the plot represents mean of four different wells. Two- way ANOVA with pair wise comparison indicates that there is significant difference in the viability of cells treated with drugs and drugs with RDT ($p<0.001$). Experiments were performed in serum free media.

TH-1245_08610607

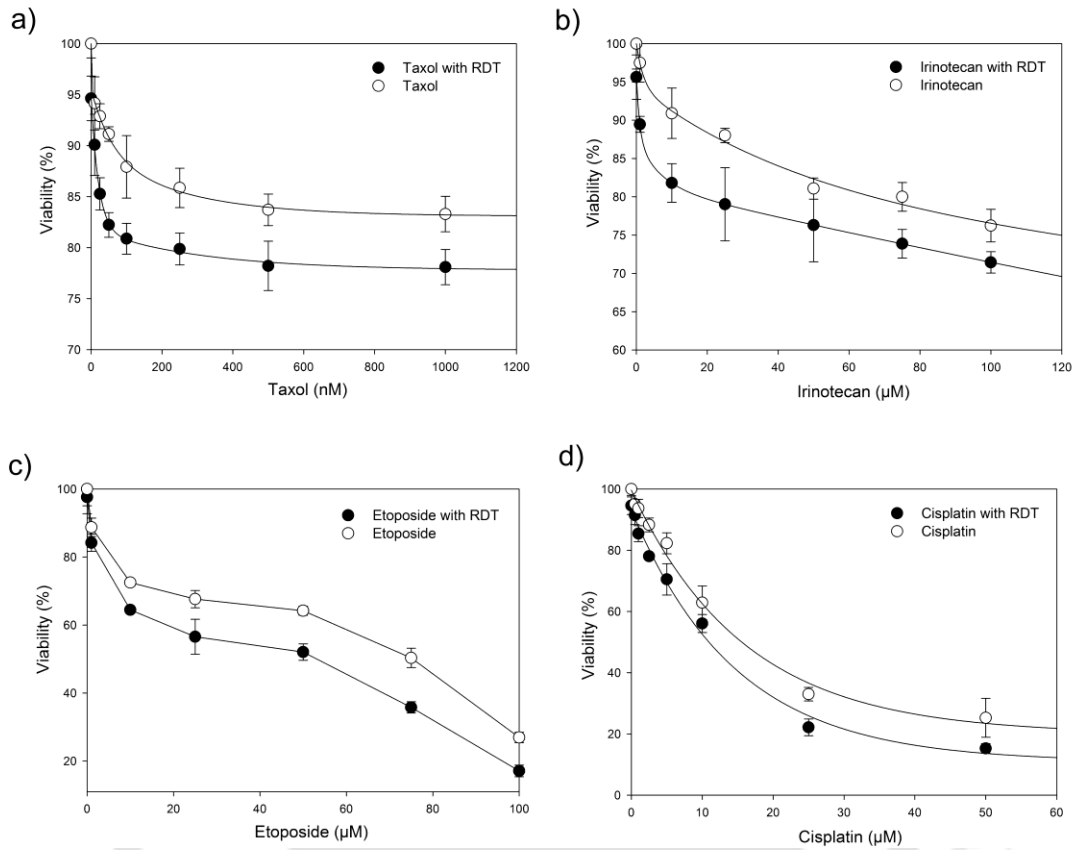

Figure 4.41: RDT potentiates chemotherapeutic agents in MCF-7 cells. Cell viability was measured by MTT assay after 48 hr of treatment with different concentrations of (a) Paclitaxel (Taxol), (b) Irinotecan, (c) Etoposide, and (d) Cisplatin in absence or presence of RDT (0.1 μM). Each data point in the plot represents mean of four different wells. Two- way ANOVA with pair wise comparison indicates that there is significant difference in the viability of cells treated with drugs and drugs with RDT ($p<0.001$). Experiments were performed in serum free media.

Based on these preliminary results, we focused on the combinatorial effect of Etoposide with RDT and Irinotecan with RDT. We treated both U-87 MG and MCF-7 cells with different doses of Etoposide or Irinotecan in combination with various doses of RDT and the cell viability were measured by MTT assay. The data of these experiments are shown in Figure 4.42 (for Etoposide) and Figure 4.43 (for Irinotecan). It is evident that RDT potentiate both the drug in a dose dependent fashion and this effect is consistent in both the cell lines.

TH-1245_08610607

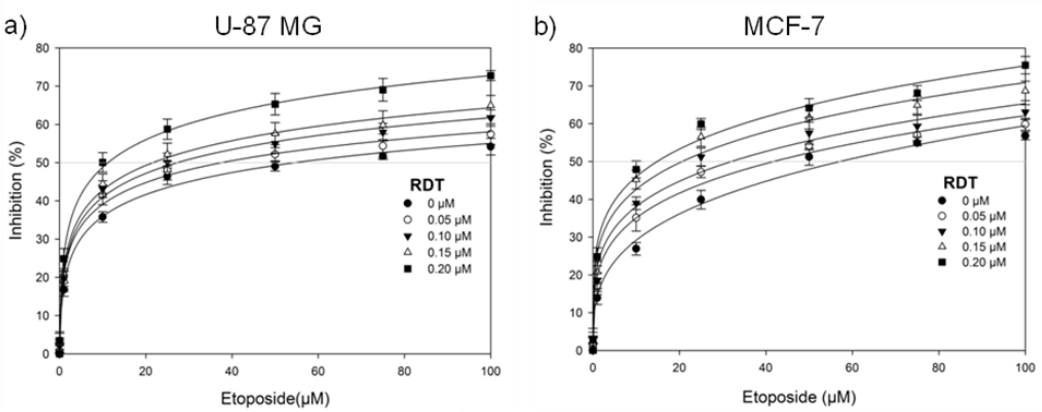

Figure 4.42: RDT potentiates Etoposide in U-87 MG and MCF-7 cells in a dose dependent fashion. Viability of cells was measured by MTT assay after 48 hr treatment in absence of serum with varied concentration of Etoposide and RDT in (a) U-87 MG cells, and (b) MCF-7 cells and % inhibition in cell viability was calculated. Each data point in the plot represents mean of four different wells. Two- way ANOVA with pair wise comparison indicates that there is significant difference among different treatment groups ($p<0.001$). The data were fitted to a power equation ($y = mx^n + c$) to calculate IC_{50}. The fitted curves are shown as solid lines.

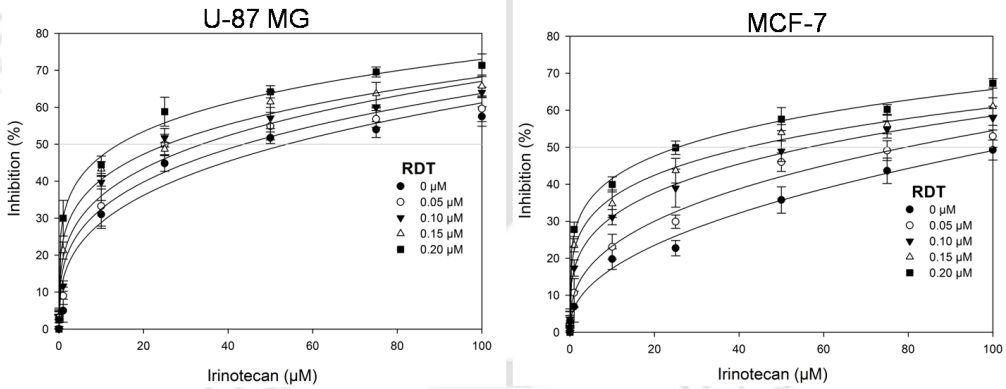

Figure 4.43: RDT potentiates Irinotecan in U-87 MG and MCF-7 cells in a dose dependent fashion. Viability of cells was measured by MTT assay after 48 hr treatment in absence of serum with varied concentration of Irinotecan and RDT in (a) U-87 MG cells, and (b) MCF-7 cells and % inhibition in cell viability was calculated. Each data point in the plot represents mean of four different wells. Two- way ANOVA with pair wise comparison indicates that there is significant difference among different treatment groups ($p<0.001$). The data were fitted to a power equation ($y = mx^n + c$) to calculate IC_{50}. The fitted curves are shown as solid lines.

TH-1245_08610607

Data of these MTT experiments were further analyzed to calculate the effect of concentration of RDT on the IC_{50} values of these drugs. The data were fitted to power equation, $y = mx^n + c$, where y = % inhibition and x = dose of the drug. IC_{50} in each case was calculated from these data fitting. Result of data fitting is shown in table 4.3. The dose dependent effects of RDT on the IC_{50} values of both the drugs are shown in figure 4.44 and figure 4.45. It is clear from these data that as expected RDT can potentiate the cytotoxic effect of these conventional chemotherapeutic agents.

Table 4.3: Results of data fitting of MTT experiments

RDT (μM)	Etoposide				Irinotecan			
	U-87 MG		MCF-7		U-87 MG		MCF-7	
	R^2	IC_{50} (μM)	R^2	IC_{50} (μM)	R^2	IC_{50} (μM)	R^2	IC_{50} (μM)
0	0.9814	**57.4842**	0.9856	**57.1607**	0.9556	**53.9328**	0.9670	**104.0623**
0.05	0.9761	**42.5689**	0.9858	**41.8224**	0.9529	**43.6597**	0.9716	**79.4532**
0.10	0.9810	**32.5654**	0.9840	**32.0254**	0.9677	**33.8146**	0.9841	**56.6011**
0.15	0.9764	**26.5666**	0.9810	**20.6357**	0.9831	**25.5990**	0.9862	**41.9083**
0.20	0.9850	**14.1773**	0.9878	**14.8658**	0.9857	**14.1777**	0.9906	**25.6005**

Data fitted to Power, 3 Parameter ($y = mx^n+c$) equation.

TH-1245_08610607

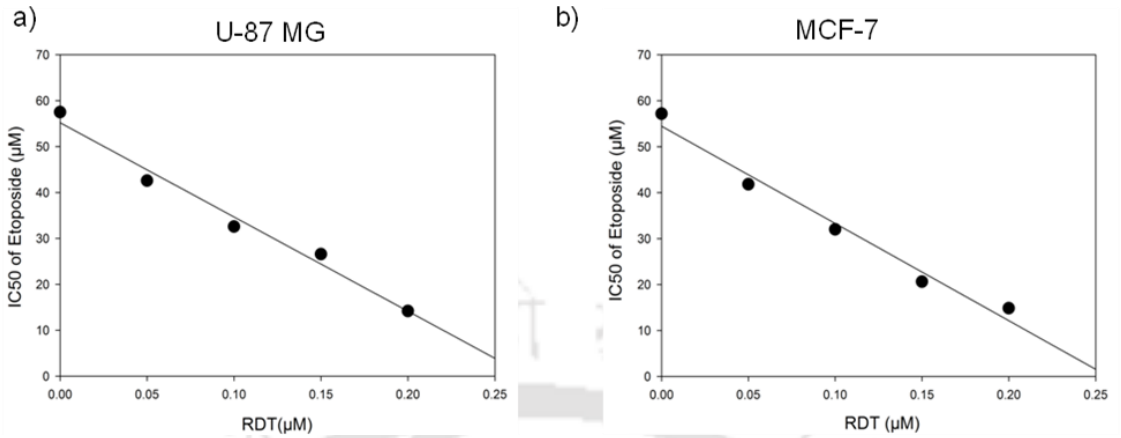

Figure 4.44: RDT decreases IC_{50} of Etoposide. Plots of RDT versus IC_{50} of Etoposide derived from MTT assays in (a) U-87 MG cells and (b) MCF-7 cells. RDT reduces the IC_{50} of Etoposide in both the cell lines in a dose-dependent manner.

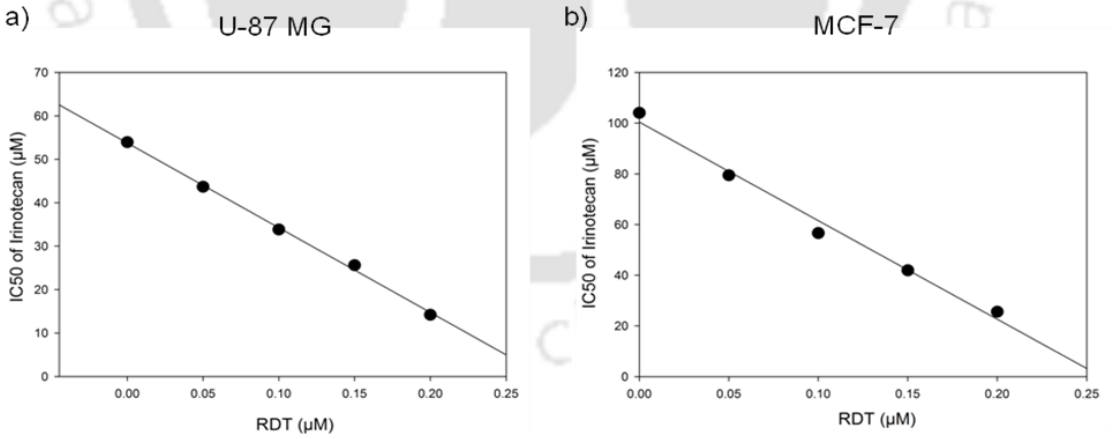

Figure 4.45: RDT decreases IC_{50} of Irinotecan. Plots of RDT versus IC_{50} of Etoposide derived from MTT assays in (a) U-87 MG cells and (b) MCF-7 cells. RDT reduces the IC_{50} of Irinotecan in both the cell lines in a dose-dependent manner.

TH-1245_08610607

4.4.3 RDT in combination with conventional chemotherapeutic agents down-regulates mitogenic pathways:

We have shown that some chemotherapeutic drugs increase expression as well as shedding of HB-EGF. We also observed that RDT in combination with these drugs, particularly Etoposide or Irinotecan, showed enhanced reduction in cell proliferation both in U-87 MG and MCF-7 cell lines. Elevated amount of soluble HB-EGF would activate two critical pro-proliferation and survival pathways, namely, MAPK and Akt pathways [74, 122]. RDT may inhibit such activities by blocking or sequestering soluble HB-EGF. This may in turn enhance the potency of these drugs as we have observed.

We performed Western blot experiment to detect the phosphorylation status of Erk1/2 and Akt in U-87 MG cells treated with RDT and Etoposide/Irinotecan for 24 hr in absence of serum. Activation of EGFR by HB-EGF induces phosphorylation of Erk1/2. As shown in Figure 4.46, treatment with Irinotecan increases phospho-Erk1/2. This indicates activation of this pathway in these drug treated cells. However, the same pathway does not get activated when cells were treated with Irinotecan in presence of RDT (Figure 4.46). This indicates that RDT is blocking the Irinotecan induced activation of Erk pathway. RDT alone does not affect the pathway (Figure 4.46). We have not observed any increase in phosphorylation of Akt in Etoposide or Irinotecan treated cells. However, cells treated with drug and RDT has lower phospho Akt than drug treated cells. RDT alone does not affect Akt phosphorylation.

These observations, together with earlier results of MTT assays suggested that RDT might be blocking EGFR trans-activation by HB-EGF. The inhibition of HBEGF reduced the strength pro-proliferative pathways that counteract the chemotherapeutic agents. Therefore, combinatorial treatment with RDT decreases IC_{50} of these drugs.

TH-1245_08610607

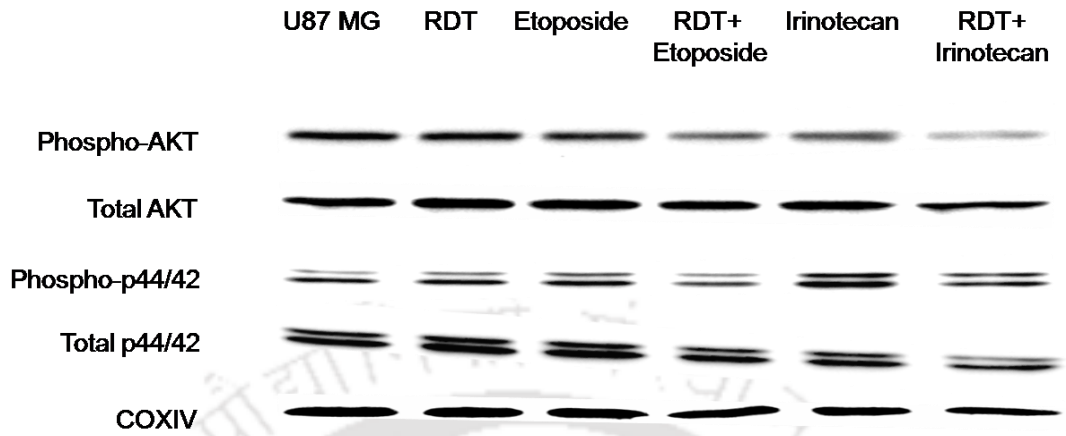

Figure 4.46: Effect of RDT on mitogenic pathways in U-87 MG cells. Western blots to detect phosphorylation of p44/42 and Akt in U-87 MG cells treated with RDT (0.2 μM), Etoposide (100 μM) or Irinotecan (100 μM) alone and RDT in combination with Etoposide or Irinotecan for 24 hr in serum free media. COXIV was used as loading control.

In this part of the work, we have shown that chemotherapeutic agents, Etoposide and Irinotecan increases expression and ectodomain shedding of HB-EGF. Our hypothesis was that such increase in HB-EGF offsets the cytotoxicity of these drugs and RDT being a binder of HB-EGF should sequester HB-EGF, thereby increasing cytotoxicity of these drugs. Using systematic experiments we have shown that our hypothesis is correct and RDT indeed acts like an adjuvant to potentiate the effect of these chemotherapeutic agents

TH-1245_08610607

5 Conclusions & Scope for future work

We have cloned and expressed the receptor-binding domain of Diphtheria toxin (RDT) using an *E. coli* expression system and purified this recombinant protein by affinity chromatography. We have used this protein to investigate its possible therapeutic utilities. Cell surface HB-EGF is a receptor for Diphtheria toxin and is over-expressed in several types of cancer and is also involved in oncogenic signaling leading to deregulated cell proliferation, migration of cancer cells, angiogenesis, and development of resistance. Therefore, HB-EGF is a good target for homing therapeutic agents. An HB-EGF binding protein can be used for homing therapeutic agents as well as for blocking oncogenic signaling. We investigated the binding ability of RDT by a series of experiments and observed that this protein retains receptor binding ability and binds to cells expressing HB-EGF and the binding affinity of RDT to HB-EGF was found to be equivalent to that of full-length DT.

Certain hydrophobic drugs have low solubility in water, low bioavailability and low cellular uptake. We explored the utility of RDT as a receptor specific drug carrier using curcumin as a representative hydrophobic therapeutic molecule. Curcumin is known to bind to proteins through hydrophobic interactions. Structural analysis of RDT showed that RDT has several hydrophobic patches on the surface. Our investigation using molecular docking revealed that curcumin may bind to RDT. Therefore, we investigated the binding ability of RDT to curcumin. We have proved that curcumin binds to RDT and binding of curcumin to RDT enhances the fluorescence of curcumin and increases the average lifetime of fluorescence decay.

TH-1245_08610607

Further, we investigated the binding ability of curcumin-RDT complex to HB-EGF. We have observed that Curcumin-RDT complex binds to HB-EGF and gets associated with human glioblastoma cells (U-87 MG) expressing the receptor. It was also observed that RDT can carry and deliver the bound curcumin to these cells leading to enhanced uptake of curcumin. Enhanced delivery of curcumin eventually leads to potentiation of the anti-proliferative effect of curcumin. Subsequently, we investigated the mechanism behind the anti-proliferative effect of curcumin-RDT complex. Curcumin is known to inhibit multiple pathways, including NF-κB and AP-1 pathways, leading to inhibition of cell proliferation and apoptosis. We have shown that when delivered as curcumin-RDT complex, curcumin induced apoptosis of these cells even at a low dose. Such increase in the effect of curcumin may also happen due to the synergistic effect of RDT. We have proved that RDT does not show any synergistic effect with curcumin. Considering these observations, we proved that RDT is potentiating the effect of curcumin by increasing its delivery to target cells.

This work demonstrates that receptor and drug-binding ability of a bacterial toxin can be used to create a system that enhances cellular uptake and potency of a drug. One can consider curcumin-RDT as a proof-of-concept. Many other therapeutically active small molecules may bind to RDT and RDT may be used to enhance their cellular uptake.

We have established that RDT increases cellular uptake of curcumin. However, the exact mechanism of enhanced uptake is unknown. In future, one can investigate whether the process involves receptor mediated endocytosis or only the passive fluid phase endocytosis. This will also establish the independent role of the receptor-binding domain of DT in its receptor–mediated endocytosis. All the experiments reported here were performed *in vitro*. In future, *in vivo* experiments should be performed using suitable animal model to explore the utility of curcumin-RDT complex in enhanced delivery to solid tumors overexpressing HB-EGF. Being smaller than full-length DT, RDT is expected to

TH-1245_08610607

have higher tissue penetration and be less immunogenic. However, suitable *in vivo* experiment can only clarify these issues. If required RDT may be modified to reduce immunogenicity and to enhance its *in vivo* stability, by chemical modifications like PEGylation. In this work, we have explored curcumin-RDT complex. One may try to develop carriers, like liposomes or nanoparticles, crowned with RDT to create HB-EGF targeted drug delivery system.

HB-EGF is known to be associated with emergence of drug resistance in cancers. It has been shown that certain chemotherapeutic agents, like Paclitaxel, enhance expression and ectodomain shedding of HB-EGF. Increase in HB-EGF counter acts the cytotoxic effects of these drugs and a blocker of HB-EGF can increase the potency of these drugs. Here, we have shown that drugs like Paclitaxel, Etoposide, Irinotecan, and Cisplatin increase expression and shedding of HB-EGF in U-87 MG and MCF-7 cells. We focused on Etoposide and Irinotecan. Results shown in this work establishes that when given in combination with these drugs, RDT reduces the IC_{50} values of these drugs in a dose dependent fashion and this is achieved possibly by blocking or sequestering HB-EGF.

This shows that RDT may be used as an adjuvant to potentiate conventional chemotherapeutic agents. We have established the drug potentiation and have provided clues to explain such potentiation. However, detail study is required on the effects of RDT alone or in combination with chemotherapeutics on key survival and oncogenic signaling pathways. Targeting HB-EGF achieves two objectives: cell specific drug delivery and blocking of oncogenic signaling. The present work has shown that RDT can be used to achieve both. One can even create a RDT-mediated targeted delivery for a conventional chemotherapeutics, like Etoposide. Such drug delivery system would ensure enhanced cell-specific delivery of the drug and would also reduce the drug induced increase in oncogenic signaling.

TH-1245_08610607

Bibliography

1. Venditti, J.M., *Preclinical drug development: rationale and methods.* Semin Oncol, 1981. **8**(4): p. 349-61.
2. Narang, A. and D. Desai, *Anticancer Drug Development*, in *Pharmaceutical Perspectives of Cancer Therapeutics*, Y. Lu and R.I. Mahato, Editors. 2009, Springer US. p. 49-92.
3. Savjani, K.T., A.K. Gajjar, and J.K. Savjani, *Drug solubility: importance and enhancement techniques.* ISRN Pharm, 2012. **2012**: p. 195727.
4. Stegemann, S., et al., *When poor solubility becomes an issue: From early stage to proof of concept.* European Journal of Pharmaceutical Sciences, 2007. **31**(5): p. 249-261.
5. Thakur Anil Kumar, N., Harikumar S L., *VARIOUS TECHNIQUES ENHANCING BIOAVAILABILTY OF POORLY WATER SOLUBLE DRUGS.* Journal of Drug Delivery & Therapeutics, 2013. **3**(2): p. 215-221.
6. Chaudhary, A., et al., *Enhancement of solubilization and bioavailability of poorly soluble drugs by physical and chemical modifications: a recent review.* J Adv Pharm Educ Res, 2012. **2**(1): p. 32-67.
7. Brewster, M.E. and T. Loftsson, *Cyclodextrins as pharmaceutical solubilizers.* Adv Drug Deliv Rev, 2007. **59**(7): p. 645-66.
8. Loftsson, T. and M.E. Brewster, *Pharmaceutical applications of cyclodextrins. 1. Drug solubilization and stabilization.* J Pharm Sci, 1996. **85**(10): p. 1017-25.
9. Becket, G., L.J. Schep, and M.Y. Tan, *Improvement of the in vitro dissolution of praziquantel by complexation with alpha-, beta- and gamma-cyclodextrins.* Int J Pharm, 1999. **179**(1): p. 65-71.
10. Carrier, R.L., L.A. Miller, and M. Ahmed, *The utility of cyclodextrins for enhancing oral bioavailability.* Journal of Controlled Release, 2007. **123**(2): p. 78-99.
11. Schwendener, R.A., *Liposomes in biology and medicine.* Adv Exp Med Biol, 2007. **620**: p. 117-28.
12. Lu, Y. and K. Park, *Polymeric micelles and alternative nanonized delivery vehicles for poorly soluble drugs.* Int J Pharm, 2013. **453**(1): p. 198-214.

TH-1245_08610607

13. Sapkal Sandip, N.M., Babhulkar Mukesh , Mehetre Gautam, Rathi Ashish., *Natural polymers: Best carriers for improving bioavailability of poorly water soluble drugs in solid dispersions. .* Marmara Pharmaceutical Journal 2013. **17**: p. 65-72.
14. Kratz, F., *Albumin as a drug carrier: Design of prodrugs, drug conjugates and nanoparticles.* Journal of Controlled Release, 2008. **132**(3): p. 171-183.
15. Elzoghby, A.O., W.M. Samy, and N.A. Elgindy, *Protein-based nanocarriers as promising drug and gene delivery systems.* Journal of Controlled Release, 2012. **161**(1): p. 38-49.
16. Fasano, M., et al., *The extraordinary ligand binding properties of human serum albumin.* IUBMB Life, 2005. **57**(12): p. 787-796.
17. Sneharani, A.H., et al., *Interaction of Curcumin with beta-Lactoglobulin-Stability, Spectroscopic Analysis, and Molecular Modeling of the Complex.* J Agric Food Chem, 2010. **58**: p. 11130-11139.
18. Cardoso, M.C. and H. Leonhardt, *Protein transduction: a novel tool for tissue regeneration.* Biol Chem, 2002. **383**(10): p. 1593-9.
19. Ziegler, A., *Thermodynamic studies and binding mechanisms of cell-penetrating peptides with lipids and glycosaminoglycans.* Adv Drug Deliv Rev, 2008. **60**(4-5): p. 580-97.
20. Madani, F., et al., *Mechanisms of cellular uptake of cell-penetrating peptides.* J Biophys, 2011. **2011**: p. 414729.
21. Wender, P.A., et al., *The design, synthesis, and evaluation of molecules that enable or enhance cellular uptake: Peptoid molecular transporters.* Proc Natl Acad Sci U S A, 2000. **97**(24): p. 13003-13008.
22. Chen, L., et al., *Molecular transporters for peptides: delivery of a cardioprotective epsilonPKC agonist peptide into cells and intact ischemic heart using a transport system, R(7).* Chem Biol, 2001. **8**(12): p. 1123-9.
23. Rothbard, J.B., et al., *Conjugation of arginine oligomers to cyclosporin A facilitates topical delivery and inhibition of inflammation.* Nat Med, 2000. **6**(11): p. 1253-7.
24. Robbins, P.B., et al., *Peptide delivery to tissues via reversibly linked protein transduction sequences.* Biotechniques, 2002. **33**(1): p. 190-2, 194.
25. Jeang, K.T., H. Xiao, and E.A. Rich, *Multifaceted activities of the HIV-1 transactivator of transcription, Tat.* J Biol Chem, 1999. **274**(41): p. 28837-40.
26. Green, M. and P.M. Loewenstein, *Autonomous functional domains of chemically synthesized human immunodeficiency virus tat trans-activator protein.* Cell, 1988. **55**(6): p. 1179-88.

TH-1245_08610607

27. Vives, E., P. Brodin, and B. Lebleu, *A truncated HIV-1 Tat protein basic domain rapidly translocates through the plasma membrane and accumulates in the cell nucleus.* Journal of Biological Chemistry, 1997. **272**(25): p. 16010-16017.
28. Tunnemann, G., et al., *Cargo-dependent mode of uptake and bioavailability of TAT-containing proteins and peptides in living cells.* FASEB J, 2006. **20**(11): p. 1775-84.
29. Booser, D.J., et al., *Phase II study of liposomal annamycin in the treatment of doxorubicin-resistant breast cancer.* Cancer Chemother Pharmacol, 2002. **50**(1): p. 6-8.
30. Lamprecht, A., et al., *Nanoparticles enhance therapeutic efficiency by selectively increased local drug dose in experimental colitis in rats.* J Pharmacol Exp Ther, 2005. **315**(1): p. 196-202.
31. Liu, Z., R. Bendayan, and X.Y. Wu, *Triton-X-100-modified polymer and microspheres for reversal of multidrug resistance.* J Pharm Pharmacol, 2001. **53**(6): p. 779-87.
32. de Verdiere, A.C., et al., *Reversion of multidrug resistance with polyalkylcyanoacrylate nanoparticles: towards a mechanism of action.* Br J Cancer, 1997. **76**(2): p. 198-205.
33. Moghimi, S.M. and A.C. Hunter, *Poloxamers and poloxamines in nanoparticle engineering and experimental medicine.* Trends Biotechnol, 2000. **18**(10): p. 412-20.
34. Thierry, A.R., et al., *Modulation of doxorubicin resistance in multidrug-resistant cells by liposomes.* FASEB J, 1993. **7**(6): p. 572-9.
35. Romsicki, Y. and F.J. Sharom, *The membrane lipid environment modulates drug interactions with the P-glycoprotein multidrug transporter.* Biochemistry, 1999. **38**(21): p. 6887-96.
36. Wong, H.L., et al., *Development of solid lipid nanoparticles containing ionically complexed chemotherapeutic drugs and chemosensitizers.* J Pharm Sci, 2004. **93**(8): p. 1993-2008.
37. Wong, H.-L., et al., *Novel solid lipid nanoparticles formulations increase the cytotoxicity and prolong the cellular accumulation of doxorubicin in human multidrug-resistant breast cancer cells.* AACR Meeting Abstracts, 2005. **2005**(1): p. 336-.
38. Veldman, R.J., et al., *Coformulated N-octanoyl-glucosylceramide improves cellular delivery and cytotoxicity of liposomal doxorubicin.* J Pharmacol Exp Ther, 2005. **315**(2): p. 704-10.

TH-1245_08610607

39. Wong, H.L., et al., *A mechanistic study of enhanced doxorubicin uptake and retention in multidrug resistant breast cancer cells using a polymer-lipid hybrid nanoparticle system.* Journal of Pharmacology and Experimental Therapeutics, 2006. **317**(3): p. 1372-1381.
40. Tallarida, R.J., *Drug synergism: Its detection and applications.* Journal of Pharmacology and Experimental Therapeutics, 2001. **298**(3): p. 865-872.
41. Pritchard, J.R., et al., *Defining principles of combination drug mechanisms of action.* Proceedings of the National Academy of Sciences, 2012.
42. Jia, J., et al., *Mechanisms of drug combinations: interaction and network perspectives.* Nat Rev Drug Discov, 2009. **8**(2): p. 111-28.
43. Lee, J.H. and A. Nan, *Combination drug delivery approaches in metastatic breast cancer.* J Drug Deliv, 2012. **2012**: p. 915375.
44. Lin, X.J., H.K. Kim, and S.B. Howell, *The role of DNA mismatch repair in cisplatin mutagenicity.* J Inorg Biochem, 1999. **77**(1-2): p. 89-93.
45. Rhee, I., et al., *DNMT1 and DNMT3b cooperate to silence genes in human cancer cells.* Nature, 2002. **416**(6880): p. 552-556.
46. van Waardenburg, R.C.A.M., et al., *Platinated DNA adducts enhance poisoning of DNA topoisomerase I by camptothecin.* Journal of Biological Chemistry, 2004. **279**(52): p. 54502-54509.
47. Lai, G.H., Z.C. Zhang, and A.E. Sirica, *Celecoxib acts in a cyclooxygenase-2-independent manner and in synergy with emodin to suppress rat cholangiocarcinoma growth in vitro through a mechanism involving enhanced Akt inactivation and increased activation of caspases-9 and -3.* Mol Cancer Ther, 2003. **2**(3): p. 265-271.
48. Cottagnoud, P., M. Cottagnoud, and M.G. Tauber, *Vancomycin acts synergistically with gentamicin against penicillin-resistant Pneumococci by increasing the intracellular penetration of gentamicin.* Antimicrobial Agents and Chemotherapy, 2003. **47**(1): p. 144-147.
49. Pegram, M.D., et al., *Rational combinations of trastuzumab with chemotherapeutic drugs used in the treatment of breast cancer.* J Natl Cancer Inst, 2004. **96**(10): p. 739-49.
50. Pinto, C., et al., *Phase II study of cetuximab in combination with FOLFIRI in patients with untreated advanced gastric or gastroesophageal junction adenocarcinoma (FOLCETUX study).* Ann Oncol, 2007. **18**(3): p. 510-7.
51. Van Cutsem, E., et al., *Efficacy results from the ToGA trial: A phase III study of trastuzumab added to standard chemotherapy (CT) in first-line human*

TH-1245_08610607

epidermal growth factor receptor 2 (HER2)-positive advanced gastric cancer (GC). Journal of Clinical Oncology, 2009. **27**(18).

52. Lammers, T., et al., *Drug targeting to tumors: principles, pitfalls and (pre-) clinical progress.* J Control Release, 2012. **161**(2): p. 175-87.
53. Orlowski, R.Z., et al., *Randomized phase III study of pegylated liposomal doxorubicin plus bortezomib compared with bortezomib alone in relapsed or refractory multiple myeloma: combination therapy improves time to progression.* Journal of Clinical Oncology, 2007. **25**(25): p. 3892-901.
54. Northfelt, D.W., et al., *Pegylated-liposomal doxorubicin versus doxorubicin, bleomycin, and vincristine in the treatment of AIDS-related Kaposi's sarcoma: results of a randomized phase III clinical trial.* Journal of Clinical Oncology, 1998. **16**(7): p. 2445-51.
55. Vergote, I., et al., *Randomized phase III study of canfosfamide in combination with pegylated liposomal doxorubicin compared with pegylated liposomal doxorubicin alone in platinum-resistant ovarian cancer.* Int J Gynecol Cancer, 2010. **20**(5): p. 772-80.
56. Sparano, J.A., et al., *Pegylated liposomal doxorubicin plus docetaxel significantly improves time to progression without additive cardiotoxicity compared with docetaxel monotherapy in patients with advanced breast cancer previously treated with neoadjuvant-adjuvant anthracycline therapy: results from a randomized phase III study.* Journal of Clinical Oncology, 2009. **27**(27): p. 4522-9.
57. Dinndorf, P.A., et al., *FDA Drug Approval Summary: Pegaspargase (Oncaspar®) for the First-Line Treatment of Children with Acute Lymphoblastic Leukemia (ALL).* Oncologist, 2007. **12**(8): p. 991-998.
58. Gradishar, W.J., et al., *Phase III trial of nanoparticle albumin-bound paclitaxel compared with polyethylated castor oil-based paclitaxel in women with breast cancer.* Journal of Clinical Oncology, 2005. **23**(31): p. 7794-803.
59. Sudimack, J., B.A.,Robert J Lee., *Targeted drug delivery via the folate receptor.* Adv Drug Deliv Rev, 2000. **41**(2): p. 147-162.
60. Kelley, V.E., et al., *Interleukin 2-diphtheria toxin fusion protein can abolish cell-mediated immunity in vivo.* Proc Natl Acad Sci U S A, 1988. **85**(11): p. 3980-4.
61. Kratz, F. and U. Beyer, *Serum proteins as drug carriers of anticancer agents: A review.* Drug Deliv, 1998. **5**(4): p. 281-299.
62. Singh, M., *Transferrin as a targeting ligand for liposomes and anticancer drugs.* Curr Pharm Des, 1999. **5**(6): p. 443-451.

TH-1245_08610607

63. Vyas, S.P. and V. Sihorkar, *Endogenous carriers and ligands in non-immunogenic site-specific drug delivery.* Adv Drug Deliv Rev, 2000. **43**(2-3): p. 101-64.
64. Kircheis, R., et al., *Tumor-targeted gene delivery: an attractive strategy to use highly active effector molecules in cancer treatment.* Gene Ther, 2002. **9**(11): p. 731-735.
65. Zhang, P., et al., *An efficient drug delivery vehicle for botulism countermeasure.* BMC Pharmacol, 2009. **9**: p. 12.
66. Townsend, S.A., et al., *Tetanus toxin C fragment-conjugated nanoparticles for targeted drug delivery to neurons.* Biomaterials, 2007. **28**(34): p. 5176-84.
67. Bouter, A., et al., *Intracellular trafficking of Shiga-toxin-B-subunit-functionalized spherulites.* Biol Cell, 2008. **100**(12): p. 717-25.
68. Mayer, A., et al., *Modifying an immunogenic epitope on a therapeutic protein: a step towards an improved system for antibody-directed enzyme prodrug therapy (ADEPT).* Br J Cancer, 2004. **90**(12): p. 2402-2410.
69. Bross, P.F., et al., *Approval summary: gemtuzumab ozogamicin in relapsed acute myeloid leukemia.* Clin Cancer Res, 2001. **7**(6): p. 1490-6.
70. Foyil, K.V. and N.L. Bartlett, *Brentuximab vedotin for the treatment of CD30+ lymphomas.* Immunotherapy, 2011. **3**(4): p. 475-85.
71. Gupta, M., et al., *Clinical implications of pathophysiological and demographic covariates on the population pharmacokinetics of trastuzumab emtansine, a HER2-targeted antibody-drug conjugate, in patients with HER2-positive metastatic breast cancer.* J Clin Pharmacol, 2012. **52**(5): p. 691-703.
72. Firer, M.A. and G. Gellerman, *Targeted drug delivery for cancer therapy: the other side of antibodies.* J Hematol Oncol, 2012. **5**: p. 70.
73. Goishi, K., et al., *Phorbol ester induces the rapid processing of cell surface heparin-binding EGF-like growth factor: conversion from juxtacrine to paracrine growth factor activity.* Molecular Biology of the Cell, 1995. **6**(8): p. 967-80.
74. Miyamoto, S., et al., *Heparin-binding epidermal growth factor-like growth factor as a novel targeting molecule for cancer therapy.* Cancer Sci, 2006. **97**(5): p. 341-347.
75. Mishima, K., et al., *Heparin-binding epidermal growth factor-like growth factor stimulates mitogenic signaling and is highly expressed in human malignant gliomas.* Acta Neuropathologica, 1998. **96**(4): p. 322-328.
76. Kobrin, M.S., et al., *Induction and expression of heparin-binding EGF-like growth factor in human pancreatic cancer.* Biochem Biophys Res Commun, 1994. **202**(3): p. 1705-9.

TH-1245_08610607

77. Shimura, T., et al., *Suppression of proHB-EGF carboxy-terminal fragment nuclear translocation: a new molecular target therapy for gastric cancer.* Clin Cancer Res, 2008. **14**(12): p. 3956-65.
78. Sato, S., et al., *A Potent Anti-HB-EGF Monoclonal Antibody Inhibits Cancer Cell Proliferation and Multiple Angiogenic Activities of HB-EGF.* PLoS One, 2012. **7**(12): p. e51964.
79. Hamaoka, M., et al., *Anti-human HB-EGF monoclonal antibodies inhibiting ectodomain shedding of HB-EGF and diphtheria toxin binding.* Journal of Biochemistry, 2010. **148**(1): p. 55-69.
80. Tsuji, I., et al., *Characterization of a variety of neutralizing anti-heparin-binding epidermal growth factor-like growth factor monoclonal antibodies by different immunization methods.* Mabs, 2012. **4**(6): p. 732-739.
81. Miyamoto, S., et al., *A Novel Anti-Human HB-EGF Monoclonal Antibody with Multiple Antitumor Mechanisms against Ovarian Cancer Cells.* Clinical Cancer Research, 2011. **17**(21): p. 6733-6741.
82. Nishikawa, K., et al., *Development of anti-HB-EGF immunoliposomes for the treatment of breast cancer.* Journal of Controlled Release, 2012. **160**(2): p. 274-280.
83. Higashiyama, S., et al., *A heparin-binding growth factor secreted by macrophage-like cells that is related to EGF.* Science, 1991. **251**(4996): p. 936-9.
84. Higashiyama, S., et al., *Structure of Heparin-Binding Egf-Like Growth-Factor - Multiple Forms, Primary Structure, and Glycosylation of the Mature Protein.* Journal of Biological Chemistry, 1992. **267**(9): p. 6205-6212.
85. Massague, J. and A. Pandiella, *Membrane-anchored growth factors.* Annu Rev Biochem, 1993. **62**: p. 515-41.
86. Raab, G., et al., *Biosynthesis and processing by phorbol ester of the cells surface-associated precursor form of heparin-binding EGF-like growth factor.* Biochem Biophys Res Commun, 1994. **204**(2): p. 592-7.
87. Higashiyama, S., et al., *A Heparin-Binding Growth-Factor Secreted by Macrophage-Like Cells That Is Related to Egf.* Science, 1991. **251**(4996): p. 936-939.
88. Fen, Z., et al., *Structural Organization and Chromosomal Assignment of the Gene Encoding the Human Heparin-Binding Epidermal Growth Factor-Like Growth-Factor Diphtheria-Toxin Receptor.* Biochemistry, 1993. **32**(31): p. 7932-7938.

TH-1245_08610607

89. Hayes, H., et al., *Regional Assignment of the Gene for Diphtheria-Toxin Sensitivity Using Subchromosomal Fragments in Microcell Hybrids.* Chromosoma, 1987. **96**(1): p. 26-32.
90. Minami, S., R. Iwamoto, and E. Mekada, *HB-EGF decelerates cell proliferation synergistically with TGFalpha in perinatal distal lung development.* Dev Dyn, 2008. **237**(1): p. 247-58.
91. Iwamoto, R. and E. Mekada, *ErbB and HB-EGF signaling in heart development and function.* Cell Struct Funct, 2006. **31**(1): p. 1-14.
92. Abraham, J.A., et al., *Heparin-binding EGF-like growth factor: characterization of rat and mouse cDNA clones, protein domain conservation across species, and transcript expression in tissues.* Biochem Biophys Res Commun, 1993. **190**(1): p. 125-33.
93. Xian, C.J. and X.F. Zhou, *EGF family of growth factors: essential roles and functional redundancy in the nerve system.* Front Biosci, 2004. **9**: p. 85-92.
94. Xie, H., et al., *Maternal heparin-binding-EGF deficiency limits pregnancy success in mice.* Proc Natl Acad Sci U S A, 2007. **104**(46): p. 18315-18320.
95. Ito, Y., et al., *Expression of heparin-binding epidermal growth factor-like growth factor in breast carcinoma.* Breast Cancer Res Treat, 2001. **67**(1): p. 81-85.
96. Kobrin, M.S., et al., *Induction and Expression of Heparin-Binding Egf-Like Growth-Factor in Human Pancreatic-Cancer.* Biochem Biophys Res Commun, 1994. **202**(3): p. 1705-1709.
97. Ito, Y., et al., *Expression of heparin-binding epidermal growth factor-like growth factor in pancreatic adenocarcinoma.* International Journal of Pancreatology, 2001. **29**(1): p. 47-52.
98. Freeman, M.R., et al., *Heparin-binding EGF-Like growth factor in the human prostate: Synthesis predominantly by interstitial and vascular smooth muscle cells and action as a carcinoma cell mitogen.* J Cell Biochem, 1998. **68**(3): p. 328-338.
99. Ito, Y., et al., *Bimodal expression of heparin-binding EGF-like growth factor in colonic neoplasms.* Anticancer Res, 2001. **21**(2B): p. 1391-1394.
100. Tanaka, Y., et al., *Clinical significance of heparin-binding epidermal growth factor-like growth factor and a disintegrin and metalloprotease 17 expression in human ovarian cancer.* Clinical Cancer Research, 2005. **11**(13): p. 4783-4792.
101. Inui, Y., et al., *Expression of Heparin-Binding Epidermal Growth-Factor in Human Hepatocellular-Carcinoma.* Gastroenterology, 1994. **107**(6): p. 1799-1804.

TH-1245_08610607

102. Thogersen, V.B., et al., *A subclass of HER1 ligands are prognostic markers for survival in bladder cancer patients.* Cancer Res, 2001. **61**(16): p. 6227-33.
103. Adam, R.M., et al., *A nuclear form of the heparin-binding epidermal growth factor-like growth factor precursor is a feature of aggressive transitional cell carcinoma.* Cancer Res, 2003. **63**(2): p. 484-490.
104. Kramer, C., et al., *Heparin-binding epidermal growth factor-like growth factor isoforms and epidermal growth factor receptor/ErbB1 expression in bladder cancer and their relation to clinical outcome.* Cancer, 2007. **109**(10): p. 2016-2024.
105. Shirakata, Y., et al., *Heparin-binding EGF-like growth factor accelerates keratinocyte migration and skin wound healing.* Journal of Cell Science, 2005. **118**(11): p. 2363-2370.
106. Marikovsky, M., et al., *Appearance of heparin-binding EGF-like growth factor in wound fluid as a response to injury.* Proc Natl Acad Sci U S A, 1993. **90**(9): p. 3889-93.
107. Lim, H.J. and S.K. Dey, *HB-EGF: A unique mediator of embryo-uterine interactions during implantation.* Experimental Cell Research, 2009. **315**(4): p. 619-626.
108. Raab, G. and M. Klagsbrun, *Heparin-binding EGF-like growth factor.* Biochimica Et Biophysica Acta-Reviews on Cancer, 1997. **1333**(3): p. F179-199.
109. Iwamoto, R., et al., *Heparin-binding EGF-like growth factor and ErbB signaling is essential for heart function.* Proc Natl Acad Sci U S A, 2003. **100**(6): p. 3221-3226.
110. Asakura, M., et al., *Cardiac hypertrophy is inhibited by antagonism of ADAM12 processing of HB-EGF: Metalloproteinase inhibitors as a new therapy.* Nat Med, 2002. **8**(1): p. 35-40.
111. Miyagawa, J., et al., *Localization of Heparin-Binding Egf-Like Growth-Factor in the Smooth-Muscle Cells and Macrophages of Human Atherosclerotic Plaques.* Journal of Clinical Investigation, 1995. **95**(1): p. 404-411.
112. Powell, P.P., et al., *Eosinophils expressing heparin-binding EGF-like growth factor mRNA localize around lung microvessels in pulmonary hypertension.* Am J Pathol, 1993. **143**(3): p. 784-93.
113. Fu, S., et al., *Heparin-binding epidermal growth factor-like growth factor, a v-Jun target gene, induces oncogenic transformation.* Proc Natl Acad Sci U S A, 1999. **96**(10): p. 5716-21.

TH-1245_08610607

114. Higashiyama, S., J.A. Abraham, and M. Klagsbrun, *Heparin-binding EGF-like growth factor stimulation of smooth muscle cell migration: dependence on interactions with cell surface heparan sulfate.* J Cell Biol, 1993. **122**(4): p. 933-40.
115. Ongusaha, P.P., et al., *HB-EGF is a potent inducer of tumor growth and angiogenesis.* Cancer Res, 2004. **64**(15): p. 5283-90.
116. Yagi, H., et al., *Clinical significance of heparin-binding epidermal growth factor-like growth factor in peritoneal fluid of ovarian cancer.* Br J Cancer, 2005. **92**(9): p. 1737-45.
117. Wang, F., et al., *Heparin-binding EGF-like growth factor is an early response gene to chemotherapy and contributes to chemotherapy resistance.* Oncogene, 2007. **26**(14): p. 2006-2016.
118. Tang, X.-h., et al., *The anti-tumor effect of cross-reacting material 197, an inhibitor of heparin-binding EGF-like growth factor, in human resistant ovarian cancer.* Biochem Biophys Res Commun, 2012. **422**(4): p. 676-680.
119. Yoshida, T., et al., *The anti-EGFR monoclonal antibody blocks cisplatin-induced activation of EGFR signaling mediated by HB-EGF.* FEBS Lett, 2008. **582**(30): p. 4125-4130.
120. Sanui, A., et al., *HB-EGF Inhibition in Combination with Various Anticancer Agents Enhances its Antitumor Effects in Gastric Cancer.* Anticancer Research, 2010. **30**(8): p. 3143-3149.
121. Johnson, F.M., B. Saigal, and N.J. Donato, *Induction of heparin-binding EGF-like growth factor and activation of EGF receptor in imatinib mesylate-treated squamous carcinoma cells.* J Cell Physiol, 2005. **205**(2): p. 218-227.
122. Yagi, H., et al., *Synergistic anti-tumor effect of paclitaxel with CRM197, an inhibitor of HB-EGF, in ovarian cancer.* International Journal of Cancer, 2009. **124**(6): p. 1429-1439.
123. Soyensen, B.S., D. Ornskov, and E. Nexo, *The chemotherapeutic agent VP16 increases the stability of HB-EGF mRNA by a mechanism involving the 3 '-UTR.* Experimental Cell Research, 2006. **312**(18): p. 3651-3658.
124. Kishida, O., et al., *Gefitinib ("Iressa", ZD1839) inhibits SN38-triggered EGF signals and IL-8 production in gastric cancer cells.* Cancer Chemother Pharmacol, 2005. **55**(4): p. 393-403.
125. Miyamoto, S., et al., *Potential for Molecularly Targeted Therapy against Epidermal Growth Factor Receptor Ligands.* Anticancer Res, 2009. **29**(3): p. 823-830.

TH-1245_08610607

126. Kunami, N., et al., *Antitumor Effects of CRM197, A Specific Inhibitor of HB-EGF, in T-Cell Acute Lymphoblastic Leukemia.* Anticancer Res, 2011. **31**(7): p. 2483-2488.
127. Cantley, L.C., *The phosphoinositide 3-kinase pathway.* Science, 2002. **296**(5573): p. 1655-7.
128. Sussman, M., *"AKT"ing lessons for stem cells: regulation of cardiac myocyte and progenitor cell proliferation.* Trends Cardiovasc Med, 2007. **17**(7): p. 235-40.
129. Wilson, K.J., et al., *Functional selectivity of EGF family peptide growth factors: Implications for cancer.* Pharmacol Ther, 2009. **122**(1): p. 1-8.
130. Pierce, K.L., L.M. Luttrell, and R.J. Lefkowitz, *New mechanisms in heptahelical receptor signaling to mitogen activated protein kinase cascades.* Oncogene, 2001. **20**(13): p. 1532-9.
131. Prenzel, N., et al., *Tyrosine kinase signalling in breast cancer: Epidermal growth factor receptor - convergence point for signal integration and diversification.* Breast Cancer Res, 2000. **2**(3): p. 184 - 190.
132. Nanba, D., et al., *Proteolytic release of the carboxy-terminal fragment of proHB-EGF causes nuclear export of PLZF.* J Cell Biol, 2003. **163**(3): p. 489-502.
133. Henson, E.S. and S.B. Gibson, *Surviving cell death through epidermal growth factor (EGF) signal transduction pathways: Implications for cancer therapy.* Cellular Signalling, 2006. **18**(12): p. 2089-2097.
134. Kinugasa, Y., et al., *The carboxyl-terminal fragment of pro-HB-EGF reverses Bcl6-mediated gene repression.* Journal of Biological Chemistry, 2007. **282**(20): p. 14797-14806.
135. Naglich, J.G., et al., *Expression cloning of a diphtheria toxin receptor: identity with a heparin-binding EGF-like growth factor precursor.* Cell, 1992. **69**(6): p. 1051-61.
136. Collier, R.J., *Diphtheria-Toxin - Mode of Action and Structure.* Bacteriological Reviews, 1975. **39**(1): p. 54-85.
137. Choe, S., et al., *The Crystal-Structure of Diphtheria-Toxin.* Nature, 1992. **357**(6375): p. 216-222.
138. Uchida, T., A.M. Pappenheimer, Jr., and R. Greany, *Diphtheria toxin and related proteins. I. Isolation and properties of mutant proteins serologically related to diphtheria toxin.* J Biol Chem, 1973. **248**(11): p. 3838-44.

TH-1245_08610607

139. Naglich, J.G., et al., *Expression Cloning of a Diphtheria-Toxin Receptor - Identity with a Heparin-Binding Egf-Like Growth-Factor Precursor.* Cell, 1992. **69**(6): p. 1051-1061.
140. Collier, R.J., *Understanding the mode of action of diphtheria toxin: a perspective on progress during the 20th century.* Toxicon, 2001. **39**(11): p. 1793-803.
141. Shen, W.H., et al., *Participation of lysine 516 and phenylalanine 530 of diphtheria toxin in receptor recognition.* J Biol Chem, 1994. **269**(46): p. 29077-84.
142. Mitamura, T., et al., *Diphtheria-Toxin Binds to the Epidermal Growth-Factor (Egf)-Like Domain of Human Heparin-Binding Egf-Like Growth-Factor Diphtheria-Toxin Receptor and Inhibits Specifically Its Mitogenic Activity.* Journal of Biological Chemistry, 1995. **270**(3): p. 1015-1019.
143. Morris, R., et al., *Receptor-mediated entry of diphtheria toxin into monkey kidney (Vero) cells: electron microscopic evaluation.* Infection and immunity, 1985. **50**(3): p. 721-727.
144. Sandvig, K. and S. Olsnes, *Diphtheria toxin entry into cells is facilitated by low pH.* J Cell Biol, 1980. **87**(3): p. 828-832.
145. Van Ness, B.G., J.B. Howard, and J.W. Bodley, *ADP-ribosylation of elongation factor 2 by diphtheria toxin. NMR spectra and proposed structures of ribosyl-diphthamide and its hydrolysis products.* Journal of Biological Chemistry, 1980. **255**(22): p. 10710-10716.
146. Piascik, P., *FDA approves fusion protein for treatment of lymphoma.* J Am Pharm Assoc (Wash), 1999. **39**(4): p. 571-2.
147. Rainov, N.G. and A. Soling, *Clinical studies with targeted toxins in malignant glioma.* Rev Recent Clin Trials, 2006. **1**(2): p. 119-31.
148. Candolfi, M., et al., *Targeted Toxins for Glioblastoma Multiforme: Pre-Clinical Studies and Clinical Implementation.* Anti-Cancer Agents in Medicinal Chemistry, 2011. **11**(8): p. 729-738.
149. Frankel, A.E., E.P. Tagge*, and M.C. Willingham†, *Clinical trials of targeted toxins.* Semin Cancer Biol, 1995. **6**(5): p. 307-317.
150. Li, Y.M., D.A. Vallera, and W.A. Hall, *Diphtheria toxin-based targeted toxin therapy for brain tumors.* Journal of Neuro-Oncology, 2013. **114**(2): p. 155-164.
151. Li, Y.M. and W.A. Hall, *Targeted Toxins in Brain Tumor Therapy.* Toxins (Basel), 2010. **2**(11): p. 2645-2662.

TH-1245_08610607

152. Buonerba, C., et al., *A comprehensive outlook on intracerebral therapy of malignant gliomas.* Critical Reviews in Oncology/Hematology, 2011. **80**(1): p. 54-68.
153. Buzzi, S., *Diphtheria-Toxin Treatment of Human Advanced Cancer.* Cancer Res, 1982. **42**(5): p. 2054-2058.
154. Miyamoto, S., et al., *New approach to cancer therapy: Heparin binding-epidermal growth factor-like growth factor as a novel, targeting molecule.* Anticancer Res, 2007. **27**(6A): p. 3713-3721.
155. Buzzi, S., et al., *CRM197 (nontoxic diphtheria toxin): effects on advanced cancer patients.* Cancer Immunology Immunotherapy, 2004. **53**(11): p. 1041-1048.
156. Tang, X.H., et al., *The anti-tumor effect of cross-reacting material 197, an inhibitor of heparin-binding EGF-like growth factor, in human resistant ovarian cancer.* Biochem Biophys Res Commun, 2012. **422**(4): p. 676-680.
157. Miyamoto, S., et al., *Heparin-binding EGF-like growth factor is a promising target for ovarian cancer therapy.* Cancer Res, 2004. **64**(16): p. 5720-5727.
158. Wang, Y.D., et al., *Cooperation between heparin-binding EGF-like growth factor and interleukin-6 in promoting the growth of human myeloma cells.* Oncogene, 2002. **21**(16): p. 2584-2592.
159. Martarelli, D., P. Pompei, and G. Mazzoni, *Inhibition of Adrenocortical Carcinoma by Diphtheria Toxin Mutant CRM197.* Chemotherapy, 2009. **55**(6): p. 425-432.
160. Horita, H., et al., *EGFR-targeted diphtheria toxin stimulates TRAIL killing of glioblastoma cells by depleting anti-apoptotic proteins.* J Neurooncol, 2009. **95**(2): p. 175-84.
161. Yotsumoto, F., et al., *HB-EGF orchestrates the complex signals involved in triple-negative and trastuzumab-resistant breast cancer.* International Journal of Cancer, 2010. **127**(11): p. 2707-2717.
162. Kunami, N., et al., *Antitumor Effects of CRM197, A Specific Inhibitor of HB-EGF, in T-Cell Acute Lymphoblastic Leukemia.* Anticancer Research, 2011. **31**(7): p. 2483-2488.
163. Gaillard, P.J., A. Brink, and A.G. de Boer, *Diphtheria toxin receptor-targeted brain drug delivery.* International Congress Series, 2005. **1277**(0): p. 185-198.
164. Gaillard, P.J. and A.G. de Boer, *A novel opportunity for targeted drug delivery to the brain.* Journal of Controlled Release, 2006. **116**(2): p. E60-E62.

TH-1245_08610607

165. Wang, P., et al., *CRM197-induced blood-brain barrier permeability increase is mediated by upregulation of caveolin-1 protein.* J Mol Neurosci, 2011. **43**(3): p. 485-92.
166. Joseph Sambrook, D.R., *Molecular Cloning: A Laboratory Manual.* Cold Spring Harbor, New York: Cold Spring Harbor Laboratory Press., (3rd edition).
167. Laemmli, U.K., *Cleavage of Structural Proteins during Assembly of Head of Bacteriophage-T4.* Nature, 1970. **227**(5259): p. 680-685.
168. Brown, J.G., et al., *Hypersensitivity to diphtheria toxin by mouse cells expressing both diphtheria toxin receptor and CD9 antigen.* Proc Natl Acad Sci U S A, 1993. **90**(17): p. 8184-8.
169. Grosdidier, A., V. Zoete, and O. Michielin, *SwissDock, a protein-small molecule docking web service based on EADock DSS.* Nucleic Acids Res, 2011. **39**(Web Server issue): p. W270-7.
170. Irwin, J.J. and B.K. Shoichet, *ZINC--a free database of commercially available compounds for virtual screening.* J Chem Inf Model, 2005. **45**(1): p. 177-82.
171. Pettersen, E.F., et al., *UCSF Chimera--a visualization system for exploratory research and analysis.* J Comput Chem, 2004. **25**(13): p. 1605-12.
172. Kunwar, A., et al., *Transport of liposomal and albumin loaded curcumin to living cells: An absorption and fluorescence spectroscopic study.* Biochimica Et Biophysica Acta-General Subjects, 2006. **1760**(10): p. 1513-1520.
173. Cooper Thomas, H., G. Clark Joseph, and A. Guzinski James, *Analysis of Curcuminoids by High-Performance Liquid Chromatography*, in *Food Phytochemicals for Cancer Prevention Ii*1994, American Chemical Society. p. 231-236.
174. Riccardi, C. and I. Nicoletti, *Analysis of apoptosis by propidium iodide staining and flow cytometry.* Nature Protocols, 2006. **1**(3): p. 1458-61.
175. Vugmeyster, Y., et al., *Pharmacokinetics and toxicology of therapeutic proteins: Advances and challenges.* World J Biol Chem, 2012. **3**(4): p. 73-92.
176. Tizard, I.R., *Immunology: An Introduction.4th ed.* Thomson Asia Pte. Ltd: Singapore, 2004.
177. Brooke, J.S., J.H. Cha, and L. Eidels, *Diphtheria toxin:receptor interaction: association, dissociation, and effect of pH.* Biochem Biophys Res Commun, 1998. **248**(2): p. 297-302.
178. Kratz, F., *Albumin as a drug carrier: design of prodrugs, drug conjugates and nanoparticles.* J Control Release, 2008. **132**(3): p. 171-83.

TH-1245_08610607

179. Stewart, K.M., K.L. Horton, and S.O. Kelley, *Cell-penetrating peptides as delivery vehicles for biology and medicine.* Org Biomol Chem, 2008. **6**(13): p. 2242-55.
180. Walker, L., et al., *Cell penetrating peptides fused to a thermally targeted biopolymer drug carrier improve the delivery and antitumor efficacy of an acid-sensitive doxorubicin derivative.* Int J Pharm, 2012. **436**(1-2): p. 825-32.
181. Bachar, M., et al., *Development and characterization of a novel drug nanocarrier for oral delivery, based on self-assembled beta-casein micelles.* Journal of Controlled Release, 2012. **160**(2): p. 164-171.
182. Koudelka, K.J. and M. Manchester, *Chemically modified viruses: principles and applications.* Curr Opin Chem Biol, 2010. **14**(6): p. 810-7.
183. Qian, Z.M., et al., *Targeted drug delivery via the transferrin receptor-mediated endocytosis pathway.* Pharmacol Rev, 2002. **54**(4): p. 561-87.
184. Anand, P., et al., *Bioavailability of curcumin: problems and promises.* Mol Pharm, 2007. **4**(6): p. 807-18.
185. Priyadarsini, K.I., *Photophysics, photochemistry and photobiology of curcumin: Studies from organic solutions, bio-mimetics and living cells.* Journal of Photochemistry and Photobiology C-Photochemistry Reviews, 2009. **10**(2): p. 81-95.
186. Leung, M.H.M. and T.W. Kee, *Effective Stabilization of Curcumin by Association to Plasma Proteins: Human Serum Albumin and Fibrinogen.* Langmuir, 2009. **25**(10): p. 5773-5777.
187. Barik, A., K.I. Priyadarsini, and H. Mohan, *Photophysical studies on binding of curcumin to bovine serum albumins.* Photochem Photobiol, 2003. **77**(6): p. 597-603.
188. Epstein, J., I.R. Sanderson, and T.T. MacDonald, *Curcumin as a therapeutic agent: the evidence from in vitro, animal and human studies.* British Journal of Nutrition, 2010. **103**(11): p. 1545-1557.
189. Gupta, S.C., et al., *Multitargeting by curcumin as revealed by molecular interaction studies.* Nat Prod Rep, 2011. **28**(12): p. 1937-55.
190. Yan, Y. and G. Marriott, *Analysis of protein interactions using fluorescence technologies.* Curr Opin Chem Biol, 2003. **7**(5): p. 635-40.
191. Bong, P.H., *Spectral and photophysical behaviors of curcumin and curcuminoids.* Bulletin of the Korean Chemical Society, 2000. **21**(1): p. 81-86.

TH-1245_08610607

192. Wang, Y.J., et al., *Stability of curcumin in buffer solutions and characterization of its degradation products.* Journal of Pharmaceutical and Biomedical Analysis, 1997. **15**(12): p. 1867-1876.

193. Shehzad, A., F. Wahid, and Y.S. Lee, *Curcumin in cancer chemoprevention: molecular targets, pharmacokinetics, bioavailability, and clinical trials.* Arch Pharm (Weinheim), 2010. **343**(9): p. 489-99.

194. Aoki, H., et al., *Evidence that curcumin suppresses the growth of malignant gliomas in vitro and in vivo through induction of autophagy: Role of Akt and extracellular signal-regulated kinase signaling pathways.* Molecular Pharmacology, 2007. **72**(1): p. 29-39.

195. Wang, L.F., et al., *Regulation of cellular growth, apoptosis, and Akt activity in human U251 glioma cells by a combination of cisplatin with CRM197.* Anti-Cancer Drugs, 2012. **23**(1): p. 81-89.

TH-1245_08610607

Appendix

General reagents: Acetic acid, chloroform, di-sodium hydrogen phosphate, glycerol, hydrochloric acid, isopropyl alcohol, isoamyl alcohol, methanol, potassium acetate, sulphuric acid, ethanol, sodium chloride (all of AR grade) – from SRL, India and Merck, India.

Molecular biology grade reagents/ chemicals: Acrylamide, APS, bis-acryl amide, EDTA, IPTG, lysozyme, TEMED, phenol, DAB, tween 20, triton X 100 - from Sigma-Aldrich, USA or SRL, India. PCR Master mix, dNTPs agarose from Bioline, UK. Magnesium chloride, disodium citrate, boric acid, SDS, Tris–base - from Merck, India. Imidazole, ampicillin, chloramphenicol, tetracycline from Himedia, India.

Components for bacterial culture medium: Bacto-agar, yeast extract, tryptone- from Himedia, India.

Components for mammalian cell culture medium: DMEM from HiMedia, antibiotic from Invitogen, fetal calf serum- from PAA, sodium bicarbonate- from Sigma-Aldrich, U.S.A.

Enzymes: Taq DNA polymerase– from Bangalore Genei, India. *BamH I* and *Xho I*, from NEB, UK. RNaseA – from Sigma-Aldrich. T4 DNA ligase from- Promega,U.S.A. Reverse transcriptase- from MBI Fermentas, Lithuania.

Blotting Membranes and Filters: PVDF membrane (0.2 μm) - from Milipore, U.S.A. 3mm filter paper - from Whatman, USA.

TH-1245_08610607

DNA and protein markers: 100 bp and 1 kb DNA ladder and protein molecular weight marker (14-100KD) - from Bangalore Genei, India.

Plastic and Glasswares: PCR tubes - from Axygen, USA; micro pipette tips, micro centrifuge tubes, petri dishes and other plastic wares- from Tarson Products Pvt. Ltd., India. Glassware- from Borosil International, India.

Cell lines: All the cell lines were procured from National Centre for Cell Science, Pune, India.

Table A1. List of Plasmid Vector

Name	Use	Promoter	Selection marker(s)	Cloning Site
pET-22b DT (Addgene)	Bacterial Expression Vector	P T7-lacO	Amp^R	Full length DT cloned at *BamH I/Xho I* site (Addgene).
pET-22b RDT (Novagen)	Bacterial expression Vector	P T7-lacO	Amp^R	ΔN-RDT cloned at *BamH I/Xho I* site.

TH-1245_08610607

Table. A2. List of Bacterial Strain

Strain	Description
Escherichia coli DH5α (Novagen)	F′ϕ80d*lac*ZΔM15 Δ (*lac*ZYA- *arg*F) U169 *end*A1 *rec*A1 *hsd*R17 ($r_K^- m_K^+$) *deo*R *thi*-1 *pho*A *sup*E44 λ^- *gyr*A96 *rel*A1
Escherichia coli BL21 (DE3) (Novagen)	F^- *ompT hsdS*$_B$ (r_B^- m_B^-) *gal dcm* (DE3).Derivation of B834.(Parental strain:B834; Resistance :none)

Table. A3. Culture Medium for Bacteria

Media	Constituents	Concentration	pH
Luria broth (LB)	Bactotryptone	1.0%	7.2
	Yeast extract	0.5%	
	NaCl	0.5%	
2xTY	Bactotryptone	1.6%	7.2
	Yeast extract	1.0%	
	NaCl	0.5%	
TYA	Bactotryptone	1.0%	7.2
	Yeast extract	0.5%	
	NaCl	0.8%	
	Agar	1.5%	
TYA/AMP	TYA media		7.2
	Ampicillin	100 µg/ ml	
TYA/AMP/Glu	TYA/AMP media		7.2
	Glucose	1%	

TH-1245_08610607

Table. A4. Culture Medium for Animal Cell

Media	Constituents	pH
DMEM	DMEM powder with high glucose for 1 liter, 3.7g $NaHCO_3$.	7.4, adjusted with 1N HCL
DMEM with serum	DMEM, 10% serum, 1 X Antibiotic.	7.4

Table. A5. List of Buffers and Solutions

Buffers / Solutions	Composition
Tris-EDTA (TE) buffer	0.01 M Tris-HCl (pH 7.4), 0.001 M Na_2-EDTA (pH 8.0)
TAE - Tris Acetate EDTA buffer, 50x (100ml)	24.2 g Tris base, 5.71 ml CH_3COOH, 10 ml of 0.5 M EDTA.
Phosphate buffer saline (PBS)	0.137 M NaCl, 2.68 mM KCl, 7.98 mM Na_2HPO_4, 1.4 mM KH_2PO_4, pH 7.2.
PBST	PBS containing 0.1% Tween -20
TBS	50mM tris base, 150mM NaCl
TBST	TBS containing 0.1% Tween -20
Trypsin- EDTA	0.05% Trypsin, 0.53mM EDTA in PBS
RIPA buffer	50 mM Tris-HCl, pH 7.5, 150 mM NaCl, 1% Nonidet P40, 0.5% sodium deoxycholat, 0.1% SDS.

TH-1245_08610607

Buffers/solutions for protein purification

Stripping Buffer	20 mM sodium phosphate, 500 mM NaCl, 50 mM EDTA, pH 7.4.
Recharging Buffer	2.5 ml of 100 mM Nickel sulphate hepta-hydrate in distilled water.
Equilibration Buffer	20 mM sodium phosphate, 500 mM NaCl, 40 mM Imidazole, pH 7.4.
Binding Buffer	20 mM sodium phosphate, 500 mM NaCl, 40 mM Imidazole, pH 7.4.
Elution Buffer	20 mM sodium phosphate, 500 mM NaCl, 500 mM Imidazole, pH 7.4

Buffers/solutions for SDS-PAGE

30 % acrylamide-bisacrylamide solution (100ml)	29.2 g Acrylamide, 0.8 g Bisacrylamide
Tris.HCl, pH 6.8, 0.5 M (100 ml)	6.06 g of Tris base, pH adjusted to 6.8 with 2 N HCl.
Tris.HCl, pH 8.8, 1.5 M (100 ml)	18.18 g of Tris base, pH adjusted to 8.8 with 2 N HCl.
Gel Running Buffer	25 mM Tris base, 250 mM, 0.1% SDS
Sample Loading Buffer (1X)	50 mM Tris-HCl pH 6.8, 2% SDS, 10% glycerol, 1% β-mercaptoethanol, 0.02 % bromophenol blue
Staining solution	50% Methanol, 10% Acetic acid, 40% Water, 0.25% CBB R250
Destaining solution	30% Methanol, 10% Acetic acid, 60% Water.

Buffers/solutions for Western Blot

Transfer buffer	25 mM Tris base, 39 mM Glycine, 20 % Methanol
Ponceau solution (Sigma)	0.1% PonceauS in 5% acetic acid
Blocking Solution	5% non fat milk in PBST or 5% BSA in TBST.

TH-1245_08610607

Washing buffer	PBST or TBST

Solutions for Plasmid Isolation

Solution I	50 mM Glucose , 25 mM Tris.HCl, 10 mM EDTA (pH 8.0)
Solution II	0.2 N NaOH, 1% SDS
Solution III	5 M potassium acetate, pH adjusted to 4.8 with acetic acid

Buffers/Solutions for Cell cycle analysis

Fixation Solution	70% ice cold ethanol in PBS , 1mM EDTA
DNA Extraction Buffer	192 ml of 0.2 M Na_2HPO4 with 8 ml of 0.1% Triton X-100 (v/v
DNA staining Solution	20 µg/ml propidium iodide and 200 µg/ml RNase A in PBS

Buffers/Solutions for SPR

Amine-coupling reagent(A)	0.4 M 1-ethyl-3-(3-dimethylamino-propyl)carbodiimide hydrochloride in water,pH 7.4.
Amine-coupling reagent(B)	0.1 M N-hydroxysuccinimide in water,pH 7.4.
Ethanolamine solution	1.0 M ethanolamine-HCl, pH 8.5
Coupling Buffer	10 mM sodium acetate, pH 4.0, 4.5, 5.0, 5.5.
Regeneration Buffer	10 mM, pH 1.5, 2.0, 2.5, 3.0
Running Buffer	10 mM Na2HPO4–NaH2PO4, 150 mM NaCl, pH 7.4
Equilibration Buffer	10 mM Na_2HPO4–NaH_2PO4, 150mM NaCl, 0.05% Tween 20, pH 7.4

TH-1245_08610607

Buffers/Solutions for ELISA

Substrate solution	O-phenylenediamine (0.4 mg/ml) diluted in 0.05 M citric acid and 0.1 M Na_2HPO_4,pH 5.0 and 0.03% H_2O_2
Stop solution	8 N Sulphuric acids.

Buffers/Solutions for HPLC

Mobile phase	40% THF and 60% water containing 1% citric acid, adjusted to pH 3.0, with concentrated KOH solution (v/v).

Table. A6. List of Antibody

Name	Sourse/ Type	Working condition	Working dilution	Use
Anti-human HB-EGF (R&D System, U.S.A, # MAB259)	Mouse/ monoclonal	RT/ 2 hr	1:1000	ELISA, WB,Imaging
Anti-Histidine-tagged protein (Calbiochem, Germany,# 0B05)	Mouse / monoclonal	RT/ 2 hr	1:1000	ELISA, WB,Imaging.
Anti-human phospho- p44/42 MAPK (Erk1/2) (Thr202/Tyr204) (Cell signaling, U.S.A, # 4370)	Rabbit/ monoclonal	4 °C/ ON	1:1000	WB
Anti-human p44/42 MAPK (Erk1/2) (Cell Signaling,U.S.A, # 4695)	Rabbit/ monoclonal	4 °C/ ON	1:1000	WB
Anti-human Phospho-Akt (Ser473) (Cell Signaling, U.S.A, # 4060)	Rabbit/ monoclonal	4 °C/ ON	1:1000	WB
Anti-human Akt (pan)	Rabbit/	4 °C/ ON	1:1000	WB

TH-1245_08610607

(Cell Signaling, U.S.A, # 4691)	Monoclonal			
Anti-human COXIV (Cell Signaling, U.S.A, # 4850)	Rabbit/ monoclonal	4 °C/ ON	1:2000	WB
Anti Mouse-HRP (Sigma, U.S.A, # A0412)	Goat	RT/ 2 hr	1:1000	ELISA, WB
Anti Rabbit-HRP (Cell Signaling, U.S.A, # 7074)	Goat	RT/ 2 hr	1:5000	WB
Anti Goat-HRP (Bangalore Genei, India, # 105500)	Rabbit	RT/ 2 hr	1:1000	WB
Anti mouse IgG-FITC (BD Pharmingen, U.S.A, #554001)	Goat /polyclonal	RT/ 2 hr	1:1000	Fluorescence Imaging.

RT: Room Temperature, ON: Over Night, W.B: Western Blot.

Table A7. List of Primers

Name	Sequence	Annealing Temp.(°C)	Final Conc (nM)
	Primers set for cloning		
RDT	DTR382 : 5′-CGCGGATCCGTCTCCGGGGCATA AAACGC-3′ DTRU : 5′TCAGTGGTGGTGGTGGTGGTGCT CGAG-3′	60	200
	Primers set for PCR		
HB-EGF	HBEGFF : 5'-TTATCCTCCAAGCCACAAGC-3' HBEGFR : 5'-CCCATGACACCTCTCTCCAT-3'	60	200

TH-1245_08610607

Beta actin	BAF : 5'-CTGTCTGGCGGCACCACCAT-3' BAR : 5'-GCAACTAAGTCATAGTCCGC-3'	60	200
GAPDH	GAPF : 5'-GAAGGTGAAGGTCGGAGTC-3' GAPR : 5'-GAAGATGGTGATGGGATTTC-3'	60	200

Table. A8. List of Antibiotic

Name	Stock Conc.(mg/ml)	Solvent	Working Conc.(µg/ml)
Ampicillin	100	Water	100

TH-1245_08610607

Publications

1. **Kumar A**, Das G., Bose B. Recombinant Receptor-binding Domain of Diphtheria Toxin Increases Potency of Curcumin by Enhancing Cellular Uptake. *Molecular Pharmaceutics.* November 2013, Epub ahead of print. (DOI: 10.1021/mp400378x) [PMID: 24224661].

Abstract:

1. **Kumar A**, Bose B. Truncated Diphtheria Toxin as a Novel Therapeutic Agent. *Carcinogenesis 2012,* New Delhi, India, November, 2012.

TH-1245_08610607